In presenting the dissertation as a partial fulfillment of the requirements for an advanced degree from the Georgia Institute of Technology, I agree that the Library of the Institute shall make it available for inspection and circulation in accordance with its regulations governing materials of this type. I agree that permission to copy from, or to publish from, this dissertation may be granted by the professor under whose direction it was written, or, in his absence, by the Dean of the Graduate Division when such copying or publication is solely for scholarly purposes and does not involve potential financial gain. It is understood that any copying from, or publication of, this dissertation which involves potential financial gain will not be allowed without written permission.

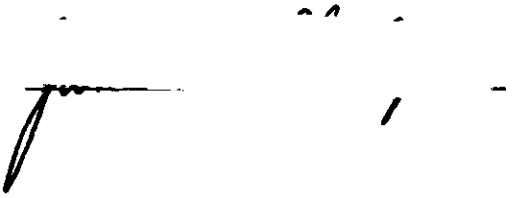

7/25/68

L-SHELL AUGER ENERGIES AND INTENSITIES IN 3D TRANSITION METALS

A THESIS

Presented to

The Faculty of the Graduate Division

By

James Daniel Phillips

In Partial Fulfillment

of the Requirements for the Degree

Doctor of Philosophy in the School of Physics

Georgia Institute of Technology

August 1972

L-SHELL AUGER ENERGIES AND INTENSITIES IN

3D TRANSITION METALS

Approved:

E. J. Scheibner, Chairman

H. A. Gersch

M. B. Sledd

Date approved by Chairman: 9/19/72

ACKNOWLEDGMENTS

I would like to extend my thanks to Dr. Edwin J. Scheibner for his able guidance and encouragement throughout the research period culminating with this dissertation. I wish to also express my gratitude to Dr. Harold A. Gersch and Dr. Marvin B. Sledd for their effective activities as members of my reading committee with a special note of thanks to Dr. Gersch for his advice and suggestions during the course of the research effort. In addition, I would like to thank Dr. Charlotte F. Fischer and Dr. Steven T. Manson for their valuable assistance in certain phases of this research and the faculty of the School of Physics for their instruction and support throughout my graduate career.

The financial basis for this research was provided under the auspices of the U. S. Atomic Energy Commission (Contract No. AT-(40-1)-2755) and the Department of Defense through the THEMIS Contract F 44620-68-C-008. This support is gratefully acknowledged.

I would also like to thank Miss Ginger Anderson and Mrs. Mary Haack for their attention and care in the typing of this dissertation in final form.

Finally, a special expression of gratitude is due my family for without their patience and confidence this work could not have been accomplished.

TABLE OF CONTENTS

LIST OF TABLES

LIST OF TABLES (Continued)

LIST OF FIGURES

SUMMARY

The Auger effect is characterized by the non-radiative de-excitation of an atom, initially singly ionized in an inner shell, to a final state consisting of a doubly ionized atom plus a free (Auger) electron in the continuum. If the initial state vacancy is in the L atomic shell while the final state vacancies are in the M shell, then one speaks of an LMM Auger transition. The current effort presents the results of a theoretical investigation of such transitions in the elements titanium (Ti), vanadium (V), chromium (Cr), zirconium (Zr), niobium (Nb), and molybdenum (Mo).

The principal results of this investigation are in the form of LMM Auger transition probabilities and energies for the cited elements. All calculations were performed in the framework of the non-relativistic theory of the Auger effect due to Wentzel. Although molecular and solid state effects were ignored in the calculations, their contribution is considered and discussed in some detail. In order to achieve the most reliable values for the transition probabilities, the pertinent electron wave functions were obtained by the Hartree-Fock approach to the atomic problem using the procedure developed by C. F. Fischer. Separate Hartree-Fock calculations were carried out for each possible initial and final state in order to account for the "relaxation" of the electron orbitals during the transition. To provide the most general formulation of the problem, the computations were performed in the formalism of

intermediate coupling (IC). One conclusion of our results is that it is unnecessary to use the IC limit when treating LMM transitions in Ti, V, and Cr; it is a necessity, however, in Zr, Nb, and Mo. As a final remark, it should be noted that the energy calculations were accomplished by first computing the total energies of the initial and final atomic states for each transition. The difference of these is, by conservation of energy, the energy of the Auger electron. In order to insure that the multiplet spectra obtained by this approach are in agreement with that predicted on the basis of the Wentzel theory, two distinct methods--the spectator and "exact"--were developed to compute the total energies. The spectator approach is used for all atoms with an incomplete M atomic shell; it was therefore used for the (Ti, V, Cr) calculations. If the M shell is completely filled, then the "exact" method is utilized. A detailed discussion is presented for both methods.

The results obtained from this procedure are given in tabular form and compared with the available experimental data. Due to a severe shortage of such data for LMM transitions, this comparison did not provide a meaningful test of the calculations. An additional experimental effort is strongly suggested in order to provide reliable data for comparison with the theoretically predicted LMM energies and transition probabilities.

CHAPTER I

INTRODUCTION

Objective

An atom ionized in an inner shell is in an unstable configuration. In a time of the order 10^{-14} - 10^{-17} seconds, the resulting system will de-excite in one of two ways. First, the vacancy may be filled by an electron from an outer shell accompanied by the emission of a photon. Such a mode of de-excitation is commonly termed a "radiative" (or an X-ray) transition. In the second mode, the outer electron again fills the inner vacancy but an electron--rather than a photon--is emitted. This "non-radiative" transition is called the Auger effect. Since the effect involves ionization of the inner levels, it is relatively insensitive to the behavior of the valence electrons. Therefore, even if the atom is chemically bound--as might be the case at or near a gas-solid interface--the Auger spectra from it will be essentially unchanged from that of a free atom (there are differences, of course; see Chapter II). It is this characteristic of the Auger process which is exploited in Auger spectroscopy.

In the typical experimental arrangement of this method, a sample is isolated in an ultra-high vacuum system and then bombarded with electrons of suitable energy. These electrons collide with surface or even sub-surface atoms and produce excited atomic states. If the excited state so formed is a result of electron ejection from the inner

shell of the atom, it may de-excite by the Auger mechanism. A monitor of the electrons emanating from the sample then provides a method of identifying the source of Auger electrons, i.e., the identity of the atoms on or near the sample surface. It follows that a knowledge of the Auger effect can provide a means of identifying surface impurities.

It is clear, however, that implementation of this approach requires an unambiguous method of identifying the Auger electrons against the background of the remaining electron current from the sample. There are two distinct physical quantities which provide this method--the Auger electron energy and the intensity of the Auger electron current. In present applications only the energy is utilized in the spectra identification, and even here the expected Auger energies are obtained primarily by semi-empirical formulae. The errors inherent in the predictions arising from such relations may be quite large--depending on the atom and the particular Auger transition--and a far more desirable procedure would be to use energies based on detailed theoretical computation. Unfortunately, rigorous results are presently available only for Auger processes arising from an initial inner vacancy in the K-shell--i.e., the K-series (the series name being determined by the shell of the initial vacancy). These are of little use in surface investigations since the energy of electrons necessary to produce K-shell ionization is so large for most atoms that the penetration past the surface is also large. Hence, the resulting spectra may not truly give a representation of the surface constituents. Instead, surface studies require a knowledge of the higher Auger series--e.g., L-, M-series--and here the theoretical work is not nearly so accurate.

Even when the energies are well known, an unambiguous spectra identification may not be possible if there are several Auger transitions with almost the same energy. It then becomes clear that to obtain maximum advantage from Auger spectroscopy, the Auger intensities should, if possible, be used. Here, however, theoretical work is lacking to a greater degree than in the case of the energies. Indeed, although the quantity of theoretical results for K-, L-, M-series transitions is steadily increasing, the quality seems to remain the same since little agreement with available experimental data is found. In order to improve upon this situation, the present investigation was undertaken. The objectives of this effort were to:

(a) aid interpretation of Auger spectra for the elements (Ti, V, Cr, Zr, Nb, Mo) by providing detailed energy predictions for LMM transitions;

(b) provide the associated transition probabilities using the best available wave functions; and

(c) compare the results obtained with current theoretical results to ascertain, if possible, where defects in the theory may exist.

Historical Survey

Theoretical

The Auger effect was first observed by P. Auger[1,2] in 1925 while performing X-ray absorption experiments on gases in a Wilson cloud chamber. He noted the presence of tracks in the chamber corresponding to electrons with energies too small to be the expected photoelectrons. By consideration of the energies involved, Auger explained the presence

of these electrons by a "conversion" process. Thus if an atom is excited in an inner level and de-excites by a radiative transition, a photon is produced. Auger proposed that in some transitions this photon does not escape the atom. Instead it is reabsorbed by a second electron which is subsequently ejected from the atomic system.

This view of the Auger process was incorrect, and it remained for Wentzel[3] in 1927 to provide the correct interpretation. Wentzel proposed that the Auger effect was actually a non-radiative process--no photon being involved--arising from the coulomb interaction of only those electrons directly involved in the Auger transition. Since only two electrons change states in such a transition, it follows that Wentzel's proposal is a two-electron view of the Auger effect. Wentzel proceeded to develop a detailed non-relativistic theory of the Auger process, a theory which is still widely used in describing Auger phenomena. Following this development, however, there was little activity relating to the Auger effect. The first significant application of Wentzel's theory was by Burhop[4] (1935) who treated the KLL transitions in silver (Ag). This effort was joined in the same year by the work of Pincherle[5] who treated K- and L-series intensities (independent of atomic number). Both Burhop and Pincherle assumed screened hydrogenic orbitals for the electron wave functions. Beyond these investigations, the only efforts until 1955 were the non-relativistic results of Ramberg and Richtmeyer[6] (1937) on gold (Au) and the first relativistic results for the Auger process by Massey and Burhop[7] (1937). There were several reasons for this lack of activity in treating Auger phenomena, but two of the more significant were (1)

the lack of an accurate means to compute electronic wave functions (the Hartree-Fock approximation is not feasible for most atoms without computers) and (2) the lack of a reliable experimental method to measure the Auger energies and intensities. Both of these drawbacks began to disappear in the early 1950's with the result that a significant amount of theoretical and experimental work has been carried out since 1955.

The resurgence of theoretical work began with the investigations of Rubenstein and Snyder[8,9] in 1955. These workers treated the K-, L-, M-series Auger transitions in argon, krypton and silver by assuming the Russell-Sanders or LS-coupling limit for the process. The inadequacy of such an assumption was demonstrated by Asaad and Burhop[10] with their formulation of Auger theory in the framework of intermediate coupling (IC). This work applied specifically to KLL and KLM transitions and predicted a 9-line Auger spectrum for the KLL case as opposed to the 5 or 6 lines expected on the basis of a pure LS- or jj-coupling treatment. Several workers--notably Erman[11] in the case of bromine and Graham et al.[12] for iodine and tellurium--have experimentally verified this prediction of the IC formulation. Despite the apparent success of IC in predicting the complexity of the Auger spectra, the quantitative predictions of intensities were still badly in error. One potential cause for this discrepancy was the lack of accurate electron wave functions to utilize in the computation of the transition amplitudes. Callan[13] (1961) attempted to remove this avenue of error by supplying for a variety of elements the requisite transition integrals for KLL transitions. Unfortunately, Callan used screened hydrogenic orbitals for the discrete states so that the KLL amplitudes were not reliable.

The results were consistent, however, since the amplitudes for different elements were all computed utilizing the same type of electron orbitals for each case. Asaad[14] (1963) took advantage of this fact and, using the IC formalism, computed the KLL intensities for the elements treated by Callan. Although the results of this computation were still in poor agreement with available experimental data, it did enable Asaad to determine the variation of the Auger intensities as a function of the atomic number Z. In order to improve upon the theoretical predictions, Asaad[15] introduced configuration interaction (CI) into the theory in 1965 and demonstrated that this inclusion could well remove some of the discrepancies between theory and experiment. Although subsequent results[16] imply that the particular success obtained by Asaad with CI was fortuitous (being due to inaccurate binding energies in the computations), it does appear that the effects of CI can be important in some Auger transitions and must be considered.

This introduction of CI into the theory has been followed by extensive computations as opposed to further examination of the theory. By assuming the basic validity of Wentzel's two-electron view of the Auger process, several investigators have studied the K-series transitions in still more detail, and treatments of L- and M-series transitions are beginning to appear. It is the L-series results which interest us in the present work, and we shall only cite the more extensive K-series efforts. Foremost among these is the work of McGuire[17] who has computed in LS-coupling the total KLL and KLM transition rates for beryllium to xenon. Unfortunately, several major approximations mar the accuracy of his results. In addition to these computations,

Walters and Bhalla[18] have treated KLL transitions with reasonable success by utilizing Hartree-Fock-Slater electron orbitals while Kostrum et al.[19] have presented similar results with the difference being their use of screened hydrogenic functions.

The L- and M-series results now becoming available represent a large percentage of all such work which has been performed. In addition to the previously cited work of Rubenstein and Snyder only the efforts by Asaad[20] and Callan[21] occurred prior to 1965. The treatment of Asaad dealt with the L-spectra for Ar, Kr, and Ag with jj-coupling assumed. This included Coster-Kronig transitions (the initial subshell vacancy is filled by an electron from the same shell but different subshell--e.g., a 2s vacancy filled by a 2p electron) as well as results for LMM and LMN transitions. The investigation of Callan was entirely concerned with the L-shell Coster-Kronig transitions. Beyond these treatments, the next consideration of L-series spectra was that by Asaad and Mehlhorn[22] who computed the transition rates for L_2MM and L_3MM spectra in argon. Only very recently have additional results become available for L-series transitions in more complex atoms. Thus McGuire[23] has presented predictions for the elements sodium (Na) through thorium (Th). These results are in the form of total transition rates so that the predictions are independent of the particular coupling scheme employed. Information concerning particular transitions such as $L_1M_1M_1$ is not given. Walters and Bhalla[24] have presented total transition rates for the $L_{2,3}$ shell transitions in the elements magnesium to cesium and a few beyond. Crasemann et al.[25] have considered L_1-shell transitions for several elements from arsenic to astatine.

Very recent results by McGuire[26] present M-shell transition rates. The agreement of these results with the small amount of L-shell experimental data has not been impressive thus far. This could be due to inaccurate experimental data or, more likely, to the use of poor wave functions and, possibly, an inaccurate theory. In any event the need for further computations is apparent.

This survey has not included a complete list of all papers relating to the Auger effect (theoretical), and the interested reader is referred to the review articles by Listengarten,[27] Bergström and Nordling,[28] Sevier[29] and the work by Burhop[30] for further information. The consideration of relativistic treatments of the Auger process has been omitted from the above survey. This was due partly to the fact that the present problem was carried out in the non-relativistic formalism and partly to the lack of relativistic calculations. Indeed, in addition to the work of Massey and Burhop[7] previously cited, only Chattarji and Tulukdar,[31] Asaad,[32] and Listengarten[33,34] have presented calculations based on the relativistic formalism of the Auger effect. Since this formalism is known to be inaccurate, we shall not comment further on this aspect of the theory.

Experimental

The measurement of Auger transition rates has not been quite as extensive as the corresponding theoretical effort. This is due primarily to the difficulty inherent in making such measurements--e.g., the requirements of the experimental apparatus include both high resolution (energy) and high sensitivity (intensities). Electrostatic and magnetic spectrometers, the chief means used thus far in Auger measurements,

possess these requisite features. In this brief survey, the experimental methods will not be discussed and for details the referenced articles are recommended. We shall further confine our comments to the more recent measurements and refer the reader to the aforementioned review articles for additional information.

Perhaps the most significant study has been that of Toburen and Albridge[35] on the K-, L-, and M-series spectra of platinum (Pt). By utilizing a magnetic spectrometer, these workers were able to identify 55 peaks in the L-series spectra, measuring both the energies and relative intensities. The comparison of these results with theory gives agreement only for the KLL energies predicted theoretically by the semi-empirical results of Hörnfeldt.[36] Similar measurements by Wolfson and Baerg[37] on KLL transitions in gold also do not find agreement with theory. The measurement of the K-series spectra of neon (Ne) has been carried out by Körber and Mehlhorn[38] while Cleff and Mehlhorn[39] have studied chlorine (Cl)--both efforts utilizing an electrostatic spectrometer. In the neon case the measured relative intensities were in disagreement with all theoretical calculations. It was shown, however, that agreement could be obtained by using improved wave functions and by incorporating CI into the formalism. The chlorine measurements provided absolute energies and relative intensities for four of the KLL transitions; once again, comparison of theory and experiment gave little agreement. Further experimental data on KLL transitions is available (e.g., Cu, Ge)--consult references 40-44 for the details.

The amount of experimental results for L-series (and higher) spectra[48] is quite limited with most of that which is available being

either for the noble gases or the heavier elements such as Tl and Bi.[45] Of the recent results Mehlhorn and Stalherm's measurement[46] of the L_2, L_3 spectra in argon is of interest since the relative intensities obtained agreed in some instances with the predictions of Rubenstein[9] but disagreed strongly in others. Such a situation indicates, probably, that the theoretical results were incorrect with the instances of agreement being fortuitous. Other measurements of L-series spectra using the traditional techniques of electrostatic or magnetic spectrometers have been carried out with Krause's results[47] for krypton being notable. In recent years, however, significant investigations of all elements have been carried out with the new tools of Auger Electron Spectroscopy (AES) and Electron Spectroscopy for Chemical Analysis (ESCA). Since AES studies on Ti, V, and Cr prompted the present investigation, we defer comment on this method to the next section. As regards ESCA, detailed reports[16,49,50] are available which describe the method and typical data arising from its use. We shall not treat this technique in more detail in this work and refer to the reports for details.

Status of Auger Phenomena

Until the advent of Auger Electron Spectroscopy (AES), the study of the Auger effect was primarily of academic interest with the goal being to understand the basic physics underlying the effect. The importance of this aspect of the study has, of course, not been diminished by AES. Due to the practical importance of the method as a tool in the investigation of surfaces, however, the basic study of the effect is now amplified by the practical desire to know the Auger

energies (and intensities) for use in the interpretation of AES spectra. In order to place the present investigation in perspective relative to AES, it will be helpful to consider the technique in more detail.

Auger Electron Spectroscopy

Since AES has been discussed exhaustively,[51-54,79-80] we shall confine our comments to those aspects of the method which can affect the interpretation of the data. In its most basic form, an electron beam is directed onto the surface of a properly oriented sample. These electrons cause excitation of electronic states in the solid and also in impurity atoms on or near the sample surface. Several types of interactions are possible for the electrons with the most prominent being those such that (1) the electrons are elastically scattered and diffracted by the lattice, (2) the electrons lose energy by exciting plasmons (collective excitation of the electron "gas"), interband excitations or both, (3) the electrons lose energy by exciting core levels of impurity atoms or low-lying bands in interband transitions. It is case (3) which is of interest here since it is for this type of excitation that an Auger process can occur. We expect, therefore, that a fraction of the electrons emanating from the surface will arise from Auger processes. Since the energies (and intensities) of Auger electrons are characteristic of the atom from which they originate, it follows that by monitoring these electrons one can obtain information about surface impurities and/or solid state effects[55-57,81-83] -- chemical shifts[58,59] have also been observed. In the AES system utilized by Tharp and Sheibner,[60] this monitoring of electron current

is accomplished by using a system of three spherical grids functioning as a retarding field analyzer.

To understand this terminology let us consider one of the grids and apply to it a retarding voltage capable of repelling all electrons from the detector with energies less than or equal to an energy E. Then the current reaching the detector of the system will be the total number of electrons emanating from the sample which have energy greater than E. By now sweeping the retarding grid voltage from a minimum (all electrons reach detector) to a maximum (none reach detector) we obtain a curve representing this total current fraction as a function of E--i.e., the retarding field curve (R(E)). Unfortunately, the information of this data is a little too general since it represents an integrated contribution of all electrons with energies greater than some energy E. The real quantity of interest is the number distribution ($N(E_o)$) of electrons in the beam from the sample--i.e., the number of electrons with a particular energy E_o. This will then identify those electrons which are elastically diffracted, excite plasmons, or those which originate from Auger transitions. One can show from quite general considerations[51] that $N(E_o)$ may be obtained (within a multiplicative factor) from the retarding field curve by taking the derivative of R(E) and evaluating at E_o. This can be accomplished experimentally by applying a small perturbing voltage to the control grid at frequency ω. As a result, ac fluctuations are induced in the current reaching the detector and by "locking-in" on that component of this current with frequency ω, the derivative of R(E) is obtained. Although this gives the desired distribution, in practice it is not generally

sufficient for observation of Auger electrons. This is due partly to the presence of a large background signal in the sample current and partly to the small intensities of the Auger currents. As a result, most AES measurements are of the second derivative of R(E) obtained by "locking-in" on the ac current component of frequency 2ω. The effect of this additional derivative is to (1) accent the position of peaks in energy and (2) totally obscure intensity information. It follows from this that AES is presently capable only of identifying Auger transitions by comparing peak energies with known (experimental or theoretical) values of Auger transition energies in the various elements. The method cannot, therefore, utilize Auger intensities at the present time (although modifications of the technique may allow it in the future--see Chapter IV). This is not too severe a restriction now since all theoretical results thus far generated show little agreement with available data, but, as more refined computations continue, one can expect the efforts of theory to become more successful. If AES is to reach full potential as a method, it follows that it must be extended to include utilization of intensities as well as energies.

Even with regard to the energies, the method is not free from confusion. Indeed, the bulk of the theoretical efforts cited previously dealt with only Auger intensities--not their energies. Only the work by Asaad and Burhop[10] considered energies, and they introduced semi-empirical expressions to describe the KLL energies. These expressions, as later modified by Hörnfeldt,[36] provide quite accurate values for KLL energies--estimated at about .05 per cent. For any other case, however, the only means to predict the expected Auger transitions for a

given transition is to utilize a rather crude relation due to Bergström and Hill.[68] Since this relation can--depending on the atom and particular transition--be considerably in error, the experimentalist has little aid in the interpretation of the observed spectra. Indeed, compilation of an experimental "encyclopedia of Auger spectra" is justifiable due to the poor state of theoretical predictions.

There is, of course, a precise, well-defined procedure for computing the Auger energies. Thus if we calculate the total energies of the initial and final atomic states and then subtract one from the other, this difference is, by conservation of energy, just the desired Auger energy. This method, developed in Chapter II, is utilized in the present work for all energy computations.

Problem and Method

This investigation was inspired as a result of difficulties encountered in the interpretation of certain structure in the AES spectra of Ti, V, and Cr. Due to the general lack of theoretical results for L- (or higher) series transitions, a natural choice for the study was the LMM transitions in these elements (Zr, Nb and Mo are also treated). In order to carry out these computations in a consistent, meaningful way, the following procedure was adopted:

(1) use Hartree-Fock wave functions thus insuring the best available electron orbitals;

(2) work in the intermediate coupling (IC) limit;

(3) consider the transitions in isolated atoms;

(4) work in non-relativistic limit; and

(5) assume basic validity of Wentzel theory.

The significance of these assumptions will be made more precise in Chapters II and III. In Chapter II we provide a detailed development of Auger theory including energy and intensity formulae, angular momentum coupling, and the changes in the theory due to solid-state and/or molecular effects. The results of this chapter, although viewed primarily as applying to LMM transitions, are given in a form which is general enough for other transitions as well. Application of the formalism to the LMM transitions in Ti, V, Cr, Zr, Nb, and Mo are then presented in Chapter III along with a comparison to available experimental data and other theoretical predictions when pertinent. An additional comment pertaining to Chapter II is in order before closing this summary.

The general lack of agreement between experiment and theoretical results based on the Wentzel formalism suggests that the formulation itself may be in error. It is, of course, true that other explanations--notably the use of poor wave functions in the calculations--are possible. The disagreement is so widespread, however, that it is meaningful to examine the Wentzel theory. In this regard, perhaps the most striking assertion of the theory is that the Auger effect is a <u>two-electron</u> process. This is not obvious, and certainly it would not be expected <u>a priori</u>. Indeed, it can be argued that a more valid view would have the Auger dynamics arising from the coulomb interaction of all electrons in the atom rather than the two of Wentzel's treatment. Such a view of the process inevitably complicates the problem since it requires the evaluation of matrix elements between many-particle states rather than two particle states. Since the complexity of the procedure for

coupling angular momentum increases rapidly with an increase in the number of particles, the calculation becomes extremely tedious. Nevertheless, a formalism capable of treating such matrix elements has been developed, independently, by Fano[61] and Shore.[62] In order to provide a complete view of the Auger theoretical formalism, we have considered the results of Fano in some detail in Chapter II. The discussion is sufficient only to indicate the basic approach, and for a detailed calculation reference must still be to the original paper.

Finally, we present in Chapter IV our conclusions and recommendations for future Auger activity.

CHAPTER II

THEORY OF AUGER EFFECT

There are two important physical quantities of interest when studying the Auger process. For a specified initial state, these are (1) the energies of the Auger electrons arising from a particular transition, and (2) the transition probabilities for each possible Auger transition. The development of the theoretical formalism for the computation of these quantities forms the basis of this chapter. The discussion is divided into three sections with the first treating the methods of computation for the Auger energies. The principal method presented is based on a total-energy approach involving the initial and final states; the Bergstrom-Hill relation is, however, briefly considered. The second section treats the problem of computing the transition probabilities. The conventional two-electron theory of Wentzel is presented with emphasis being on selection rules and matrix element evaluation in the LS- and intermediate angular momentum coupling schemes. A more general Auger theory is also considered--one which requires the evaluation of N-electron matrix elements instead of the two-electron variety encountered in the Wentzel theory. A formalism, due to Fano[61], is presented for the computation of such matrix elements. It should be mentioned that all of the discussion in these sections assumes that the transitions occur in isolated atoms. Since much of the current interest in the Auger effect arises from transitions in molecular or solid-state

systems, the third section presents the principal changes in the formalism due to the effects of such systems.

Energies

The energy of the Auger electron is obtained directly by considering the general features of the Auger effect in conjunction with conservation of energy. Thus the de-excitation of an atom, initially singly ionized in an inner shell, by the Auger process is characterized by the transition from a well-defined initial state to a final state consisting of a doubly ionized atom plus a free (Auger) electron. By conservation of energy, the total energies of the initial and final states must be equal so that

$$E_{initial} = E_{SI} = E_{final} = E_{DI} + E_{Auger} , \tag{1}$$

where E_{SI}, E_{DI} are the total energies of the singly and doubly ionized atomic states, respectively, and E_{Auger} is the energy of the Auger electron. It follows immediately that

$$E_{Auger} = E_{SI} - E_{DI} \tag{2}$$

so that, if the total energies (E_{SI}, E_{DI}) can be determined, the Auger energy is easily obtained. Unfortunately, the determination of these energies is generally a non-trivial task involving the solution of Schrödinger's equation for the relevant atomic states. Exact solutions of this equation are possible only for hydrogen and, perhaps, the ground state of helium so that most computations of E_{SI}, E_{DI} necessarily

involve approximations. The use of (2) is further complicated by the multiple line spectra associated with Auger transitions--e.g., for a specified initial and final atomic state the Auger electron can have several different energies. It is then evident from (2) that either E_{SI} or E_{DI} (or both) must also possess a spectrum of values. Since these multiple spectra originate from angular momentum coupling effects, it is useful to examine these in some detail.

Angular Momentum States

The relationship of angular momentum to the energy of an atomic system is most easily illustrated by considering a typical atomic Hamiltonian (H). The Hamiltonian, of course, determines the energy of the system through Schrödinger's equation

$$H\Psi = E\Psi \ , \tag{3}$$

where Ψ represents the state vector or wave function of the atom and E is the corresponding total energy. It is this equation which must be solved in order to obtain the E_{SI}, E_{DI} of equation (2). The form of the Hamiltonian dictates the complexity of this problem and, in the present investigation, it is assumed that for an N-electron atom

$$H = \underbrace{\sum_{k=1}^{N} \left[(KE)_k - \frac{2Z}{r_k} \right]}_{I} + \alpha^2 \underbrace{\sum_{k=1}^{N} \xi(r_k) \underline{\ell}_k \cdot \underline{s}_k}_{II} + \underbrace{\sum_{k<j} \frac{2}{r_{kj}}}_{III} \tag{4}$$

where the separate terms are the electron kinetic (KE) and electron-nuclear potential energies (I), the spin-orbit energy (II), and the

mutual electron electrostatic energies (III)--all being expressed in Rydbergs. We now wish to examine the solutions of equation (3) using this form for H with particular emphasis on the angular momentum dependence in the solutions. Detailed consideration of the actual solution of (3) is not pertinent here, however, and for such details one should consult the general references.[63-65] In addition, the nature of the various angular momenta which enter in the solutions is rather involved so that the following discussion is confined only to general results; details are given in Appendix A.

The nature of the angular dependence in the solutions of (3) may be described by considering the relative sizes of the terms I, II, III contained in H. Four of the more important relationships between these terms will be discussed here. In the first case, the spin-orbit (II) and mutual electrostatic (III) energies are very small contributors to the total energy of the system. This case, therefore, reduces the problem to essentially a collection of hydrogen-like systems (Appendix A). As a result, the electrons are well described by the familiar one-electron labels 1s, 2s, 2p... encountered in solutions of the hydrogen atom, and the energy is then given simply by specifying the electron configuration in the atom--i.e., the occupancies of the various $n\ell$ levels. Hence in this limit each separate configuration (such as $1s^2 2s^2$ and $1s^2 2s2p$ in Be) would have only one energy level [compare with Figure 1, case (a)].

As the terms II, III increase in their contribution to the total energy, this situation changes and the energy of a given configuration "splits" into several levels. Thus if the spin-orbit term (II) remains

negligible but the electrostatic energy (III) becomes significant, then the atomic energy levels [E(L,S)] are characterized by definite values of the total orbital (L) and spin (S) angular momenta of the atom. The number of such levels is just the number of distinct (L,S) pairs which are possible, and this can be computed easily by the method of vector addition. For example, if one has a two-electron configuration $(n_1\ell_1 n_2\ell_2)$, then the total momenta L,S are constructed from the coupling

$$\begin{aligned} \underline{L} &= \underline{\ell}_1 + \underline{\ell}_2 \quad , \\ \underline{S} &= \underline{s}_1 + \underline{s}_2 \quad ; \end{aligned} \tag{5}$$

and then the possible L,S values are constrained to the limits

$$\begin{aligned} |\underline{L}| &= |\ell_1 - \ell_2|,\ |\ell_1 - \ell_2| + 1, \ldots,\ \ell_1 + \ell_2 \\ |\underline{S}| &= |s_1 - s_2|,\ |s_1 - s_2| + 1, \ldots,\ s_1 + s_2 \quad . \end{aligned} \tag{6}$$

Since individual electrons have spin ½, it follows from (6) that S = 0,1 for any two-electron configuration considered. For configurations of three or more electrons this same procedure can be applied successively to yield the L,S values and hence the number of energy levels in this LS- (or Russell-Saunders)[66] coupling scheme. A word of caution is required if the electrons are equivalent $(n_1\ell_1 \equiv n_2\ell_2)$ for in this case the Pauli exclusion principle acts to forbid certain states. Indeed, for two equivalent electrons it is such that (L+S) is an even

integer. This can be illustrated for an np^2 configuration; one obtains from (6) that

$$|\underline{L}| = 0,\ 1,\ 2$$

$$|\underline{S}| = 0,\ 1$$

are the possibilities in the general case. However, the exclusion principle acts to allow only the cases

$$L = 0,\ S = 0$$

$$L = 1,\ S = 1$$

$$L = 2,\ S = 0$$

so that in the traditional spectroscopic notation $[^{(2S+1)}L]$ for LS-states, the allowed levels for a p^2 configuration are ^1S, ^1D, ^3P (the correspondence is S,P,D,F,G... $\sim$ L = 0,1,2,3,4...). It may be also observed that the <u>total</u> angular momentum of the atom may be constructed from $\underline{L}$,$\underline{S}$ by

$$\underline{J} = \underline{L} + \underline{S}$$

$$|\underline{J}| = |L-S|,\ |L-S| + 1,\ldots,\ L+S \qquad (7)$$

so that there are several different values of J for specified L,S values. In the limit of validity of LS-coupling (very small or zero spin-orbit energy), however, the energy levels of the atom are all degenerate in J [compare Figure 1, case (b)].

This degeneracy is lifted as the spin-orbit energy becomes comparable in importance with the electrostatic contribution. Thus

the Russell-Saunders levels [E(L,S)] are now each split into a set of levels--one for each J obtained from the coupling (7). As the spin-orbit term increases further, this splitting becomes so pronounced that it is no longer meaningful to designate the atomic levels by values of L,S; instead it is only the total angular momentum J which characterizes the energy states [E(J)]. The occurrence of this phenomenon then marks the onset of the intermediate coupling (IC) region. It is in this region, therefore, that the most general form of angular momentum dependence, using the Hamiltonian (4), enters the solutions of Schrödinger's equation (3). Since it is also the IC scheme which is applied to LMM Auger transitions in this investigation, a detailed consideration of IC functions is in order. For convenience, this is reserved for Appendix A; the important point required here is that the energy levels in the IC region are characterized only by the values of the total angular momentum J [compare Figure 1, case (c)].

The final coupling case is approached if the spin-orbit term (II) becomes so large that the electrostatic energy (III) is negligible. In this region, the separate energy levels again become degenerate in J with the relevant angular momenta instead being individual total angular momenta. Thus, for the two-electron configuration $(n_1\ell_1 n_2\ell_2)$, the individual orbital and spin momenta, $(\ell_1 s_1)$ and $(\ell_2 s_2)$, are coupled as

$$\begin{aligned} \underline{j}_1 &= \underline{\ell}_1 + \underline{s}_1 \\ \underline{j}_2 &= \underline{\ell}_2 + \underline{s}_2 \\ \underline{J} &= \underline{j}_1 + \underline{j}_2 \end{aligned} \qquad (8)$$

with the vector addition formulae (6) still valid. The values of j_1, j_2 then characterize the energy of the atom in analogy to the L,S characterization in Russell-Saunders coupling. This jj-coupling scheme is of interest since it has been applied extensively to Auger studies. Indeed, much of the interpretation of Auger spectra utilizes notation arising from this scheme. For example, if one states that a $L_1L_2M_3$ transition occurs, it is implicitly assumed that the jj-coupling limit is valid when describing the electron energy states in the atom. Thus from (8) one obtains for s, p, and d electrons the results

$$\begin{aligned} s(\ell = 0) &: \underline{j} = \underline{0} + \underline{\tfrac{1}{2}} \rightarrow j = \tfrac{1}{2} \quad , \\ p(\ell = 1) &: \underline{j} = \underline{1} + \underline{\tfrac{1}{2}} \rightarrow j = \tfrac{1}{2}, \ \tfrac{3}{2} \ , \\ d(\ell = 2) &: \underline{j} = \underline{2} + \underline{\tfrac{1}{2}} \rightarrow j = \tfrac{3}{2}, \ \tfrac{5}{2} \ ; \end{aligned} \tag{9}$$

and for the K, L, and M shells the notation ($n\ell_j \sim \underline{j} = \underline{\ell} + \underline{\tfrac{1}{2}}$)

$$\begin{aligned} &K_1 \sim 1s_{\frac{1}{2}}; \ L_1 \sim 2s_{\frac{1}{2}}; \ L_2 \sim 2p_{\frac{1}{2}}; \ L_3 \sim 2p_{\frac{3}{2}}; \ M_1 \sim 3s_{\frac{1}{2}} \\ &M_2 \sim 3p_{\frac{1}{2}}; \ M_3 \sim 3p_{\frac{3}{2}}; \ M_4 \sim 3d_{\frac{3}{2}}; \ M_5 \sim 3d_{\frac{5}{2}} \end{aligned} \tag{10}$$

is then introduced. The designation of a $L_1L_2M_3$ transition, therefore, asserts that the individual 2s,2p,3p levels--degenerate in the LS-limit--

are split as in (9) so that there are two 2p, two 3p (but only one 2s) levels. If this were not true, then the transitions $L_1L_2M_3$, $L_1L_3M_3$, $L_1L_2M_2$ and $L_1L_3M_2$ could not be distinguished.

In order to illustrate these ideas, the energy level diagram expected for a KLL Auger transition is presented in Figure 1 for the various coupling limits. The splitting of levels in these limits is well indicated. It is assumed that the coupling is in the almost closed shells of the final state so that the spectrum is in accordance with conventional Auger theory. The diagram is then precisely that expected for KLL transitions in a noble gas, such as argon, when the energy is computed by relation (2). For other elements, however, the level diagram is based on an approximation to be discussed later. To understand the diagram, note that there are three possible final configurations in a KLL transition--i.e.,

$$2s^o2p^6 \qquad 2s2p^5 \qquad 2s^22p^4 \tag{11}$$

In the hydrogenic limit, (a), each of these gives rise only to a single energy. As the Russell-Saunders limit is approached, these single levels each split as indicated. The ^3S, ^3D and ^1P levels of the $2s^22p^4$ configuration are forbidden by the exclusion principle in accordance with previous remarks--these levels are thus shown dotted. In addition, the ^3p level is shown crossed since it is also forbidden in the pure LS- limit due to parity restrictions--i.e., the parity of the initial singly ionized state differs from that of the ^3P final state (this

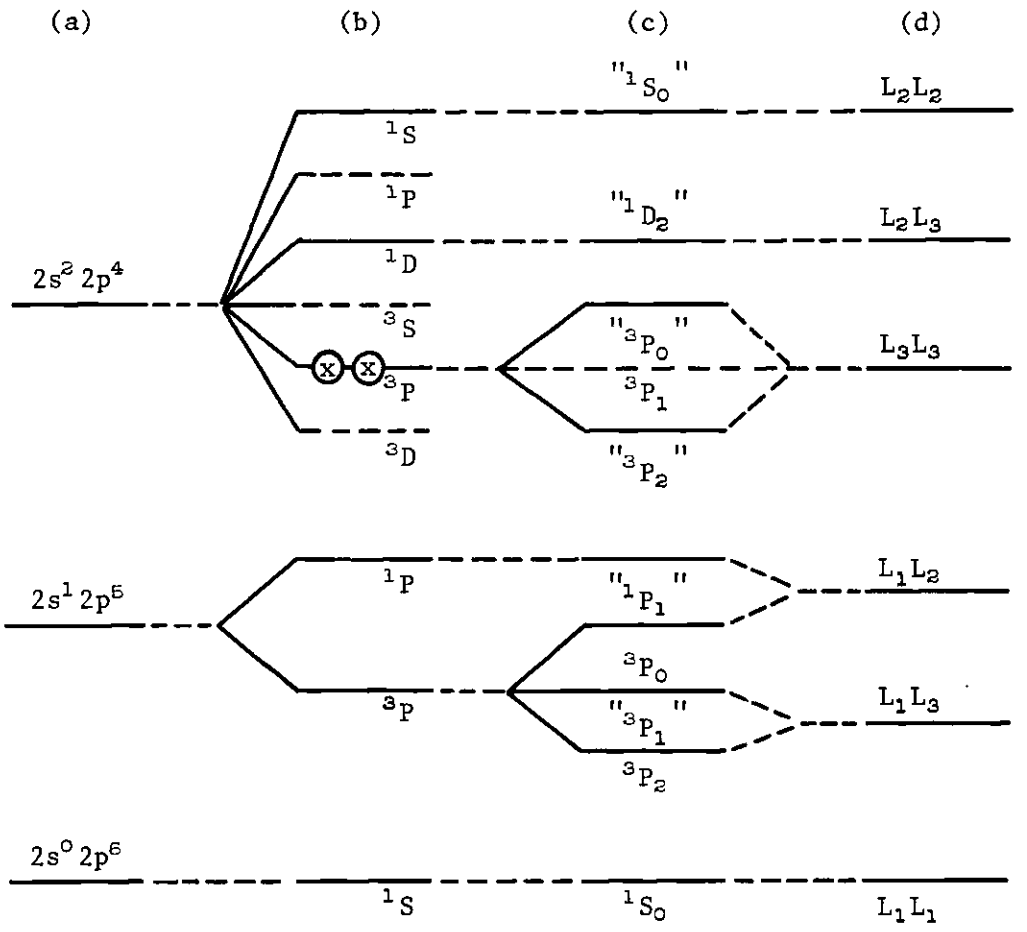

(a) Central Field Limit [I >> II, III]

(b) Russell-Saunders (LS-) Coupling Limit [I ~ III >> II]

(c) Intermediate Coupling Region [I ~ II ~ III]*

(d) jj-Coupling Limit [I ~ II >> III]

*General Notation for Auger Levels $L_1L_1(^1S_0)$, $L_1L_3(^3P_1)$, etc.

Figure 1. Schematic Energy Level Diagram for KLL Auger Transitions.

evidently depends on the dynamics assumed for the Auger process; for details consult the section on transition probabilities). By simply counting the levels in case (b), it is then evident that--if LS-coupling is the valid limit for a KLL transition--one expects a 5-line spectrum.

In the intermediate coupling (IC) region, the degeneracy in J is lifted. Note the quotation marks on some of the states. This indicates that, since J is the only identifier of the energy levels in this limit, the true (J = 0,1) states are mixtures of the pure (J = 0,1) functions obtained directly from the LS-states (or, for that matter, the jj-states). Thus in the $2s^2 2p^4$ configuration, the existence of the ^1S_o, $^1D_2$ levels means that the true (J = 0,2) states are mixtures--[^1S_o and ^3P_o] and [$^1D_2$ and $^3P_2$]--so that transitions into the original $^3P_2$, ^3P_o levels are then allowed. This follows since the levels, no longer being pure states, are not forbidden by the parity restriction (recall that transitions into ^1S_o, $^1D_2$ are allowed). It is then evident that the IC formulation predicts a 9-line KLL spectrum, a prediction that has been verified in some cases.[11,12]

The onset of jj-coupling is indicated by the coalescing of the IC levels into L_1L_1, L_2L_3, etc., with a 6-line spectrum being anticipated. For application to the LMM transitions, it is well to note that the correspondence of the jj-levels with the appropriate IC levels is different for complementary configurations (here complementary refers to configurations such as [p^2 and p^4], [d^2 and d^8], [d^4 and d^6], etc.). Thus it can be shown that for the configurations [2s2p and $2s2p^5$], [$2p^2$ and $2p^4$], one has the correspondences

$$
\begin{aligned}
&2s2p : [{}^1P_1 \text{ and } {}^3P_2] \rightarrow L_1L_3, [{}^3P_1 \text{ and } {}^3P_o] \rightarrow L_1L_2 \ , \\
&2s2p^5 : [{}^1P_1 \text{ and } {}^3P_o] \rightarrow L_1L_2, [{}^3P_1 \text{ and } {}^3P_2] \rightarrow L_1L_3 \ , \\
&2p^2 : [{}^1S_o \text{ and } {}^1D_2] \rightarrow L_3L_3, [{}^3P_2 \text{ and } {}^3P_1] \rightarrow L_2L_3, \ {}^3P_o \rightarrow L_2L_2 \ , \\
&2p^4 : [{}^1D_2 \text{ and } {}^3P_1] \rightarrow L_2L_3, [{}^3P_o \text{ and } {}^3P_2] \rightarrow L_3L_3, \ {}^1S_o \rightarrow L_2L_2 \ .
\end{aligned}
\tag{12}
$$

The importance of these differences is essentially that between a two electron and two "hole" view of the Auger process.

Before closing the discussion on angular momentum coupling, it may be noticed that the labeling of a state or level in the IC region is ambiguous since neither the LS- or jj-nomenclature is valid for these levels. For purposes of Auger transitions[10], this ambiguity is removed by the specification of both the LS- and jj-coupling limits of a particular IC level. Thus in the $2s2p^5$ level of Figure 1, one writes the four IC levels as $L_1L_2({}^1P_1)$, $L_1L_2({}^3P_o)$, $L_1L_3({}^3P_1)$ and $L_1L_3({}^3P_2)$.

This section has sought to demonstrate the significance of angular momentum coupling effects in explaining the complexity of Auger transitions; explicit attention has been given to KLL transitions. Although much detail has been relegated to Appendix A, it is hoped that this goal has been attained. In the next section, the application of these ideas to the general case of Auger energies, primarily through equation (2), is presented.

Energies for LMM Transitions

A general procedure for computing Auger electron energies can now be described. Thus it is assumed that, for a given transition, the complexity of the Auger energy spectrum is due to angular momentum coupling effects in the initial and final atomic states. By specifying the particular coupling limit (i.e., LS-, IC, or jj-), the total energies E_{SI}, E_{DI} can be computed in this scheme and by equation (2), the Auger energies then follow immediately. In outline form, the steps for this computational procedure are:

(a) decide on appropriate coupling scheme;

(b) compute initial and final state energies in this scheme;

(c) compute Auger energies by equation (2).

Since this procedure is exact in principle, it is unfortunate that it cannot be performed exactly in practice. This is, of course, due primarily to our inability to solve Schrödinger's equation, but other difficulties also exist. Since these can be significant, they are discussed below, where the computation of Auger energies for KLL and LMM transitions is considered.

The case of KLL transitions is included in order to introduce notation and to illustrate the above computational scheme. For these reasons, the present analysis for argon is carried out in some detail--argon being chosen for simplicity. It is assumed that KLL transitions in argon can be adequately treated in the LS-coupling limit with the coupling mechanism being applied to the initial and final states separately. The configurations for these states can be written down

at once. Thus the initial state is just an argon ion with a single 1s vacancy so that the configuration is

$$(SI) : 1s2s^2 2p^6 3s^2 3p^6 \quad . \tag{13}$$

The final atomic state is somewhat more complex since there are several different configurations. Indeed, the possible configurations represent an argon atom doubly ionized in the L shell so that there are the three possibilities

$$\begin{aligned} (DI) : \text{(a)}\ & 1s^2 2s^o 2p^6 3s^2 3p^6 \ , \\ \text{(b)}\ & 1s^2 2s\ 2p^5 3s^2 3p^6 \ , \\ \text{(c)}\ & 1s^2 2s^2 2p^4 3s^2 3p^6 \ . \end{aligned} \tag{14}$$

The first of these corresponds to the $(2s^2)$ transition in that both of the electrons which change states are from the 2s subshell. Similarly, the second and third configurations correspond to the (2s2p) and $(2p^2)$ transitions respectively. In order to proceed, it is now necessary to obtain the energies of these configurations in the LS-coupling formalism. This is easily done if it is recalled[63,64] that closed atomic shells (e.g., $2p^6$, $3d^{10}$, $3s^2$, etc.) behave like ^1S $(L = S = 0)$ states when coupling of angular momentum is considered. Since the coupling of a ^1S state has no effect on multiplet structure, it follows that closed subshells can be ignored when one is determining this structure for a

given configuration. Hence the multiplet of configuration (13) is simply that of a single 1s electron--viz., a ^2S state--while for the configurations (14) the multiplets are obtained from the open shells (the multiplet structure of complementary configurations are the same)

$$\begin{aligned} &\text{(a)} \quad \rightarrow 2s^o \rightarrow {}^1S \quad , \\ &\text{(b)} \quad \rightarrow 2s2p^5 \rightarrow {}^1P, {}^3P \quad , \\ &\text{(c)} \quad \rightarrow 2p^4 \rightarrow {}^1S, {}^1D, {}^3P \quad . \end{aligned} \tag{15}$$

This structure is to be compared with the previous comments on KLL transitions illustrated in Figure 1. Since the initial ^2S state is a single level, it follows from (2) and (5) that the possible Auger energies are

$$\begin{aligned} &E_{SI}({}^2S) - E_{DI}((2s^o)^1S) \quad , \\ &E_{SI}({}^2S) - E_{DI}((2s2p)^1P) \quad , \\ &E_{SI}({}^2S) - E_{DI}((2s2p)^3P) \quad , \\ &E_{SI}({}^2S) - E_{DI}((2p^4)^1S) \quad , \\ &E_{SI}({}^2S) - E_{DI}((2p^4)^1D) \quad , \\ &E_{SI}({}^2S) - E_{DI}((2p^4)^3P) \quad . \end{aligned} \tag{16}$$

Here the notation $E_{DI}((C)^1S)$ is used with (C) referring to the configuration or transition which produces the ^1S multiplet level. These equations imply a six-line KLL Auger spectrum, but a computation of the transition probabilities, in the two-electron view, indicates that the transition

$$(1s)^2S \rightarrow (2p^2)^3P$$

is forbidden by parity restrictions (compare with Figure 1 and consult discussion of transition probabilities for further details). The results obtained in (16) are thus complete, and all that is needed now is a computation of the relevant energies. The approximate method used in this work for solving this aspect of the problem is that of the Hartree-Fock approximation. Although it is possible to obtain direct evaluation of the energies (16) by this method,[67] this is not the case for the corresponding expressions in the IC limit. It is then convenient to rewrite the energies in (16) in order to facilitate application to this IC scheme.

Using the results of Slater,[63] recall that the multiplet energies arising from a given configuration can be expressed relative to the average energy of the configuration. This energy includes only those contributions to the multiplet energies which are the same for each--i.e., the kinetic energies, the electron-nuclear potential energies, and the average electrostatic interaction energies. These latter quantities are easily obtained and, for convenience, expressions for pertinent interactions (e.g., p^2,s^2,d^2,sp,sd,pd) are given in Appendix B along with a general formula for computing the average configuration energy.

It is worthwhile to note that the spin-orbit energy (term II in equation (3)) is not included in this definition of average energy. As a result, the terminology is primarily suited for application to LS-states, but it is possible to use the average energy in the IC formalism as well. The same definition of the average is used, however, in these latter cases. Now if one denotes the average energy of configuration C by

$$E_{avg}(C) \ ,$$

then the energy E_{SI} can be written as

$$\begin{aligned} E_{SI}(^2S) &\equiv E(1s2s^2 2p^6 3s^2 3p^6; {}^2S) \\ &= E_{avg}(1s2s^2 2p^6 3s^2 3p^6) + St(1s; {}^2S) \ , \end{aligned} \tag{17}$$

where St(1s) is the "structure" term which describes the departure of the multiplet energy (here the ^2S level) from the average energy. This is, of course, zero for the single electron and, in fact, the energy of any configuration with only a single unpaired electron is just the average energy.[63] Similarly, one can write

$$\begin{aligned} E_{DI}((2s^o)^1S) &= E_{avg}(1s^2 2s^o 2p^6 3s^2 3p^6) \\ E_{DI}((2s2p)^{1,3}P) &= E_{avg}(1s^2 2s2p^5 3s^2 3p^6) + St(2s2p^5({}^{1,3}P)) \\ E_{DI}((2p^4)^1S, {}^1D, {}^3P) &= E_{avg}(1s^2 2s^2 2p^4 3s^2 3p^6) + St(2p^4({}^1S, {}^1D, {}^3P)) \end{aligned} \tag{18}$$

so that now it is only necessary to obtain the expressions for the

various structure energies. In terms of the traditional electrostatic integrals $F^k(ab)$ and $G^k(ab)$ defined in Appendix B, these are just

$$
\begin{aligned}
St(2s2p^5(^3P)) &= -\frac{1}{6}\ G^1(2s2p) = St(2s2p(^3P)) \\
St(2s2p^5(^1P)) &= +\frac{1}{2}\ G^1(2s2p) = St(2s2p(^1P)) \\
St(2p^4(^1S)) &= +\frac{12}{25}\ F^2(2p2p) = St(2p^2(^1S)) \\
St(2p^4(^1D)) &= +\frac{3}{25}\ F^2(2p2p) = St(2p^2(^1D)) \\
St(2p^4(^3P)) &= -\frac{3}{25}\ F^2(2p2p) = St(2p^2(^3P))
\end{aligned}
\tag{19}
$$

where the structure terms for the complementary configurations are also included. It is to be emphasized that these expressions are valid only if the average interaction energies of $2s2p^5$, $2p^4$, $2s^2p$ and $2p^2$ are included in the expression for E_{avg}; this is to be understood in all future work as well. The energies for KLL transitions in argon can now be expressed in terms of the average energies by combining (16), (17), (18), and (19) with the result being

$$
\begin{aligned}
E_{Auger}((2s^o)^1S) &= E_{avg}(1s) - E_{avg}(2s^o) \\
E_{Auger}((2s2p)^1P) &= [E_{avg}(1s) - E_{avg}(2s2p)] - \frac{1}{2}\ G^1(2s2p) \\
E_{Auger}((2s2p)^3P) &= [\qquad\qquad\qquad\quad] + \frac{1}{6}\ G^1(2s2p) \\
E_{Auger}((2p^4)^1S) &= [E_{avg}(1s) - E_{avg}(2p^4)\ ] - \frac{12}{25}\ F^2(2p2p) \\
E_{Auger}((2p^4)^1D) &= [\qquad\qquad\qquad\quad] - \frac{3}{25}\ F^2(2p2p) \\
E_{Auger}((2p^4)^3P) &= [\qquad\qquad\qquad\quad] + \frac{3}{25}\ F^2(2p2p)
\end{aligned}
\tag{20}
$$

where the notation

$$
\begin{aligned}
E_{avg}(1s) &\equiv E_{avg}(1s2s^2 2p^6 3s^2 3p^6) \\
E_{avg}(2s^o) &\equiv E_{avg}(1s^2 2s^o 2p^6 3s^2 3p^6) \\
E_{avg}(2s2p) &\equiv E_{avg}(1s^2 2s2p^5 3s^2 3p^6) \\
E_{avg}(2p^4) &\equiv E_{avg}(1s^2 2s^2 2p^4 3s^2 3p^6)
\end{aligned}
\tag{21}
$$

is utilized. It is only necessary now to obtain by some means, such as the Hartree-Fock approximation, the relevant average energies and the indicated electrostatic integrals; the KLL Auger energies then follow from (20).

Before proceeding to develop similar results for LMM transitions, there remains one point of interest. Thus the spectrum obtained above for the KLL transitions agrees with that exhibited in Figure 1 which, in turn, is that obtained by the conventional two-electron theory of the Auger process. This agreement is unfortunately fortuitous since, in general, computation of spectra on the basis of the initial and final state configurations will <u>not</u> agree with the <u>two-electron</u> coupling predictions. In order to see this, consider the configurations for KLL transitions in potassium--they are

$$
\begin{aligned}
(SI) &: 1s2s^2 2p^6 3s^2 3p^6 4s \\
(DI) &: 1s^2 2s^0 2p^6 3s^2 3p^6 4s \\
&\quad 1s^2 2s2p^5 3s^2 3p^6 4s \\
&\quad 1s^2 2s^2 2p^4 3s^2 3p^6 4s \ .
\end{aligned}
\tag{22}
$$

The uncoupled 4s electron prevents, in each case, the spectra obtained with these configurations from being the same as that for the argon configurations in (13) and (14). As an example, note that the initial state (SI) is a ^2S for argon while for potassium it can be either a ^1S or ^3S (obtained from coupling the 1s, 4s electrons). Results similar to this are, of course, obtained for other than KLL transitions; the only requirement is the existence of an open shell(s). If it is desired that the Auger spectrum be that predicted via the conventional two-electron theory, it then follows from these remarks that some type of approximation is necessary when the total energy approach is used to compute E_{Auger}. Such approximations have been considered in this work and are discussed below where the expressions for the LMM transition energies are derived.

This derivation will be carried out in the formalism of intermediate coupling thus insuring that the results represent the most general treatment for LMM transitions. In order to understand the computations, it is necessary to consider the form of the energy problem in the IC limit. The wave function can be expressed in terms of linear combinations of LS-states (see Appendix A); denoting by $|LSJM\rangle$ these latter functions and by $\Psi_K(JM)$ the IC function, one finds

$$\Psi_K(JM) = \sum_{L,S}^{N} C_K(LSJ)\,|LSJM\rangle \ , \tag{23}$$

where the sum is over all the L,S pairs such that

$$\underline{L} + \underline{S} = \underline{J} \ ,$$

N is the number of such pairs, and $C_K(LSJ)$ are expansion coefficients. The energy problem then is given by Schrödinger's equation (3), i.e.,

$$H\Psi_K(JM) = E(J)\Psi_K(JM) \tag{24}$$

or from (23)

$$\sum_{L,S}^{N} C_K(LSJ)H|LSJM\rangle = E(J) \sum_{L,S}^{N} C_K(LSJ)|LSJM\rangle \quad . \tag{25}$$

The LS-functions satisfy the orthonormality properties

$$\langle L'S'J'M'|LSJM\rangle = \delta_{L'L}\delta_{S'S}\delta_{J'J}\delta_{M'M} \tag{26}$$

where $\delta_{L'L}\delta_{S'S}$ are the ordinary Kronecker deltas. It follows that by premultiplying (25) by the function $|L'S'JM\rangle$ and integrating over all coordinates one obtains

$$\sum_{L,S}^{N} C_K(LSJ)\langle L'S'JM|H|LSJM\rangle = E(J)C_K(L'S'J) \tag{27}$$

which can be written in the form

$$\sum_{L,S}^{N} C_K(LSJ)[\langle L'S'JM|H|LSJM\rangle - E(J)\delta_{L'L}\delta_{S'S}] = 0 \quad . \tag{28}$$

Since it is assumed that L', S' are one of N pairs which couple to give J, it is evident that (28) constitutes a system of linear equations in

the expansion coefficients $C_K(LSJ)$. For non-trivial solutions of these quantities, the form of (28) then requires that the energies E(J) must satisfy an NxN secular equation. This is easily illustrated for the particular case where N is two so that there exist two (L,S) pairs, say L_1S_1 and L_2S_2, which can couple to give a specified J. Since in (28) $L'S'$ can be either L_1S_1 or L_2S_2, one obtains at once the set of equations

$$C_K(L_1S_1J)\left[\langle L_1S_1JM|H|L_1S_1JM\rangle - E(J)\right] + C_K(L_2S_2J)\langle L_1S_1JM|H|L_2S_2JM\rangle = 0$$

$$C_K(L_1S_1J)\langle L_2S_2JM|H|L_1S_1JM\rangle + C_K(L_2S_2J)\left[\langle L_2S_2JM|H|L_2S_2JM\rangle - E(J)\right] = 0 \ . \tag{29}$$

If the solutions $C_K(L_1S_1J)$, $C_K(L_2S_2J)$ for this system are to be non-trivial, the determinant of the coefficient matrix must vanish (Cramer's rule). Hence the requirement is

$$\det \begin{bmatrix} \langle L_1S_1JM|H|L_1S_1JM\rangle - E(J) & \langle L_1S_1JM|H|L_2S_2JM\rangle \\ \langle L_2S_2JM|H|L_1S_1JM\rangle & \langle L_2S_2JM|H|L_2S_2JM\rangle - E(J) \end{bmatrix} = 0 \tag{30}$$

which is then the 2x2 secular equation obtained from (28); the analogous NxN equation for N values greater than two follows in the same fashion. Now when a secular equation of order N is solved, there will be N solutions (or energies, E(J)) obtained. The K subscript in $C_K(LSJ)$ is then used to distinguish the solutions $\Psi_K(JM)$ which correspond to

these different energy values. To complete this discussion, the procedure for obtaining $C_K(LSJ)$, once the energies are known, should be mentioned. This, however, is primarily a mathematical exercise and not necessary for the present development; it may be found in Appendix D.

The above formalism will now be used to obtain the Auger electron energies for LMM transitions. In order to demonstrate the two different approximations which are introduced, the analysis will be carried out by using vanadium (V) and zirconium (Zr) as specific examples. To begin, note that there are two possible initial states for an LMM transition as compared with one for KLL transitions. This situation corresponds to the possibility that the initial state vacancy can be in either the 2s or 2p subshells. Since the ground state configurations of V and Zr are assumed to be

$$\begin{aligned} \text{V} &: 1s^2 2s^2 2p^6 3s^2 3p^6 3d^3 4s^2 \\ \text{Zr} &: 1s^2 2s^2 2p^6 3s^2 3p^6 3d^{10} 4s^2 4p^6 4d^2 5s^2 \end{aligned} \tag{31}$$

one finds that the initial state configurations are

$$\begin{aligned} \text{V} &: [\text{I}] \quad 1s^2 2s 2p^6 3s^2 3p^6 3d^3 4s^2 \\ &\quad [\text{II}] \quad 1s^2 2s^2 2p^5 3s^2 3p^6 3d^3 4s^2 \\ \text{Zr} &: [\text{I}] \quad 1s^2 2s 2p^6 3s^2 3p^6 3d^{10} 4s^2 4p^6 4d^2 5s^2 \\ &\quad [\text{II}] \quad 1s^2 2s^2 2p^5 3s^2 3p^6 3d^{10} 4s^2 4p^6 4d^2 5s^2 \quad . \end{aligned} \tag{32}$$

From these, one obtains the final state configurations of vanadium as

$$
\begin{aligned}
V : \ &(a)\ 1s^2 2s^2 2p^6 3s^o 3p^6 3d^3 4s^2 \\
&(b)\qquad 3s\ 3p^5 3d^3 \\
&(c)\qquad 3s\ 3p^6 3d^2 \\
&(d)\qquad 3s^2 3p^4 3d^3 \\
&(e)\qquad 3s^2 3p^5 3d^2 \\
&(f)\qquad 3s^2 3p^6 3d
\end{aligned}
\tag{33}
$$

while for zirconium

$$
\begin{aligned}
Zr : \ &(a)\ 1s^2 2s^2 2p^6 3s^o 3p^6 3d^{10} 4s^2 4p^6 4d^2 5s^2 \\
&(b)\qquad 3s\ 3p^5 3d^{10} \\
&(c)\qquad 3s\ 3p^6 3d^9 \\
&(d)\qquad 3s^2 3p^4 3d^{10} \\
&(e)\qquad 3s^2 3p^5 3d^9 \\
&(f)\qquad 3s^2 3p^6 3d^8 \ .
\end{aligned}
\tag{34}
$$

As discussed previously, the existence of the open 3d and 4d shells in these elements leads to difficulties if the Auger spectrum obtained by (2) is to agree with the traditional two electron predictions. These latter predictions are fairly well established experimentally and, therefore, it is assumed that our computations should generate similar spectra. This result can be accomplished by either of two approaches which will now be explained.

Direct Approach. To begin, consider the initial state [I] of zirconium. If one does the problem exactly, the coupling of the 2s

electron with the open 4d shell electrons should be taken into account. This would, of course, introduce a splitting of the single 2s energy level into several levels. But the 4d electrons are screened from the 2s electron by six closed shells, which weakens the 2s4d coupling. As a result, the splitting introduced by the coupling will be extremely small--too small to be observed experimentally--so that it is a good approximation to treat the open 4d subshell in an average way. One way to accomplish this is to include the 4d electrons only through their contribution to the average energy of the configuration, structure effects due to coupling being explicitly ignored. This then gives the initial state configuration (Zr[I]) the same multiplet structure as an analogous configuration with either an empty or completely filled 4d shell--i.e., the structure corresponding to a single 2s vacancy. Thus one has in this approximation

$$\begin{aligned} E([I]) &= E(1s^2 2s 2p^6 3s^2 3p^6 3d^{10} 4s^2 4p^6 4d^2 5s^2) \\ &\simeq E_{avg}([I]) + St(2s) \end{aligned} \tag{35}$$

with the analogous results for the other configurations being

$$\begin{aligned} E([II]) &\simeq E_{avg}([II]) + St(2p^5) \\ E([a]) &\simeq E_{avg}([a]) + St(3s^o) \\ E([b]) &\simeq E_{avg}([b]) + St(3s3p^5) \\ E([c]) &\simeq E_{avg}([c]) + St(3s3d^9) \\ E([d]) &\simeq E_{avg}([d]) + St(3p^4) \\ E([e]) &\simeq E_{avg}([e]) + St(3p^5 3d^9) \\ E([f]) &\simeq E_{avg}([f]) + St(3d^8) \quad . \end{aligned} \tag{36}$$

The spectrum obtained in this approximation is then clearly the same as that encountered in the conventional two electron formalism; this is true since the complementary configurations

$$[3s^{o} - 3s^{2}],[3s3p^{5} - 3s3p],[3s3d^{9} - 3s3d],[3p^{5}3d^{9} - 3p3d]$$

$$[3d^{8} - 3d^{2}]$$

have the same multiplet structure (e.g., 3s3p and $3s3p^{5}$ both have the LS- multiplets $^{1}P,^{3}P$). Hence the above approximation does yield the desired result. It is evident, in fact, that it will always do so unless the open shell(s) happens to be directly involved in the Auger transition. This occurs for the 3d transition metals when LMM transitions are involved. Vanadium provides an excellent example of the problems encountered, and it will now be examined.

In a cursory glance at the vanadium configurations in (31) and (33), one may conclude that the method discussed above is applicable. This is incorrect, however, as is evident when an application is actually tried. Thus in the two vanadium initial states and the final configurations [a,b,d], it is necessary that the open 3d shell be treated in an average way as in the zirconium case. This will then give the appropriate two-electron spectrum. In those final states arising from transitions which directly involve the 3d subshell, however, it is not possible to carry through the approximation. In order to illustrate this difficulty, consider final state (c) of (33)--i.e.,

$$1s^2 2s^2 2p^6 3s 3p^6 3d^2 4s^2 \quad . \tag{37}$$

This final state corresponds to a transition in which the initial 2s (or 2p) vacancy is filled by a 3s electron with the Auger electron arising from the 3d subshell (or vice-versa). Hence one can designate this as the 3s3d configuration and, on the basis of two-electron theory, it is then expected that the Auger spectrum will be that arising from a 3s3d coupling. In order to get such a spectrum from (37), part of the 3d subshell must be ignored while the other is not, clearly a confusing way to proceed. The problem is made even more obvious if the $3d^2$configuration

$$1s^2 2s^2 2p^6 3s^2 3p^6 3d\ 4s^2 \tag{38}$$

is considered. In this case, the spectrum anticipated is that of a $3d^2$ coupling and there is no way that such a spectrum can be achieved from the single 3d electron in (38). It is then evident from these observations that application of the first method introduced is incorrect for elements in which the transition considered is from an open shell. In these cases the method is, at best, inconsistent and can, in cases such as (38), be completely inapplicable. It was for this reason that the alternate spectator approximation was developed.

Spectator Approach. Consider the configurations of vanadium which correspond to the 3s3d transition filling an initial 2s vacancy--i.e.,

$$\begin{aligned} \text{(initial)} &: 1s^2 2s\ 2p^6 3s^2 3p^6 3d^3 4s^2 \\ \text{(final)} &: 1s^2 2s^2 2p^6 3s\ 3p^6 3d^2 4s^2 \end{aligned} \tag{39}$$

where it is understood that the complete final state also includes the Auger electron. By comparing the occupation numbers of the various subshells in these two configurations, one finds that the only changes are in the (2s, 3d, 3d) subshells. All electrons in other subshells apparently remain passive to the transition--i.e., they seem to behave as spectators.* The (2s, 3s, 3d) shells also contain spectators; for example, the 2s subshell contains at least one electron in both configurations which qualifies it as a spectator. Similarly, one finds a single 3s and two 3d electron spectators. It follows that a spectator configuration can be specified from the configurations (39) and it is

$$Sp \sim 1s^2 2s 2p^6 3s\ 3p^6 3d^2 4s^2 \quad . \tag{40}$$

The fundamental assumption of the spectator approach is that this configuration behaves like a ^1S state--i.e., like a collection of closed shells. If this is true, then one can separate the spectator state, $|Sp(^1S)\rangle$, from the complete configurations (39) and obtain the initial and final states as

$$\begin{aligned} &\text{(initial)} : |Sp(^1S);\ 3s3d(^{2S+1}L_J)\rangle \\ &\text{(final)} \quad : |Sp(^1S);\ 2s(^2S_{\frac{1}{2}})\rangle \quad . \end{aligned} \tag{41}$$

---

*A justification for this view can be found from consideration of the coulomb matrix element

$$\langle i|1/r_{12}|f\rangle$$

where $|i\rangle$, $|f\rangle$ are given in (39)--see section on transition probabilities, Fano formalism, for details (equation (120)).

The energies of these states can be computed, and it is clear that the only structure will arise from the non-spectator electrons. Indeed, one obtains

$$\begin{aligned} E(\text{initial}) &\simeq E(Sp(^1S);3s3d(^{2S+1}L_J)) \\ &= E_{avg}(Sp(^1S);3s3d) + St(3s3d(^{2S+1}L_J)) \end{aligned} \tag{42}$$

$$\begin{aligned} E(\text{final}) &\simeq E(Sp(^1S);2s(^2S_{\frac{1}{2}})) \\ &= E_{avg}(Sp(^1S);2s) + St(2s(^2S_{\frac{1}{2}})) \end{aligned}$$

where the notation assumes that E_{avg} contains the average electrostatic energies not only of the spectator configuration but of (1) the interaction of 3s3d with this configuration and (2) the interaction of the 3s3d electrons as well. Note that the spin orbit energies are specifically excluded from E_{avg} so that these are still included in the structure term exactly as they are computed. The use of this type of notation insures that the structure terms are identical with those obtained for a two-electron configuration. Thus if one has a 3s3d configuration and writes the energy as

$$E(3s3d(^{2S+1}L_J)) = E_{avg}(3s3d) + St(3s3d(^{2S+1}L_J)) \ , \tag{43}$$

then the structure terms in (42) and (43) are identical. The above notation for E_{avg} also allows a simplification in computing the relative average energies in (42). Since it is true that

$$E_{avg}(Sp(^1S);2s) = E_{avg}(1s^2 2s 2p^6 3s 3p^6 3d^2 4s^2;2s)$$

$$= E_{avg}(1s^2 2s^2 2p^6 3s 3p^6 3d^2 4s^2) \qquad (44)$$

$$= E_{avg}(\text{final})$$

and similarly

$$E_{avg}(Sp(^1S);3s3d) = E_{avg}(\text{initial}) \ , \qquad (45)$$

it follows that (42) can be written as

$$E(\text{initial}) \simeq E_{avg}(\text{initial}) + St(3s3d(^{2S+1}L_J))$$

$$E(\text{final}) \simeq E_{avg}(\text{final}) \qquad (46)$$

where the fact that

$$St(2s) = 0 \qquad (47)$$

is used. These expressions for the energies are analogous to those obtained by the direct approach in (35) and (36) so that a comparison of the two methods--direct and spectator--can be easily carried out. Before doing this, it should be noted that the forms obtained in (35), (36), and (46) are general. Thus the same results are obtained in (35) and (36), for any element, such as zirconium, with <u>closed</u> M subshells when treated by the direct approach. Similarly, the spectator approach leads to expressions like (46) regardless of the transition or element involved.

Both of these approximations then lead to a two-electron type spectrum. We now wish to examine how the predictions of the Auger energies vary, if at all, in the two methods. For this purpose, the discussion will again be confined to the case of 3s3d transitions but only zirconium will be considered. In analogy with the results of (46), it can be shown that the spectator approach applied to zirconium yields

$$\begin{aligned} E(\text{initial}) &\simeq E_{avg}(\text{initial}) + St(3s3d(^{2S+1}L_J)) \\ E(\text{final}) &\simeq E_{avg}(\text{final}) \end{aligned} \tag{48}$$

where (initial, final) refer to the configurations [Zr(I)] in (32) and [Zr(c)] respectively. But, from (35) and (36), the direct approach gives

$$\begin{aligned} E(\text{initial}) &\simeq E_{avg}(\text{initial}) \\ E(\text{final}) &\simeq E_{avg}(\text{final}) + St(3s3d^9(^{2S+1}L_J)) \end{aligned} \tag{49}$$

where (47) is used. If one now uses (2) to compute the Auger energy, the two approaches give

$$\begin{aligned} (\text{Direct}) &: E_{Auger}(^{2S+1}L_J) = E_{avg}(\text{initial}) - E_{avg}(\text{final}) \\ &\quad -St\ (3s3d^9(^{2S+1}L_J)) \\ (\text{Spectator}) &: E_{Auger}(^{2S+1}L_J) = E_{avg}(\text{initial}) - E_{avg}(\text{final}) \\ &\quad +St(3s3d(^{2S+1}L_J)) \end{aligned} \tag{50}$$

which are remarkably similar in appearance. There are two distinct differences, however, which must be mentioned. The most obvious of these is the difference in sign (±) with which the structure terms contribute to the Auger energy. The minus sign in the direct case is expected since this is the result for an LMM transition in an element such as krypton (Kr) where no approximation is required. Indeed, this sign will prefix the structure term for any transition if the element involved is a noble gas. These facts suggest that the expression obtained by the spectator approach should also contain a minus sign on the structure term in order to achieve the most accurate predictions. One can examine this question in detail, however, only by considering the differences of the structure term expressions. For this purpose, recall that these terms arise from two sources--the coulomb interaction between electrons and the spin-orbit interaction (compare (3)). The convention adopted for E_{avg}, however, insures that the structure arising from the coulomb interaction is identical for complementary configurations. Thus, if one ignores the spin-orbit interaction temporarily, it is easily shown that

$$E(3s3d(^{2S+1}L_J)) = E_{avg}(3s3d) + St(3s3d(^{2S+1}L_J))$$

and (51)

$$E(3s3d^9(^{2S+1}L_J)) = E_{avg}(3s3d^9) + St(3s3d(^{2S+1}L_J))$$

in analogy with the results given in (19). It follows that the structure terms in (50) can be divided into an electrostatic (E_{EL}) and a spin-orbit

(E_{SO}) portion with the former being the same in each case. One has

$$\begin{aligned} St(3s3d(^{2S+1}L_J)) &= E_{EL}(3s3d(^{2S+1}L_J)) + E_{SO}(3s3d(^{2S+1}L_J)) \\ St(3s3d^9(^{2S+1}L_J)) &= E_{EL}(3s3d(^{2S+1}L_J)) + E_{SO}(3s3d^9(^{2S+1}L_J)) \end{aligned} \tag{52}$$

so that the difference in the predictions of the direct and spectator approaches is, by (50) and (52), just

$$\begin{aligned} &E_{EL}(3s3d(^{2S+1}L_J))(q+1) + [qE_{SO}(3s3d(^{2S+1}L_J)) + \\ &E_{SO}(3s3d^9(^{2S+1}L_J)) \end{aligned} \tag{53}$$

where q is ($\pm$ 1) according as the sign on the structure term in the spectator approach is positive or negative. This is inserted in order to check the discrepancies between the two approaches. It is evident that a minimum difference in the predictions is obtained for a minus sign since then

$$[\text{Spectator-Direct}] = E_{SO}(3s3d^9(^{2S+1}L_J)) - E_{SO}(3s3d(^{2S+1}L_J)) \ . \tag{54}$$

Hence if agreement between the two approximations is desired, it follows that the structure term sign in the spectator result of (50) should be changed to a minus. Since the direct approach is considered to be the

most accurate, our future applications of the spectator approach will, therefore, use a minus sign in the structure terms. For generality in the present discussion, however, the sign will be left somewhat arbitrary with q inserted instead; for example, one would write

$$E(Sp(^1S);3s3d(^{2S+1}L_J)) = E_{avg}(\text{initial}) + qSt(3s3d(^{2S+1}L_J))$$

in place of (42).

In summary of this discussion, two approximation methods have been developed which predict a two-electron spectrum while using the total energy expression (2). These methods are presented in schematic form in Figures 2 and 3. Note once again that the applicability of the direct approach (Figure 2) is to be confined to transitions from closed shells or subshells. If transitions from open shells are involved, such as the LMM transitions in 3d transition metals, then the spectator approach should be used. The important point of each method is, of course, the two-electron type spectrum. As a consequence, only two-electron matrix elements need be considered when obtaining the Auger energies through the equations (29) and (30). The first item we need in order to obtain the LMM energies is, therefore, the possible two-electron configurations resulting from these transitions. These are obtained from (35) and (36) for the direct approach and the spectator configurations are then the complements of these--i.e., one has

$$\begin{aligned} \text{Direct} &: 3s^o,\ 3s3p^5,\ 3s3d^9,\ 3p^53d^9,\ 3p^4,\ 3d^8 \\ \text{Spectator} &: 3s^2,\ 3s3p,\ 3s3d,\ 3p3d,\ 3p^2,\ 3d^2 \end{aligned} \tag{55}$$

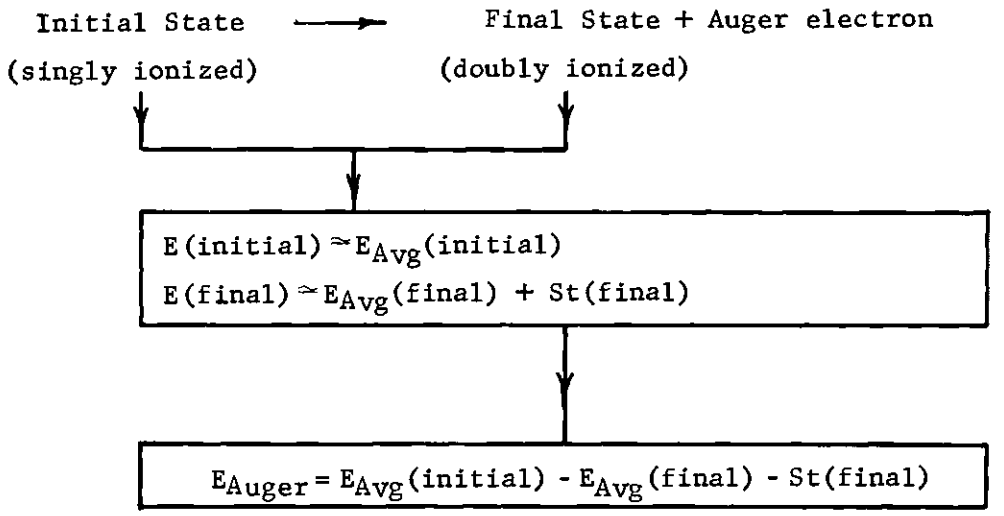

Figure 2. Direct Computation of Auger Energy: Block Diagram

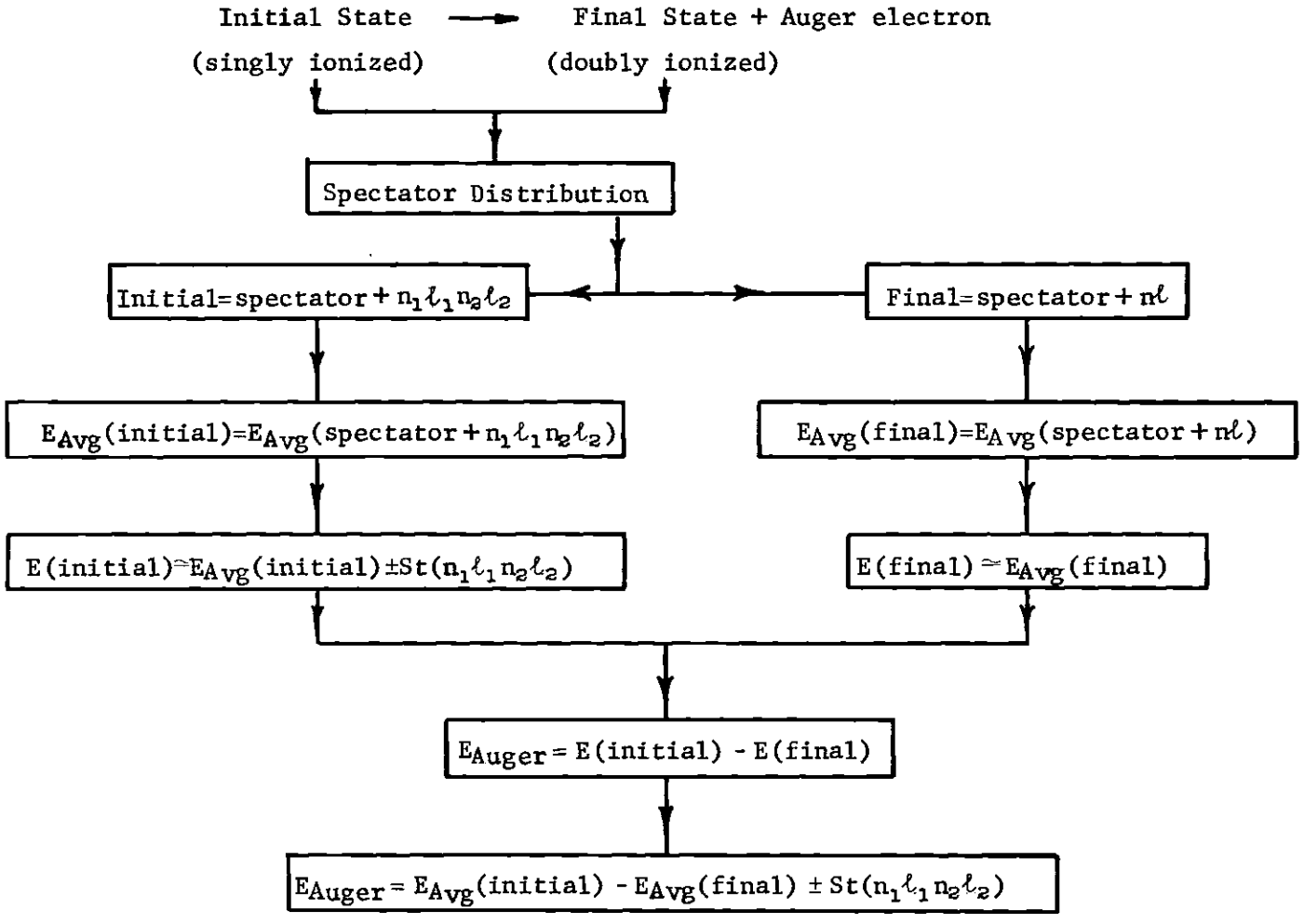

Figure 3. Computation of Auger Energy by Spectator Approach: Block Diagram

and the multiplets obtained for these configurations using the vector addition formulae of (6) and the notation $(^{2S+1}L_J)$, are then given by

$$
\begin{aligned}
&(3s^o, 3s^2) && : {}^1S_0 \\
&(3s3p^5, 3s3p) && : {}^1P_1;\ {}^3P_{0,1,2} \\
&(3s3d^9, 3s3d) && : {}^1D_2;\ {}^3D_{1,2,3} \\
&(3p^5 3d^9, 3p3d) && : {}^1P_1;\ {}^3P_{0,1,2};\ {}^1D_2;\ {}^3D_{1,2,3};\ {}^1F_3;\ {}^3F_{2,3,4} \\
&(3p^4, 3p^2) && : {}^1S_0;\ {}^1D_2;\ {}^3P_{0,1,2} \\
&(3d^8, 3d^2) && : {}^1S_0;\ {}^1D_2;\ {}^1G_4;\ {}^3P_{0,1,2};\ {}^3F_{2,3,4} \ .
\end{aligned}
\tag{56}
$$

These will now be utilized in the IC formalism presented in equations (23) - (30) to obtain the LMM energies. Note that there are 35 states defined here so that with the two initial states, one expects a 70-line Auger spectrum in the IC limit. Due to the relationship of complementary configurations and our convention for the average energies, it is sufficient to examine only the configurations encountered in the spectator approach. The Hamiltonian used in computing the LMM energies can, therefore, be confined to that of only two electrons; all effects for other electrons are automatically included in the average energy. In this respect, it is also to be noted that the average energy of the two-electron configurations need not be written down since it is also included in the average energy of the system. For example, if the energy of the $|3p3d(^3P_0)\rangle$ state is needed, it will be written as (spin-orbit interaction not included here)

$$\langle 3p3d(^3P_0)\,|H|\,3p3d(^3P_0)\rangle = E(3p3d(^3P_0)) = \frac{1}{5}\,F^2(3p3d) - \frac{105}{490}\,G^3(3p3d) \quad (57)$$

rather than

$$E_{avg}(3p3d) + \frac{1}{5}\,F^2(3p3d) - \frac{105}{490}\,G^3(3p3d) \quad .$$

As regards the actual expressions for the energies, these will not be explicitly computed here. Instead, the electrostatic energies are obtained from the results of Slater[63] while the spin-orbit energies are from the work of Condon and Shortley.[64] We can now proceed to the actual computation of the structure terms and begin by considering the order of the secular equations which one obtains by the IC formalism. Recall that this is determined by the number of (L,S) pairs which couple to give a particular J (only within a configuration since configuration interaction is not included) so that the results are

$$\begin{aligned}
&3s^2 \;:\; J=0(1x1)\\
&3s3p \;:\; J=0(1x1);\; J=1(2x2);\; J=2(1x1)\\
&3s3d \;:\; J=1(1x1);\; J=2(2x2);\; J=3(1x1)\\
&3p3d \;:\; J=0(1x1);\; J=1(3x3);\; J=2(4x4);\; J=3(3x3);\; J=4(1x1)\\
&3p^2 \;:\; J=0(2x2);\; J=1(1x1);\; J=2(2x2)\\
&3d^2 \;:\; J=0(2x2);\; J=1(1x1);\; J=2(3x3);\; J=3(1x1);\; J=4(2x2) \quad .
\end{aligned} \quad (58)$$

The solution of the secular equations is trivial for the (1x1) cases since the results are only written down; the (2x2) cases are also quite easy. The cases of the (3x3) and (4x4) equations are more tedious, however, and explicit evaluation is not attempted here. Instead, only the general framework for the problems is presented. The case of the (2x2) equation is well illustrated by the 3s3d transition; thus from (30) and (56) it is clear that the secular equation for this case is

$$\det\begin{bmatrix} E(3s3d(^1D_2)) - E(2) & \langle 3s3d(^1D_2)|H|3s3d(^3D_2)\rangle \\ \langle 3s3d(^3D_2)|H|3s3d(^1D_2)\rangle & E(3s3d(^3D_2)) - E(2) \end{bmatrix} = 0 \ . \quad (59)$$

The non-diagonal elements are easily obtained since only the spin-orbit interaction gives non-zero results. Using results from Appendix B and the work of Condon and Shortley, one then has

$$E(3s3d(^1D_2)) = \frac{3}{10} G^2(3s3d)$$

$$E(3s3d(^3D_2)) = -\frac{1}{10} G^2(3s3d) - \frac{1}{2} \xi_{3d} \quad (60)$$

$$\langle 3s3d(^1D_2)|H|3s3d(^3D_2)\rangle = \sqrt{\frac{3}{2}}\, \xi_{3d} = \langle 3s3d(^3D_2)|H|3s3d(^1D_2)\rangle$$

so that the secular equation takes the form

$$\det\begin{bmatrix} \frac{3}{10} G^2(3s3d) - E & \sqrt{\frac{3}{2}}\, \xi_{3d} \\ \sqrt{\frac{3}{2}}\, \xi_{3d} & -\frac{1}{10} G^2(3s3d) - \frac{1}{2} \xi_{3d} - E \end{bmatrix} = 0 \quad (61)$$

which gives (write $G^2(3s3d)$ as G^2)

$$(\frac{3}{10}\,G^2 - E)(-\frac{1}{10}\,G^2 - \frac{1}{2}\,\xi_{3d} - E) - \frac{3}{2}\,\xi_{3d}{}^2 = 0$$

or

$$E^2 + E(-\frac{G^2}{5} + \frac{\xi_{3d}}{2}) - (3(\frac{G^2}{10})^2 + \frac{3}{20}\,G^2\,\xi_{3d} + \frac{3}{2}\,\xi_{3d}{}^2) = 0\,. \qquad (62)$$

This is clearly a quadratic in E and the solutions are just

$$E_{\pm} = \frac{G^2(3s3d)}{10} - \frac{\xi_{3d}}{4} \pm \sqrt{(\frac{G^2}{5} + \frac{\xi_{3d}}{4})^2 + \frac{3}{2}\,\xi_{3d}{}^2} \qquad (63)$$

which gives the required IC energies. A similar analysis can be carried out for the other (2x2) secular equations which arise.

The case of a (3x3) secular equation can be illustrated by the $3d^2$ transition with the multiplets $^1D_2$, $^3P_2$, and $^3F_2$. The secular equation is

$$\det\begin{bmatrix} E(3d^2(^1D_2)) - E & \langle 3d^2(^1D_2)|H|3d^2(^3P_2)\rangle & \langle 3d^2(^1D_2)|H|3d^2(^3F_2)\rangle \\ \langle 3d^2(^3P_2)|H|3d^2(^1D_2)\rangle & E(3d^2(^3P_2)) - E & \langle 3d^2(^3P_2)|H|3d^2(^3F_2)\rangle \\ \langle 3d^2(^3F_2)|H|3d^2(^1D_2)\rangle & \langle 3d^2(^3F_2)|H|3d^2(^3P_2)\rangle & E(3d^2(^3F_2)) - E \end{bmatrix} = 0 \qquad (64)$$

but it is more convenient to write this in the form

$$\det \begin{bmatrix} B1 - E & P1 & P2 \\ P1 & B2 - E & P3 \\ P2 & P3 & B3 - E \end{bmatrix} = 0 \qquad (65)$$

where B1, B2,..., P3 are the relevant matrix elements from the first expression. This form is not only easier to write, but it also makes the nature of the secular equation more evident. Thus the equation may be reduced at once to the cubic

$$(-E)^3 + C_3(-E)^2 = C_2(-E) + C_1 = 0$$

where

$$\begin{aligned} C_3 &= B1+B2+B3 \\ C_2 &= B2\cdot B3+B1\cdot B3+B1\cdot B2-(P1)^2-(P2)^2-(P3)^2 \\ C_3 &= B1\cdot B2\cdot B3+2\cdot P1\cdot P2\cdot P3-B2\cdot(P2)^2-B1\cdot(P3)^2-B3\cdot(P1)^2 \end{aligned} \qquad (66)$$

and this may be solved in a straightforward, though tedious, fashion. The solutions for all 3x3 secular equations will, however, not be listed explicitly. Instead, it will be assumed that the equation is in the form (65) with the parameters B1, B2,..., P3 being given. For example, the $3d^2$ transition is specified by

$$\begin{aligned} B1 &= E(3d^2(^1D_2)) = -\frac{13}{441}F^2(3d3d) + \frac{50}{441}F^4(3d3d) \\ B2 &= E(3d^2(^3P_2)) = \frac{77}{441}F^2(3d3d) - \frac{70}{441}F^4(3d3d) + \xi_{3d} \\ B3 &= E(3d^2(^3F_2)) = -\frac{58}{441}F^2(3d3d) + \frac{5}{441}F^4(3d3d) - 2\xi_{3d} \\ P1 &= \frac{1}{2}\sqrt{\frac{42}{5}}\,\xi_{3d};\quad P2 = -2\sqrt{\frac{3}{5}}\,\xi_{3d};\quad P3 = 0 \quad . \end{aligned} \qquad (67)$$

A convention similar to this is established for the 4x4 secular equation. Thus the form for the 3p3d case is

$$\det \begin{bmatrix} B1 - E & \frac{3\sqrt{2}}{4} P1 & \frac{3\sqrt{3}}{4} P2 & 0 \\ \frac{3\sqrt{2}}{4} P1 & B2 - E & P3 & -\sqrt{\frac{42}{36}} P1 \\ \frac{3\sqrt{3}}{4} P2 & P3 & B3 - E & \frac{\sqrt{7}}{3} P2 \\ 0 & -\sqrt{\frac{42}{36}} P1 & \frac{\sqrt{7}}{3} P2 & B4 - E \end{bmatrix} = 0 \qquad (68)$$

and the parameters are the quantities listed in the table of energies (Table I). For completeness we note that this equation reduces to the quartic

$$(-E)^4 + D_4(-E)^3 + D_3(-E)^2 + D_2(-E) + D_1 = 0$$

where

$$\begin{aligned} D_4 &= B1+B2+B3+B4 \\ D_3 &= B1\cdot B2+B1\cdot B3+B1\cdot B4+B2\cdot B3+B2\cdot B4+ \\ &\quad B3\cdot B4 - \frac{355}{144}(P2)^2 - (P3)^2 - \frac{55}{24}(P1)^2 \\ D_2 &= B1\cdot B3\cdot B4+B2\cdot B3\cdot B4+B1\cdot B2\cdot B3+B1\cdot B2\cdot B4 \\ &\quad + \frac{25\sqrt{6}}{72} P1\cdot P2\cdot P3 - (P1)^2[7/6(B1+B3)+9/8(B3+B4)] \\ &\quad - (P2)^2[7/9(B1+B2) + \frac{27}{16}(B2+B4)] - (P3)^2(B1+B4) \end{aligned} \qquad (69)$$

$$D_1 = B1 \cdot B2 \cdot B3 \cdot B4 + P1 \cdot P2 \cdot P3\left(\frac{9\sqrt{6}}{8} B4 - \frac{7\sqrt{6}}{9} B1\right) - (P3)^2 B1 \cdot B4$$

$$- (P1)^2 (7/6\ B1 \cdot B3 + 9/8\ B3 \cdot B4) - (P2)^2 (7/9\ B1 \cdot B2 + \frac{27}{16} B2 \cdot B4)$$

$$+ \frac{175}{32} (P1)^2 (P2)^2$$

The solutions of this equation are easily obtained by computer techniques.

The intermediate coupling energies may now be written down, and this is done in Table I. As discussed above, the (1x1) and (2x2) secular equations are the only cases for which explicit solutions, in terms of the coulomb integrals and the spin-orbit parameters, are given. One more point needs to be made before these results are complete, and this concerns the energies for the configurations complementary to those in (56); these are the values needed when the direct approximation is used. As discussed previously, the electrostatic contribution is the same in the two approaches due to our convention regarding the average energies. It is, therefore, only the spin-orbit energies which one needs to consider and this has been done by Condon and Shortley.[64] They show that spin-orbit energies of complementary configurations differ only in the sign of the spin-orbit parameter(s). For example, one has

$$E_{SO}(p^2(^3P_o)) = -\xi_p \text{ and } E_{SO}(p^4(^3P_o)) = +\xi_p$$

$$E_{SO}(pd(^3F_3)) = -2\xi_d - \xi_p \text{ and } E_{SO}(p^5d^9(^3F_3)) = 2\xi_d + \xi_p \qquad (70)$$

with similar results for other configurations. It follows from this

that the only changes required in Table I in order to be applicable to the direct approach are given by the substitutions

$$\xi_p \rightarrow -\xi_p \qquad \text{and} \qquad \xi_d \rightarrow -\xi_d \tag{71}$$

whenever the parameters occur. The table of results is thereby applicable to both cases.

Bergström-Hill Relation. This section on Auger energies should not be concluded without a brief discussion of the principal method for computation now being used--i.e., the Bergström-Hill relation. To understand this relation, let V correspond to the subshell of the initial vacancy while T,S are the subshells of the final vacancies. Then if an electron from T transits to fill the V vacancy, one would expect--in the simple Bohr picture--the energy liberated to be

$$E_V(Z) - E_T(Z) \tag{72}$$

where $E_V(Z)$, $E_T(Z)$ are the electron binding energies in an atom of atomic number Z. If this energy is given to the electron in S which then exits the atom as the Auger electron, this simple view would give the Auger energy as

$$E_V(Z) - E_T(Z) - E_S(Z) \ . \tag{73}$$

Bergström and Hill[68] pointed out that this approximate view of the process could be made more precise by considering the fact that the S electron "sees" a doubly ionized atom as it exists the system. Hence the binding energy of this level would be expected to increase beyond

Table 1. Structure terms for LMM Auger Energies in Intermediate Coupling. To obtain the Auger energy, add the appropriate quantity $(E_{avg}(\text{initial})-E_{avg}(\text{final})$, obtained by the spectator (method 1) or direct (method 2) approaches, to the elements of the table. Notation is ZPM, ZDM = ξ_{3p}, ξ_{3d}(method 1) and $-\xi_{3p}$, $-\xi_{3d}$(method 2)

$3s^2\,(^1S_0)$	0
$3s3p(^3P_0)$	$-G^1(3s3p)/6 - ZPM$
$3s3p(^3P_1)$	$G^1(3s3p)/6 - ZPM/4 - \sqrt{(G^1/3-ZPM/4)^2 + \xi_{3p}^2}$
$3s3p(^1P_1)$	$G^1(3s3p)/6 - ZPM/4 + \sqrt{\quad}$
$3s3p(^3P_2)$	$-G^1(3s3p)/6 + ZPM/2$
$3s3d(^3D_1)$	$-G^2(3s3d)/10 - \frac{3}{2}\,ZDM$
$3s3d(^3D_2)$	$G^2(3s3d)/10 - ZDM/4 - \sqrt{(G^2/5+ZDM/4)^2 + \frac{3}{2}\,\xi_{3d}^2}$
$3s3d(^1D_2)$	$G^2(3s3d)/10 - ZDM/4 + \sqrt{\quad}$
$3s3d(^3D_3)$	$-G^2(3s3d)/10 + ZDM$
$3p^2\,(^3P_1)$	$-(3/25)F^2(3p3p) - ZPM/2$
$3p^2\,(^3P_0)$	$(9F^2/25 - ZPM)/2 - \frac{1}{2}\sqrt{(3F^2/5+ZPM)^2 + 8\xi_{3p}^2}$
$3p^2\,(^1S_0)$	$(9F^2/25 - ZPM)/2 + \frac{1}{2}\sqrt{\quad}$
$3p^2\,(^3P_2)$	$ZPM/4 - \frac{1}{2}\sqrt{(6F^2/25 - ZPM/2)^2 + 2\xi_{3p}^2}$
$3p^2\,(^1D_2)$	$ZPM/4 + \frac{1}{2}\sqrt{\quad}$
$3p3d(^3P_0)$	$F^2(3p3d)/5 - 105\,G^3(3p3d)/490 + (ZPM - 3\,ZDM)/2$
$3p3d(^3F_4)$	$2F^2(3p3d)/35 - G^1(3p3d)/3 + 15G^3(3p3d)/490 + ZDM + ZPM/2$

Table 1. (continued)

$3p3d(^3P_2)$	$B1 = F^2(3p3d)/5 - 3\,G^3(3p3d)/14 - (ZPM - 3ZDM)/4;$	$P1 = (ZPM + ZDM)/\sqrt{5}$
$3p3d(^1D_2)$	$B2 = -F^2(3p3d)/5 - 2G^1(3p3d)/15 + 9G^3(3p3d)/70;$	$P2 = (ZDM - ZPM)/\sqrt{5}$
$3p3d(^3D_2)$	$B3 = -F^2/5 + 4G^1/15 - 3G^3/70 - (ZPM + 5ZDM)/12;$	$P3 = \sqrt{6}(ZPM - 5ZDM)/12$
$3p3d(^3F_2)$	$B4 = 2F^2/35 - G^1/3 + 15G^3/490 - 2(ZPM + 2ZDM)/3$	
$3p3d(^1P_1)$	$B1 = F^2/5 + 2G^1/15 + 147G^3/490;$	$P1 = \sqrt{2}(ZPM + 3ZDM)/4$
$3p3d(^3P_1)$	$B2 = F^2/5 - 3G^3/14 + (ZPM - 3ZDM)/4;$	$P2 = \sqrt{6}(ZPM + ZDM)/4$
$3p3d(^3D_1)$	$B3 = -F^2/5 + 4G^1/15 - 3G^3/70 - (ZPM + 5ZDM)/4;$	$P3 = \sqrt{3}(ZDM - ZPM)/4$
$3p3d(^3D_3)$	$B1 = -F^2/5 + 4G^1/15 - 3G^3/70 + (ZPM + 5ZDM)/6;$	$P1 = (ZPM + ZDM)/\sqrt{6}$
$3p3d(^1F_3)$	$B2 = 2F^2/35 + 7G^1/15 + 27G^3/490;$	$P2 = \sqrt{2}(ZDM - ZPM)/3$
$3p3d(^3F_3)$	$B3 = 2F^2/35 - G^1/3 + 15G^3/490 - (ZPM + ZDM)/6;$	$P3 = -(2ZDM - ZPM)/\sqrt{3}$
$3d^2(^1D_2)$	$B1 = -13\,F^2(3d3d)/441 + 50F^4(3d3d)/441\ ;$	$P1 = \sqrt{21}\ ZDM/\sqrt{10}$
$3d^2(^3P_2)$	$B2 = 11\,F^2/63 - 10F^4/63 + ZDM/2\ ;$	$P2 = -2\sqrt{.6}\ ZDM$
$3d^2(^3F_2)$	$B3 = -58\,F^2/441 + 5F^4/441 - 2ZDM;$	$P3 = 0$
$3d^2(^1S_0)$	$(31F^2/63 + 10F^4/63 - ZDM)/2 + \frac{1}{2}\sqrt{(F^2/7+10F^4/21+ZDM/2)^2 - 8ZDM(F^2+10F^4/3)/7}$	
$3d^2(^3P_0)$	$(31F^2/63 + 10F^4/63 - ZDM)/2 - \frac{1}{2}\sqrt{\quad}$	
$3d^2(^3P_1)$	$11F^2/63 - 10F^4/63 - ZDM/2$	
$3d^2(^3F_3)$	$-58F^2/441 + 5F^4/441 - ZDM/2$	
$3d^2(^1G_4)$	$\frac{1}{2}(-8F^2/441 + 20F^4/441 + 3/2ZDM) + \frac{1}{2}\sqrt{(108F^2/441 + 10F^4/441 + \frac{5}{2}\ ZDM)^2 - 8ZDM(108F^2+10F^4)/441}$	
$3d^2(^3F_4)$	$(-8F^2/441 + 20F^4/441 + 3/2\,ZDM)/2 - \frac{1}{2}\sqrt{\quad}$	

the value for the neutral atom. A better approximation would be to use the binding energy of the S level for the element with next higher atomic number--i.e., Z+1--or some value in between the two values. Bergström and Hill then introduced the parameter ΔZ and write the Auger energy as

$$E_{Auger} \simeq E_V(Z) - E_T(Z) - E_S(Z) + \Delta Z[E_S(Z) - E_S(Z+1)] \tag{74}$$

where $0 \leq \Delta Z \leq 1$. With this relation, quite reasonable estimates of the Auger energy can be obtained although the accuracy varies. A comparison of the predictions of this relation with the methods described earlier will be carried out in the next chapter to illustrate the use of the relation. It should be noted that the scheme is expected to be most accurate for heavy elements, such as lead (Pb), since it is strictly valid only in the jj-coupling limit. This follows since the specification of the levels V, T, S as distinct is meaningful only in the jj-limit. The relation can be applied to LS-states if V, T, S are interpreted in an appropriate fashion but an application to intermediate coupling states is not possible. In this region, the ΔZ parameter becomes a J dependent variable thus destroying the simplicity of the relation.

Transition Probabilities

The starting point for our consideration of transition probabilities is the "golden rule" of time dependent perturbation theory.

This rule asserts that the probability for the transition of a system in state $|i\rangle$ to a final state $|f\rangle$ is given by

$$\omega_{i \rightarrow f} = \frac{2\pi}{\hbar} |\langle f|A|i\rangle|^2 \rho \qquad (75)$$

where A is an operator representing the dynamics of the transition, P is the density of states available to the system during the transition, and h is Planck's constant divided by 2π. The application of this relation to an Auger process evidently requires that the Auger dynamics (A) be known. In this section two possibilities (or views) for A are considered and, for each, the requisite formalism is developed. The simplest and conventional view, due to Wentzel, is the two-electron theory for Auger transitions.

Conventional Theory

In order to understand the nature of this theory, consider Figure 4 where a schematic level diagram for a KL_1L_2 transition is shown. Such a transition is, of course, characterized by a single 1s vacancy in the initial atomic state, a double L shell vacancy in the final atomic state, plus the Auger electron in the continuum. It is clear from this description that two electrons change states in the transition, and this suggests a possible dynamics for the process. Thus the conventional theory assumes that the transition arises from the electrostatic interaction of only those electrons directly involved in the process--i.e., those which change their states. This assumption, for KLL transitions, means that in the initial state the two L shell electrons interact and, as a result, one transits to fill the 1s

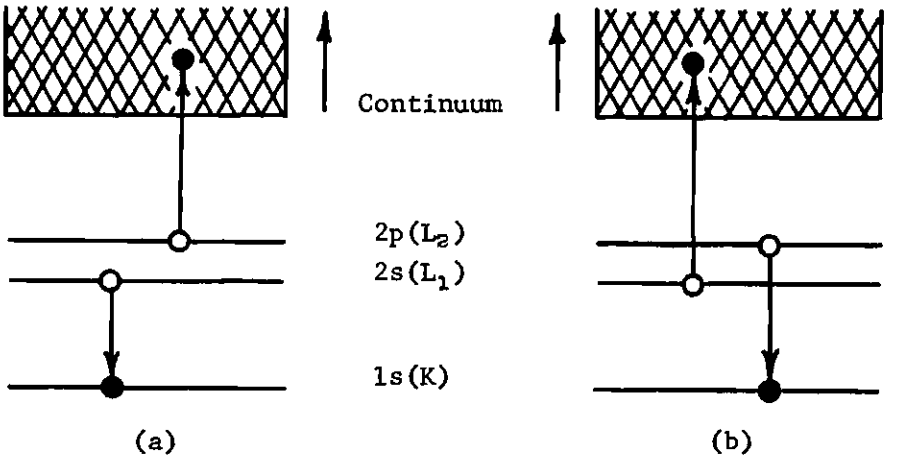

Figure 4. Schematic Diagram for the Two Electron Interaction in the Auger Process

vacancy while the other is ejected from the atom. For the final state, the interaction is between the continuum (Ek) electron, as it exits the system, with the "new" 1s electron. If the particular case of the KL_1L_2 transition is used, these comments when combined with (75) then give the pertinent transition probability as

$$\omega_{KL_1L_2} = \frac{2\pi}{\hbar} \left| \langle 1sEk \left| \frac{e^2}{r_{12}} \right| 2s2p \rangle \right|^2 \rho \qquad (76)$$

where

$$|i\rangle = |2s2p\rangle$$

$$|f\rangle = |1sEk\rangle \quad .$$

This expression indicates that the dynamics A, in the conventional theory, is just the electrostatic operator $\frac{e^2}{r_{12}}$. It is to be noted that this form is not really complete since there are two ways (see Figure 4) in which the (2s,2p) electrons can fill the 1s vacancy. Thus the 2s electron can transit to the 1s level with the 2p electron being ejected from the atom or the reverse case can occur in which the 2p electron fills the 1s level. This "exchange" case can be incorporated into (76) merely by requiring that the states by anti-symmetrized and, unless otherwise stated, this assumption will be made in all future work. The direct and exchange contributions will thus be automatically included.

In order to make the discussion more general, it is worthwhile to rewrite (76) for an arbitrary transition. Thus the initial vacancy

will be assumed to have the quantum numbers $n_i \ell_i$ while the final vacancies are in the subshells characterized by $(n_1\ell_1, n_2\ell_2)$. Then it is straightforward to show that (76) is replaced by

$$\omega = \frac{2\pi}{\hbar} \left| \langle n_i \ell_i E k \right| \frac{e^2}{r_{12}} \left| n_1 \ell_1 n_2 \ell_2 \rangle \right|^2 \rho \quad . \tag{77}$$

This may be extended still further by incorporating angular momentum coupling into the formalism. From Appendix A, one has the two electron LS-coupled function as

$$\left|(n_1\ell_1 n_2\ell_2)LSJM\right\rangle_{12} = \sum \langle L\bar{M}_L S\bar{M}_S | JM\rangle \langle \ell_1 \bar{m}_1 \ell_2 \bar{m}_2 | L\bar{M}_L \rangle * \tag{78}$$

$$\langle \tfrac{1}{2} \bar{\mu}_1 \tfrac{1}{2} \bar{\mu}_2 | S\bar{M}_S \rangle \left| n_1 \ell_1 \bar{m}_1 \bar{\mu}_1 \right\rangle_1 \left| n_2 \ell_2 \ \bar{m}_2 \bar{\mu}_2 \right\rangle_2$$

where $\langle j_1 m_1 j_2 m_2 | j_3 m_3 \rangle$ are Clebsch-Gordan coefficients and the $\left| n_j \ell_j \ m_j \mu_j \right\rangle$ are one-electron functions; the sum is over all barred quantities. The subscripts (1,2) correspond to the coordinates r_1 and r_2 respectively; if no subscripts are included, it is assumed that the function is anti-symmetrized. It then follows that, in the LS-coupling limit, the transition probabilities are given by

$$\omega_{LS} = \left(\frac{2\pi}{\hbar} \rho \right) \left| \langle (n_i' \ell_i E k) L' S' J' M' \right| e^2/r_{12} \left| (n_1' \ell_1 n_2 \ell_2) LSJM \right\rangle \right|^2 \quad . \tag{79}$$

The selection rules for an Auger transition follow at once from this relation. Thus it may be shown[69] that

$$\langle L' S' J' M' |^1/r_{12} | LSJM \rangle = \delta_{L'L} \delta_{S'S} \delta_{J'J} \delta_{M'M} \langle LSJM |^1/r_{12} | LSJM \rangle \qquad (80)$$

so that only those transitions with

$$\Delta L = \Delta S = \Delta J = 0 \qquad (81)$$

are allowed. We can, therefore, simplify (78) somewhat and write

$$\omega_{LS} = \left(\frac{2\pi}{\hbar} \rho \right) | \langle (n_i \ell_i Ek) LSJM | e^2/r_{12} | (n_1 \ell_1 n_2 \ell_2) \quad LSJM \rangle |^2 \qquad (82)$$

as the form for the Auger transition probability in the LS-limit. One further comment is necessary when $n_1 \ell_1$ is the same as $n_2 \ell_2$--i.e., the electrons are equivalent. Thus the form (82) assumes that the $|LSJM\rangle$ states are both normalized and anti-symmetrized. It may be shown from (78) that

$$|(n_1 \ell_1 n_2 \ell_2) LSJM\rangle = \frac{1}{\sqrt{2}} \left[|(n_1 \ell_1 n_2 \ell_2) LSJM\rangle_{12} + (-1)^{\ell_1 + \ell_2 - L - S} |(n_2 \ell_2 n_1 \ell_1) LSJM\rangle_{12} \right] \qquad (83)$$

and, if $n_1 \ell_1 \neq n_2 \ell_2$, this state is normalized. For equivalent electrons, however, one obtains

$$|(n_1 \ell_1)^2 LSJM\rangle = \frac{1}{\sqrt{2}} \left[1 + (-1)^{L+S} \right] |(n_1 \ell_1)^2 LSJM\rangle_{12} \qquad (84)$$

which is not normalized. To see this, note that only L,S pairings such that

$$L + S = \text{ even integer} \qquad (85)$$

are allowed and for such cases

$$\langle (n_1\ell_1)^2 LSJM | (n_1\ell_1)^2 LSJM \rangle = 2 \ . \tag{86}$$

It is then clear that for equivalent electrons, the expression (83) should be multiplied by $(1/\sqrt{2})$ in order that the function be normalied. The general anti-symmetrized two electron LS-state is then

$$|(n_1\ell_1 n_2\ell_2)LSJM\rangle = \frac{1}{\sqrt{2}}[\,|n_1\ell_1 n_2\ell_2)LSJM\rangle_{12} + (-1)^{\ell_1+\ell_2-L-S}\,|(n_2\ell_2 n_1\ell_1)LSJM\rangle_{12}\,] \tag{87}$$

where

$$\begin{aligned} C &= 1 \qquad && n_1\ell_1 \neq n_2\ell_2 \\ &= 1/\sqrt{2} && n_1\ell_1 = n_2\ell_2 \ . \end{aligned} \tag{88}$$

Now, from (82), the general matrix element of interest is

$$\langle (n_i\ell_i Ek)LSJM | e^2/r_{12} | (n_1\ell_1 n_2\ell_2)LSJM \rangle \tag{89}$$

which can be written as[69]

$$C[DIR + (-1)^{\ell_1+\ell_2-L-S}\ EXC] \ . \tag{90}$$

Here the quantities DIR, EXC are the matrix elements

$$\mathrm{DIR} = {}_{12}\langle (n_i \ell_i E k) LSJM | e^2/r_{12} | (n_1 \ell_1 n_2 \ell_2) LSJM \rangle_{12}$$

$$= \sum_{\ell} (-1)^{\ell_1 - \ell_2 + L} [\ell_i, \ell_2]^{\frac{1}{2}} \langle k0 | \ell 0 \ell_2 0 \rangle \langle \ell_1 0 | \ell 0 \ell_i 0 \rangle \begin{Bmatrix} \ell_1 & \ell_2 & L \\ k & \ell_i & \ell \end{Bmatrix} R^{\ell}(n_i \ell_i E k, n_1 \ell_1 n_2 \ell_2) \tag{91}$$

$$\mathrm{EXC} = {}_{12}\langle (n_i \ell_i E k) LSJM | e^2/r_{12} | (n_2 \ell_2 n_1 \ell_1) LSJM \rangle_{12}$$

$$= \sum_{\ell} (-1)^{\ell_2 - \ell_1 + L} [\ell_i, \ell_1]^{\frac{1}{2}} \langle k0 | \ell 0 \ell_1 0 \rangle \langle \ell_2 0 | \ell 0 \ell_i 0 \rangle \begin{Bmatrix} \ell_2 & \ell_1 & L \\ k & \ell_i & \ell \end{Bmatrix} R^{\ell}(n_i \ell_i E k, n_2 \ell_2 n_1 \ell_1) \tag{92}$$

with the notation

$$[a,b,c\ldots]^{\frac{1}{2}} = \sqrt{2a+1} \quad \sqrt{2b+1} \quad \sqrt{2c+1} \ \ldots \tag{93}$$

being used. The quantities

$$\begin{Bmatrix} a & b & e \\ d & c & f \end{Bmatrix}$$

are the 6j symbols as defined by Edmonds.[70] If follows from (89), (90), (91), (92), and (82) that the Auger transition probability in the LS-coupling limit may be written as

$$w_{LS} = \left(\frac{2\pi}{\hbar} \rho \right) \left| C[\mathrm{DIR} + (-1)^{\ell_1 + \ell_2 - L - S} \mathrm{EXC}] \right|^2 . \tag{94}$$

It remains to consider the form for the transition probability

if intermediate coupling is assumed in either the initial or final states. This is straightforward from the formal standpoint. Thus one has the IC functions

$$\Psi_B^N(JM) = \sum_{(LS)} C_B^N(LSJ) \,|(n_i \ell_i Ek) LSJM\rangle$$

$$\Psi_K^N(JM) = \sum_{(LS)} C_K^N(LSJ) \,|(n_1 \ell_1 n_2 \ell_2) LSJM\rangle \qquad (95)$$

from which the IC transition probability is

$$\omega_{IC} = \left(\frac{2\pi}{\hbar}\rho\right) |\langle \Psi_B^N(JM) | e^2/r_{12} | \Psi_K^N(JM)\rangle|^2 \ . \qquad (96)$$

This can be simplified by using (94) and (95) to obtain

$$\omega_{IC} = \left(\frac{2\pi}{\hbar}\rho\right) \left| \sum_{(LS)} C_B^N(LSJ) C_K^N(LSJ) C[DIR + (-1)^{\ell_1+\ell_2-L-S} EXC] \right|^2 \ , \qquad (97)$$

and the result is quite general. There are complications, however, which stem from the difficulty of applying the IC formalism to the continuum state as in $\Psi_B^N(JM)$. Indeed, it is not at all clear that this is meaningful since the interaction of $n_i \ell_i$ and Ek is expected to be primarily electrostatic. A better formulation of the problem is to include IC only in the interaction of the $(n_1 \ell_1, n_2 \ell_2)$ electrons and confine the $n_i \ell_i$, Ek coupling to the LS-limit. If this is done, then

one obtains the result

$$\omega = \left(\frac{2\pi}{\hbar}\sigma\right) \left|\langle n_i \ell_i Ek)LSJM\right|^{e^2}/r_{12} \sum_{(L'S')} C^N(L'S'J) \left|(n_1\ell_1 n_2\ell_2)L'S'JM\rangle\right|^2 \tag{98}$$

which, with (80) and (82), can be written as

$$\omega = \left|C^N(LSJ)\right|^2 \omega_{LS} \ . \tag{99}$$

This expression, though formally correct, is not complete due to the dependence on a particular set of L,S values. In order to understand this, recall from the section on Auger energy analysis that the structure is determined by the coupling of the $(n_1\ell_1, n_2\ell_2)$ electrons and <u>not</u> by the $n_i\ell_i$, Ek coupling. This latter interaction serves to determine if the transition is allowed through the selection rules in (81), but it does not influence the observed structure. It then follows that the intensities for a particular J value should include the contribution from all possible L,S pairings and, therefore, the appropriate expression for the transition probabilities is given by

$$W_{IC} = \sum_{(LS)} \left|C^N(LSJ)\right|^2 \omega_{LS} \tag{100}$$

where W_{IC}, rather than ω_{IC}, is used to distinguish (100) from the more general result of (96), (97). This expression is evidently dependent only on J and the C^N values so that it does represent a meaningful

quantity in comparison with the transition lines obtained by the two-electron energy analysis. Note that the above result holds since the IC functions in (95) are assumed normalized so that

$$S(NJ) = \sum_{(LS)} |C^N(LSJ)|^2 = 1 \tag{101}$$

If this is not the case, then (100) should be divided by S(NJ).[10]

Only a few more comments are necessary to complete this discussion. We first observe that the orbital angular momentum, k, carried by the Auger electron is not measured experimentally. As a result, the expressions for ω_{LS}, ω_{IC}, and/or W_{IC} must be summed over all possible values of k. This requirement is not as complicated as one might initially expect since, for a specified (L,S) pairing, it is necessary that

$$\underline{\ell}_i + \underline{k} = \underline{L}$$

which restricts k to those values such that

$$|\ell_i - L| \leq k \leq \ell_i + L \ . \tag{102}$$

Further restrictions on k arise due to the requirement that parity be conserved in the transition. Thus it may be shown[71-72] that the parity of the two-electron LS-state in (78) is given by

$$\begin{aligned} P|(n_1\ell_1 n_2\ell_2)LSJM\rangle_{12} &= |(n_1\ell_1 n_2\ell_2)LSJM\rangle_{21} \\ &= (-1)^{\ell_1+\ell_2-L}|(n_1\ell_1 n_2\ell_2)LSJM\rangle_{12} \end{aligned} \tag{103}$$

where P is the parity operator. Since the operator $(1/r_{12})$ is even under parity, it then follows from parity conservation in the matrix elements of (91), (92) that

$$(-1)^{\ell_i+k-L} = (-1)^{\ell_1+\ell_2-L}$$

or

$$(-1)^{\ell_i+k} = (-1)^{\ell_1+\ell_2} \quad . \tag{104}$$

Using the fact that $(\ell_i, k, \ell_1, \ell_2)$ are all integers this can also be written as

$$\ell_i + k = \ell_1 + \ell_2 \tag{105}$$

where the equality is modulo 2--i.e., the combinations $(\ell_i + k)$ and $(\ell_1+\ell_2)$ are both even or both odd. For any given transition, one then has that the possible k values are limited by (105) as well as (102). Finally, it must be noted that all the states involved in the transition are degenerate in the J_Z value, M. Hence it is necessary that the expressions for the transition probabilities be summed over all possible final states with the same J but different M and averaged over the initial states. This is accomplished quite easily and introduces a factor of (2J+1) into the results. Similarly, it is not possible to ascertain the particular state of the initial $n_i\ell_i$ vacancy so this must also be averaged, a procedure which introduces a factor of $\left(\frac{1}{2(2\ell_i+1)}\right)$. When these various comments are combined, the requisite relation for the computation of Auger transition probabilities, in the

conventional theory, is given by

$$W_{IC} = \sum_{k} \sum_{(LS)} \frac{(2J+1)}{2(2\ell_i+1)} \left|C^N(LSJ)\right|^2 \omega_{LS} \qquad (106)$$

with k being subject to the restrictions in (102) and (105). The approximations introduced to obtain this relation should, of course, be recalled in any application.

"Exact" Theory

Although the conventional theory described above provides a very concise picture of the Auger progess, one may well ask if the problem is not being oversimplified. This possibility is suggested by the poor agreement between experimental intensities and those predicted by conventional formulae such as (106). In addition, it is not at all clear from the principal characteristic of the Auger effect--i.e., a singly ionized initial state $|i\rangle$ de-exciting to a doubly ionized final state plus a free electron $|f;a\rangle$--that the dynamics for this transition is simply the coulomb interaction of only two electrons. Alternate possibilities to this view certainly exist and, in this section, one of the most obvious will be considered.

The dynamics in this alternate view is also provided by electrostatic interactions but not between just two electrons. Instead, the total coulomb interaction between the initial ($|i\rangle$) and final ($|f;a\rangle$) electrons is assumed to link these states. This is clearly a multi-electron view for the Auger process since, for an N-electron system, the total coulomb interaction is given by the operator

$$A = \sum_{i<j}^{N} e^2/r_{ij} = \sum_{i<j}^{N} g_{ij} = g \ . \tag{107}$$

If one uses this result in (75), it then follows that the Auger transition probabilities are given by

$$\omega = \left(\frac{2\pi}{\hbar} \rho \right) |\langle f;a|g|i\rangle|^2 \tag{108}$$

where now

$$|i\rangle = |\text{singly ionized atomic state}\rangle$$

$$|f;a\rangle = |\text{doubly ionized atomic state + Auger electron}\rangle.$$

The primary difference between this form and the conventional results is then in the type of matrix elements which are computed. Thus the calculations are no longer confined to the simple case of two-electron matrix elements and, instead the general case of N interacting electrons must be considered. The requisite analysis for evaluating these multi-electron matrix elements has been carried out by several workers--notably by Fano[61] and Shore[62]--but the formalism is quite complex. Since much of the problem is one of obtaining a precise notation for the coupled, N-electron wave functions, we shall confine the present discussion to an exposition of the notation introduced in the work by Fano. Detailed formulae for the matrix elements are not given, and the analytical details are reserved for the original Fano paper.

The basic problem is the evaluation of a matrix element such as

$$\langle 1s^{\alpha'} 2s^{\beta'} 2p^{\gamma'} \ldots \Big| \sum_{i<j} g_{ij} \Big| 1s^{\alpha} 2s^{\beta} 2p^{\gamma} \ldots \rangle$$

where the occupation numbers of the various subshells need not be the same. In order to obtain a definite notation for treating these elements, the subshells will be denoted by $n_\lambda \ell_\lambda$ where $\lambda = 1,2,3,\ldots$ and

$$n_1\ell_1 = 10(1s)$$

$$n_2\ell_2 = 20(2s) \qquad n_3\ell_3 = 21(2p)$$

$$n_4\ell_4 = 30(3s) \qquad n_5\ell_5 = 31(3p) \qquad n_6\ell_6 = 32(3d)$$

etc.

It follows that an atom with N_λ electrons in the λ subshell is represented by

$$1s^{N_1}2s^{N_2}2p^{N_3} \ldots = \prod_\lambda n_\lambda \ell_\lambda^{N_\lambda} \tag{109}$$

where $[\prod_\lambda]$ is the conventional product symbol. Now the evaluation of matrix elements with these configurations requires that the corresponding wave functions be anti-symmetric in all electron spin(s_i) and spatial ($\underline{r}_i$) coordinates. To obtain such functions, note first that it is fairly easy to form the anti-symmetric function for any individual subshell (e.g., $2p^4$, $3d^8$,...) and, indeed, these functions have been obtained by Racah[73] for the cases of (s,p,d) electrons. One procedure to take, therefore, in obtaining the total wave function is to begin with the anti-symmetrized functions of each λ subshell. It will be assumed that these are coupled in the LS-limit. The notation for these functions is then obtained by noting that the λ subshell is specified by the N_λ coordinates (s_i,$\underline{r}_i$) which constitute the set

$$q_\lambda = \{s_i, \underline{r}_i\} = \{i\} \ .$$

Since each possible ordering of these coordinates is present in the anti-symmetrized function, the set q_λ is prescribed to be ordered in the direction of increasing (i). Any deviation from this ordering then gives a factor of (± 1) in the function, the particular value being obtained only by considering the number of permutations required to return to the natural or prescribed order. With these definitions, the LS-coupled function for the λ subshell is then denoted by

$$\langle q_\lambda \, | n_\lambda \ell_\lambda^{N_\lambda} \alpha_\lambda L_\lambda S_\lambda \rangle \tag{110}$$

which includes all possibilities for M_{L_λ}, M_{S_λ}. The quantity, α_λ, represents any other quantum numbers required to define the state.

An unsymmetrized total atomic wave function is now obtained by successively coupling these anti-symmetrized subshell functions. In order to illustrate the procedure and to introduce the notation, suppose that one has three LS-states as

$$|L_1 S_1 M_L \, M_{S_1}\rangle; \ |L_2 S_2 M_{L_2} M_{S_2}\rangle; \ |L_3 S_3 M_{L_3} M_{S_3}\rangle \ . \tag{111}$$

Then the composite LS-state formed from these functions is obtained by first coupling $L_1 S_1$ and $L_2 S_2$ as

$$|L_{12} S_{12} M_{L_{12}} M_{S_{12}}\rangle = \sum \langle L_1 \bar{M}_{L_1} L_2 \bar{M}_{L_2} | L_{12} M_{L_{12}}\rangle \langle S_1 \bar{M}_{S_1} S_2 \bar{M}_{S_2} | S_{12} M_{S_{12}}\rangle \, |L_1 S_1 \bar{M}_{L_1} \bar{M}_{S_1}\rangle |L_2 S_2 \bar{M}_{L_2} \bar{M}_{S_2}\rangle \tag{112}$$

and then couple L_3S_3 to get

$$|LSM_LM_S\rangle = \sum \langle L_{12}\bar{M}_{L_{12}} L_3\bar{M}_{L_3}|LM_L\rangle\langle S_{12}\bar{M}_{S_{12}} S_3\bar{M}_{S_3}|SM_S\rangle \\ |L_{12}S_{12}\bar{M}_{L_{12}}\bar{M}_{S_{12}}\rangle|L_3S_3M_{L_3}M_{S_3}\rangle \ . \tag{113}$$

The sums here are over the barred quantities. If one now inserts (112) into (113) and replaces the notation in (111) by that of (110), the result is

$$|\alpha LSM_LM_S\rangle = \sum \langle L_{12}\bar{M}_{L_{12}} L_3\bar{M}_{L_3}|LM_L\rangle\langle S_{12}\bar{M}_{S_{12}} S_3\bar{M}_{S_3}|SM_S\rangle \ . \\ \langle L_1\bar{M}_{L_1} L_2\bar{M}_{L_2}|L_{12}\bar{M}_{L_{12}}\rangle\langle S_1\bar{M}_{S_1} S_2\bar{M}_{S_2}|S_{12}\bar{M}_{S_{12}}\rangle \ . \\ \langle q_1|n_1\ell_1^{N_1}\alpha_1L_1S_1\bar{M}_{L_1}\bar{M}_{S_1}\rangle\langle q_2|n_2\ell_2^{N_2}\alpha_2L_2S_2\bar{M}_{L_2}\bar{M}_{S_2}\rangle\langle q_3|n_3\ell_3^{N_3}\alpha_3L_3S_3\bar{M}_{L_3}\bar{M}_{S_3}\rangle \tag{114}$$

This is then a coupled, unsymmetrized wave function for $(N_1+N_2+N_3)$ electrons. It is anti-symmetric in the coordinates of the N_1 electrons of group q_1, N_2 electrons of group q_2, and N_3 electrons of group q_3--but it is not anti-symmetric under interchange of coordinates in separate groups. This must still be accomplished.

The procedure outlined above for three groups or subshells can evidently be extended easily. For an arbitrary number of such groups, however, the exact expressions such as (114) will be too cumbersome to write out, and a notation for these states must be specified. This is done by replacing (114) by

$$\Psi_u(q,\alpha LSM_L M_S) = \left[\prod_{\lambda=1}^{3} \langle q_\lambda | n_\lambda \ell_\lambda^{N_\lambda} \alpha_\lambda L_\lambda S_\lambda \rangle\right]^{(\alpha LS)}_{M_L M_S} \tag{115}$$

where the (u) subscript indicates that the state is unsymmetrized in the coordinates of different groups and $q = \{q_\lambda\}$ represents one distribution of N electrons arranged in groups of N_λ electrons each. This notation then implicitly contains all sums over the relevant angular momentum components--such as M_{L1}, M_{S1}, M_{L2}, M_{S2}, etc.--which appear in the precise expression of (114). In order to obtain a function anti-symmetric in all coordinates, we now note that such a function must necessarily contain all possible distributions, q, for the N electrons--i.e., all interchanges of electrons in different subshells must be included (recall that the function is already anti-symmetric for interchange of coordinates within subshells). But if one is given a particular distribution (q), then any interchange between subshells gives a different distribution--say q'--and the number of such distributions is required if the final function is to be normalized. This result follows at once if one notes that only interchanges between groups--not within--produce different distributions. Hence the number of distributions is just that obtained by permuting N objects for which permutations of objects within the groups $\{q_1, q_2 \ldots\}$ are indistinguishable; the result is then

$$\Omega(N_\lambda) = \frac{N!}{N_1! N_2! \ldots} = \frac{N!}{\prod N_\lambda!} \tag{116}$$

since the number of elements of the set q_λ is N_λ. The distribution q_n which has the coordinates in the natural order 1,2,3,... is assigned an

even parity and the corresponding state (115) appears with a plus sign. The functions for all other distributions enter the total anti-symmetrized function with the factor

$$(-)^{P_q} \tag{117}$$

where Pq is the number of permutations required to take the arbitrary distribution into q_n. It then follows that the total wave function for the N electrons is obtained by combining functions like (115) for each distribution and inserting the permutation factor (117) for each function so that we have

$$\Psi(\alpha LSM_L M_S) = \frac{1}{\sqrt{\Omega(N_\lambda)}} \sum_q (-1)^{P_q} \psi_u(q, \alpha LSM_L M_S) \; ; \tag{118}$$

the factor $\left(\frac{1}{\sqrt{\Omega(N_\lambda)}}\right)$ is present for purposes of normalization.

The fundamental matrix element of interest may now be written in terms of these anti-symmetrized states as

$$\langle \Psi' | g | \Psi \rangle \; . \tag{119}$$

Since the functions are anti-symmetric, it follows that the contributions of each term in this expression are identical. Further, there are $\left[\frac{N(N-1)}{2}\right]$ such terms so that (119) becomes

$$\frac{N(N-1)}{2} \langle \Psi' | g_{N-1,N} | \Psi \rangle \tag{120}$$

where one term is chosen for definiteness. This prescription thus reduces

the problem to one in which only those electrons with coordinates (N-1,N) interact. All others observe the process as "spectators" and comprise the spectator configuration (compare with (39) and the subsequent discussion). If we now insert the result (118) for Ψ and Ψ', the matrix element takes the form

$$\langle \Psi' | g | \Psi \rangle = \frac{N(N-1)}{2} \left[\Omega(N_\lambda') \Omega(N_\lambda) \right]^{-\frac{1}{2}} \sum_{q'q} (-1)^{P_q + P_{q'}} * \tag{121}$$

$$\langle \psi_u(q', \alpha' L' S' M'_{L'} M'_{S'}) | g_{N-1,N} | \psi_u(q, \alpha L S M_L M_S) \rangle$$

so that the calculation is reduced to essentially a two-electron problem. In order to further simplify the computation, note that the spectator configurations are the same in the initial and final states. Thus a given distribution q is such that the coordinates are as

$$q = \overset{\text{Spectator}}{(1 \to N-2)} + \overset{\text{Active}}{(N-1,N)}$$

$$= \bar{q} + (\text{active})$$

where $\bar{q}$ is the spectator configuration for q. But the matrix element in (121) is then of the form

$$\langle \bar{q}'(\text{active}) | g_{N-1,N} | \bar{q}(\text{active}) \rangle$$

with $\bar{q}'$, $\bar{q}$ being completely unaffected by the interaction. The relevant atomic orbitals being assumed orthonormal, it then follows at once that

$$\langle \bar{q}' | \bar{q} \rangle = \delta_{\bar{q}\,\bar{q}'} \quad , \tag{122}$$

i.e., the spectator configurations are the same. This configuration is then specified by giving the occupation number $\bar{N}_\lambda$ for each subshell so that

$$Sp = \prod_\lambda n_\lambda \ell_\lambda^{\bar{N}_\lambda} \quad . \tag{123}$$

As mentioned in the discussion on Auger energies, the values of $\bar{N}_\lambda$ are just the smaller occupation numbers of the initial and final states--i.e.,

$$\bar{N}_\lambda \leq \min(N_\lambda', N_\lambda) \quad . \tag{124}$$

It is also clear that

$$\sum_\lambda \bar{N}_\lambda = N - 2 \tag{125}$$

since all but two electrons are spectators. These two criteria on $\bar{N}_\lambda$ are sufficient to uniquely determine the spectator configuration if the initial and final states differ by two electrons; this is, of course, the case for Auger transitions. For the case where they differ by only one or no electrons, however, several spectator configurations (i.e., various values for $\bar{N}_\lambda$) are permitted and a separate computation must be performed for each.

For Auger transitions, we can thus restrict our consideration to a single spectator configuration $\{\bar{N}_\lambda\}$. The "active" or interacting

electrons will be assumed to be in the subshells with $\lambda = \rho$ or $\lambda = \sigma$ so that one can define three possibilities for $\bar{N}_\lambda$. Thus if a subshell is such that $\lambda \neq (\rho,\sigma)$, then clearly the number of spectators in this shell is just N_λ--i.e.,

$$\bar{N}_\lambda = N_\lambda \qquad \lambda \neq \rho, \sigma \quad ; \tag{126a}$$

similarly, if $\lambda = \rho$, $\lambda \neq \sigma$ then

$$\bar{N}_\lambda = N_\lambda - 1 \tag{126b}$$

while $\lambda = \rho = \sigma$ gives

$$\bar{N}_\rho = N_\rho - 2 \ . \tag{126c}$$

With these results, the matrix elements in (121) can be simplified still further. Thus the sums over q',q in that expression can be written as sums over spectator distributions plus sums over the non-spectator states. But from (122) the spectator configurations are the same so that (121) becomes

$$\frac{N(N-1)}{2}\left[\Omega(N_\lambda')\Omega(N_\lambda)\right]^{-\frac{1}{2}} \sum_{a',a} \sum_{\bar{q}} (-1)^{P_q+P_{q'}} \langle \psi_u(\bar{q};a';\alpha'L'M_L'M_S') \left| g_{N-1,N} \right| \psi_u(\bar{q};a;\alpha LSM_LM_S) \rangle \tag{127}$$

where (a', a) refer to the active non-spectator distributions. Since the spectator electrons are not affected by the operator $(g_{N-1,N})$, it

follows that the value of the matrix element in this result is independent of the particular spectator distribution $\bar{q}$. Hence one need specify only one $\bar{q}$ for the spectators and then multiply by all such possibilities. The number of these is, in analogy with (116), just

$$\Omega'(\bar{N}_\lambda) = \frac{(N-2)!}{\pi \bar{N}_\lambda !} \tag{128}$$

and (127) then becomes

$$\frac{N(N-1)}{2}\left[\Omega(N_\lambda')\Omega(N_\lambda)\right]^{-\frac{1}{2}}\Omega'(\bar{N}_\lambda)\sum_{a',a}(-1)^{P_q+P_{q'}}\langle\psi_u(\bar{q};a';\alpha'L'S'M_L'M_S')|g_{N-1,N}| \tag{129}$$

$$\psi_u(\bar{q};a;\alpha LSM_L MS)\rangle$$

where $\bar{q}$ is now a particular spectator distribution. The sums over the non-spectator distributions can also be treated in a simple fashion since these distributions are specified essentially by the two coordinates (N-1,N). Thus, using previous notation, if

$$\lambda \neq \rho,\sigma$$

so that all electrons in the subshell are spectators, it must be true that

$$q_\lambda = \bar{q}_\lambda \tag{130}$$

But if

$$\lambda = \rho \quad \text{or} \quad \lambda = \sigma$$

the situation is changed; in order to illustrate this, we first consider the case

$$\rho \neq \sigma \ .$$

The distribution of the ρ subshell contains the spectator portion $\{\bar{q}_\rho\}$ plus an electron with one of the coordinates (N-1,N); the σ subshell then contains the spectator portion $\{\bar{q}_\sigma\}$ plus an electron with the other coordinate. There are thus two possibilities for these distributions and they are

$$\begin{aligned} q_\rho &= \{\bar{q}_\rho;\ N-1\} & & q_\rho\{\bar{q}_\rho;\ N\} \\ & & \text{or} & \\ q_\sigma &= \{\bar{q}_\sigma;\ N\} & & q_\sigma = \{\bar{q}_\sigma;\ N-1\} \ . \end{aligned} \tag{131}$$

These then specify the two non-spectator distributions to be included in (129). Note that these can be combined by introducing the parameter (ϵ) and writing

$$\begin{aligned} q_\rho^{(\epsilon)} &= \{\bar{q}_\rho;\ N-1+\epsilon) \\ q_\sigma^{(\epsilon)} &= \{\bar{q}_\sigma;\ N-\epsilon\} \ . \end{aligned} \tag{132}$$

Then if (ϵ = 0,1) are the allowed values, it is easily shown that (132) produces the distributions in (131). It follows from this that the sum over the distributions ($\{a'\}$, $\{a\}$) in (129), which essentially interchanges the (N-1, N) coordinates, may be replaced by a sum over ϵ(ϵ' for $\{a'\}$). Indeed, one obtains the result

$$\sum_{\epsilon',\epsilon=0}^{1} \frac{N(N-1)}{2}\left[\Omega(N'_\lambda)\,\Omega(N_\lambda)\right]^{-\frac{1}{2}}\Omega'(\bar{N}_\lambda)(-1)^{P_q+P_{q'}}(1-\epsilon\delta_{\rho\sigma})(1-\epsilon'\delta_{\rho'\sigma'})\ \cdot$$

$$\langle\psi_u(q'^{(\epsilon')}\alpha' L'S'M_L'M_S')\,|\,g_{N-1,N}\,|\,\psi_u(q^{(\epsilon)};\alpha LSM_L MS)\rangle \tag{133}$$

where the substitution

$$q_\lambda \rightarrow q_\lambda^{(\epsilon)}$$

is made throughout and the relations

$$q_\lambda^{(\epsilon)} = \bar{q}_\lambda \qquad \lambda \neq \rho, \sigma$$

$$q_\lambda^{(\epsilon)} = (\bar{q}_\rho;\ N-1,N)\delta_{\epsilon o} \qquad \lambda = \rho = \sigma$$

are used in addition to (132). The factors

$$(1-\epsilon\delta_{\rho\sigma})(1-\epsilon'\delta_{\rho'\sigma'})$$

insure that the distributions $(q_{\rho'}^{(\epsilon')}\ldots q_\sigma^{(\epsilon)})$ are properly included in the sums over (ϵ,ϵ') when one has $(\rho=\sigma)$ or $(\rho'=\sigma')$. It remains to evaluate the parity or permutation values, P_q and $P_{q'}$, in terms of the parameters which have been introduced. This can be accomplished by noting that the distribution q is now specified by (assume $\rho \leq \sigma$ for a definite ordering)

$$\begin{aligned} q = q^{(\epsilon)} &= \{\bar{q}_\lambda\}_{\lambda\neq\rho,\sigma} + \{\bar{q}_\rho;\ N-1+\epsilon\} + \{\bar{q}_\sigma;\ N-\epsilon\} \\ &= \{\bar{q}_\lambda\} + (N-1+\epsilon)_\rho + (N-\epsilon)_\sigma \end{aligned} \tag{134}$$

where the case $(\rho \neq \sigma)$ is used and the notation

$$(N - 1 + \epsilon)_{\rho}$$

simply means that the ρ subshell has the coordinate $(N-1+\epsilon)$ within it. The permutation P_q is then composed of the permutations required to return the spectator distribution

$$\bar{q} = \{\bar{q}_\lambda\} \tag{135}$$

to a natural order $(P_{\bar{q}}^{-})$ plus that required to return the (N-1,N) coordinates to a natural order. But one has the correspondence, for $\epsilon = 0$,

$$\lambda = 1,2,3,\ldots, \overset{(N-1)}{\rho},\ldots, \overset{(N)}{\sigma},\ldots$$

so that, to obtain a natural order, the N coordinate must be permuted through each subshell from $(\lambda = \sigma + 1)$ to the maximum required to exhaust all filled subshells. Since each subshell has $\bar{N}_\lambda$ electrons it follows that the number of permutations for the N coordinate is

$$\sum_{\lambda=\sigma+1}^{\infty} \bar{N}_\lambda$$

Similarly, for the (N-1) coordinate, the number of permutations is just

$$\sum_{\lambda=\rho+1}^{\infty} \bar{N}_\lambda$$

and one then has that

$$P_q(0) = P_q^- + \sum_{\lambda=\rho+1}^{\infty} \bar{N}_\lambda + \sum_{\lambda=\sigma+1}^{\infty} \bar{N}_\lambda$$

$$= P_q^- + \sum_{\lambda=\rho+1}^{\sigma} \bar{N}_\lambda \quad . \tag{136}$$

If (ϵ=1) is the situation, then (N-1,N) are interchanged and one extra permutation is then required; a one (1) must then be added to (136). The general case may, therefore, be written as

$$P_q^{(\epsilon)} = P_q^- + \sum_{\lambda=\rho+1}^{\sigma} \bar{N}_\lambda + \epsilon \; ; \tag{137}$$

since it is also true that

$$P_{q'}(\epsilon') = P_q^- + \sum_{\lambda=\rho'+1}^{\sigma'} \bar{N}_\lambda + \epsilon'$$

one has

$$P_q(\epsilon) + P_{q'}(\epsilon') = \sum_{\lambda=\rho+1}^{\sigma} \bar{N}_\lambda + \sum_{\lambda=\rho'+1}^{\sigma'} \bar{N}_\lambda + \epsilon + \epsilon' \quad . \tag{138}$$

But this equality is modulo 2--i.e., the only restriction is that both sides be even or both odd--so that the same result is obtained for either sign in the quantity

$$(-1)^{P_q(\epsilon) \pm P_{q'}(\epsilon')} .$$

It is more convenient to use the minus case and we shall thus replace (138) by

$$P_q(\epsilon) - P_{q'}(\epsilon') = \sum_{\lambda=\rho+1}^{\sigma} \bar{N}_\lambda - \sum_{\lambda=\rho'+1}^{\sigma'} \bar{N}_\lambda + \epsilon - \epsilon' = \Delta P + \epsilon - \epsilon' . \quad (139)$$

If these results are now combined with

$$\frac{\Omega'(\bar{N}_\lambda)}{\sqrt{\Omega(N'_\lambda)\Omega(N_\lambda)}} = \frac{\sqrt{N_\rho (N_\sigma - \delta_{\rho\sigma}) N'_{\rho'} (N'_{\sigma'} - \delta_{\rho'\sigma'})}}{N(N-1)} \quad (140)$$

it follows that

$$\langle \Psi' | g | \Psi \rangle = \tfrac{1}{2} \sqrt{N_\rho (N_\sigma - \delta_{\rho\sigma}) N'_{\rho'} (N'_{\sigma'} - \delta_{\rho'\sigma'})}\ (-1)^{\Delta P} .$$

$$\sum_{\epsilon', \epsilon = 0}^{1} (-1)^{\epsilon - \epsilon'} (1 - \epsilon \delta_{\rho\sigma}) (1 - \epsilon' \delta_{\rho'\sigma'}) \langle \psi_u (q^{(\epsilon')}; \alpha' L' S' M'_L M'_S) | g_{N-1,N} | \psi_u (q^{(\epsilon)}; \alpha L S M_L M_S) \rangle \quad (141)$$

and the problem is thus reduced to one of evaluating the matrix elements for unsymmetrized states. The computations for these, though straightforward, are tedious and the details are relegated to the Fano paper.[61]

A procedure for computing the N-electron matrix elements is thus available, and it may evidently be applied to the computation of Auger transition probabilities when the multi-electron model for the transition dynamics is assumed. Unfortunately, the calculations are quite prohibitive if the number of open atomic subshells is very large for, in this case, the number of angular momentum states is also large. As a result of this, very few computations based on this model have yet been performed. It should be recognized, however, that this is not due to restrictions on the method.

Before closing this section, the effect of the density of states factor (ρ) must be mentioned. Our comments will be confined to atomic transitions here since the next section considers the difficulties introduced by the solid state. Since the discussion is for atomic systems, all of the orbital states (such as $(n_i\ell_i, n_1\ell_1, n_2\ell_2)$ in the conventional view) are discrete. The density of states is thereby just that available to the continuum electron. It is shown in Messiah[65] that the density of states for such an electron is determined by its normalization. Indeed, if one normalizes the continuum state as

$$\langle E'\ell | E\ell \rangle = \delta(E' - E) \quad , \tag{142}$$

the density of energy states is just

$$\rho(E) = 1 \tag{143}$$

and, for this case, the factor (ρ) can be dropped from the relevent formulae for the transition probabilities. This normalization is "per

unit energy" and for Auger transitions it can be interpreted as one Auger electron emitted per unit energy. It is sometimes convenient, however, to normalize to one electron emitted per unit energy per unit time. This means that (142) is replaced by

$$\langle E'\ell | E\ell \rangle = h\delta(E' - E) \ , \tag{144}$$

where h is Planck's constant, and (143) then becomes

$$\rho(E) = 1/h \ . \tag{145}$$

In this normalization, therefore, the factor $\left(\frac{2\pi}{\hbar}\rho\right)$ in the transition formulae becomes

$$\left(\frac{1}{\hbar}\right)^2 \tag{146}$$

One must thus be cautious when considering the results obtained for Auger transition probabilities since the normalization chosen for the continuum function will affect the predicted values.

Solid State Effects

We now will consider briefly the effects introduced for Auger transitions in molecular or solid state systems. The obvious new feature in both systems involves the changes in the valence state wave functions. The overlap of these states in the molecular or solid state leads to a broadening of the energy levels as well as an alteration in the wave function properties. Instead of atomic orbitals, therefore,

one must use molecular orbitals or the appropriate solid state functions. A second feature of the molecular and/or solid state is the importance of the density of states factor, ρ. As we shall see, the structure in this factor can have a pronounced effect on the observed Auger spectra. Finally, the broadening of the intrinsic energy level widths can have an effect on the observed Auger peak widths. Since this broadening is most pronounced in solid state systems where energy bands are formed, we will restrict the following comments to the solid (for a more detailed treatment of solid state difficulties and for additional references, consult Amelio[74]). The same conclusions, however, follow to a lesser extent for the molecular case.

Now consider Figure 5 where a schematic level diagram, such as might exist in a solid, is given. The band is labeled M_1 while the relatively unperturbed L_1, L_2, L_3, K levels remain distinct. We have the top of the band an energy ϕ below the so-called vacuum level while the bottom of the band is ϵ below this level. Two types of Auger transitions involving the band are indicated--one in which both final vacancies are in the band and the second where only one vacancy is in the band. Only the former case will be discussed here. Assuming a Bergstrom-Hill type expression for the energy, the Auger electron will have the energy

$$E = E_k - |E_B| - |E_C| \ . \tag{147}$$

Since E_b, E_C are band energies, it is then clear that the Auger electron may have a continuous range of values with the maximum value given when $E_B + E_C$ is a minimum--i.e., when both electrons originate at the top of

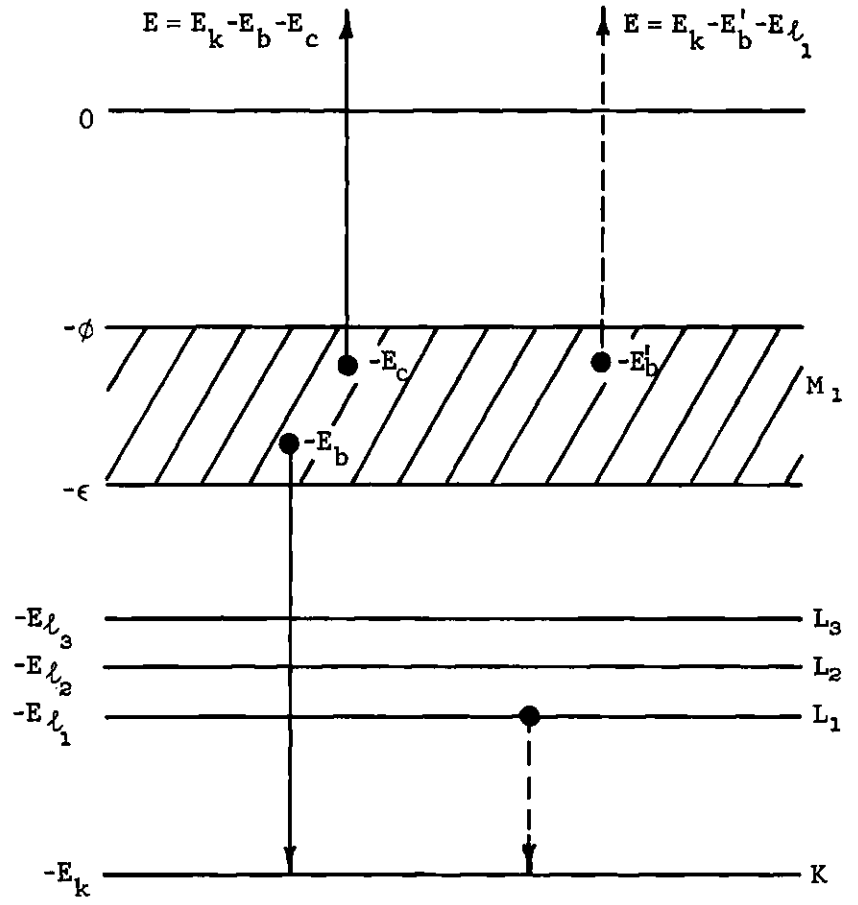

Figure 5. Level Diagram for Auger Transitions from an Energy Band.

the band. Similarly, the minimum Auger energy occurs if $E_B + E_C$ is a maximum--i.e., both electrons originate at the bottom of the band. Thus we can list explicitly the maximum and minimum energies as

$$E_{max} = E_k - 2\phi \ , \qquad E_{min} = E_k - 2\epsilon \tag{148}$$

so that the intrinsic width of the Auger peak can be expected to have at least a spread in energy of

$$\Delta E = E_{max} - E_{min} = 2(\epsilon - \phi) = 2E_W \ , \tag{149}$$

i.e., twice the band width. Now such a broadening of the energy widths may give rise to difficulty in interpreting Auger spectra if the peaks are separated by amounts comparable with the band widths. In such cases, the adjacent peaks will overlap and their resolution will thus become increasingly difficult.

It is, therefore, of interest to examine what information --if any--one may obtain from the peak intensities. Before this can be properly done, however, observe that in addition to the use of solid state band functions and the importance of the density of states, there is one other complication to be included. Thus we note that the two electrons may originate at different places within the band and still give rise to the same Auger energy. It follows that the transition probability or intensity of the peak for a given energy is actually a sum of individual intensities. In order to understand how this situation occurs, consider Figure 6 where the transition of two electrons

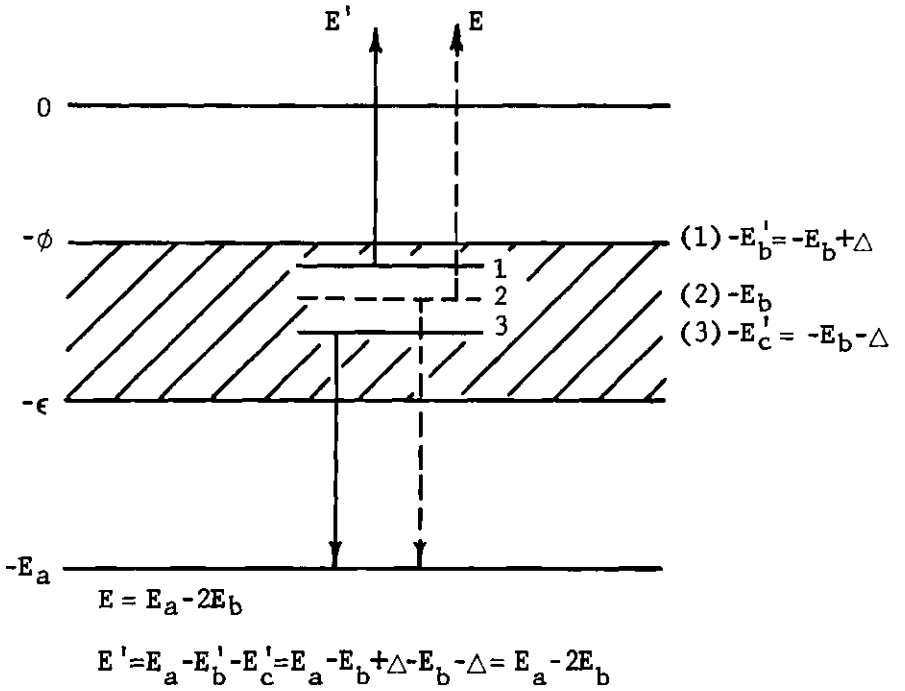

Figure 6. Illustration of the Same Auger Energy for Different Band Transitions.

from the same level, $-E_B$, is shown. The Auger energy is clearly just

$$E = E_A - 2E_B \tag{150}$$

for this case. But it is evident that electrons which originate in the symmetric levels

$$\begin{aligned} -E_B' &= -E_B + \Delta \\ -E_C' &= -E_B - \Delta \end{aligned} \tag{151}$$

will necessarily give the same Auger energy. Now all values of the Δ parameter are not allowed since the energies (151) must lie within the band--i.e., one has

$$\begin{aligned} -E_B + \Delta &\leq -\phi \\ -E_C - \Delta &\geq -\epsilon \end{aligned} \tag{152}$$

which can be written as

$$\Delta \leq E_B - \phi = \Delta_1$$

$$\text{and} \qquad \Delta \leq -E_B + \epsilon = \Delta_2 \quad .$$

It follows that one must have

$$0 \leq \Delta \leq \min(\Delta_1, \Delta_2) \tag{153}$$

and one can show that

$$\min(\Delta_1, \Delta_2) = \begin{cases} \Delta_1 & -\left(\frac{\epsilon+\phi}{2}\right) \leq -E_B - \phi \\ \Delta_2 & -\epsilon \leq -E_B \leq -\left(\frac{\epsilon+\phi}{2}\right) \end{cases} . \tag{154}$$

From this the allowed values of Δ are determined by (153). If one now sums all transition probabilities associated with a particular energy E, the result is

$$TP(E) \propto \int_0^{\Delta_{max}} |\langle f|1/r_{12}|i\rangle|^2 \rho(\Delta) d\Delta \tag{155}$$

where the conventional view of an Auger transition is assumed. Recall that this expression requires the use of solid state band functions and/or molecular orbitals in place of the atomic orbitals assumed previously. This clearly complicates the computations in (155). In addition, the calculation of the density of states (ρ) is extremely complex in itself. It follows from this that the introduction of the solid state into an Auger problem significantly increases the labor involved in making the computation for transition probabilities.

A final comment on computing energies for Auger transitions in a solid is in order. Thus it was assumed above that the Bergstrom-Hill relation was valid in computing the energy. But from previous remarks we expect that a far better procedure would utilize the total energy approach of (2). Unfortunately, this approach is not feasible for extremely large systems since (a) the computation of the energies

become more complex and (b) the percentage change in the total energy for the emission of a single electron decreases for such systems. For these reasons, it is probably better to use a relation of the Bergstrom-Hill type for solid state or large molecular systems.

CHAPTER III

COMPUTATIONAL RESULTS

The formalism developed in the previous chapter is now applied to the computation of LMM transition probabilities and energies for the elements titaninum (Ti), vanadium (V), chromium (Cr), zirconium (Zr), niobium (Nb), and molybdenum (Mo). Before presenting the results, however, it is worthwhile to consider the procedure adopted for carrying out the necessary calculations. This procedure has already been briefly described in Chapter I but, for convenience, the procedural steps are repeated below:

(a) use Hartree-Fock wave functions;

(b) work in the intermediate coupling (IC) limit;

(c) treat transitions in isolated atoms;

(d) work in the non-relativistic limit; and

(e) assume basic validity of Wentzel two-electron theory.

In order to clarify the significance of these steps, each will be discussed separately; following this, the data obtained for the above elements is presented.

The choice of Hartree-Fock wave functions was dictated by the fact that this approach represents the best approximation to the actual solutions obtained by solving Schrödinger's equation (3). It may be recalled that exact solutions of (3) are not feasible for most atoms so

the approximation is a necessity. By utilizing the Hartree-Fock functions, it then follows from equations (94) and (106) that the results obtained for the computed transition probabilities should be the most accurate attainable in the absence of exact solutions to (3). In addition, the coulomb integrals, $F^k(n_1 \ell_1 n_2 \ell_2)$ and $G^k(n_1 \ell_1 n_2 \ell_2)$, are produced in the Hartree-Fock treatment so that the energy calculations are also improved by the approach. The particular computation carried out in this work utilized the multi-configuration Hartree-Fock (MCHF) program of C. F. Fischer.[67] With this program it is possible to specify the configuration of the atom in the LS-coupling limit and then obtain the Hartree-Fock wave-functions, the average and total energy of the configuration, and the relevant coulomb integrals for the calculations.

The use of this MCHF procedure was not restricted to the computation of a single configuration per element. Instead, an attempt was made to account for the "relaxation" of the electron orbitals following the excitation of the atom. Thus the removal of the inner shell electron to produce the excited initial state would be expected to alter the electron binding energies and wave functions from that obtained for the neutral atom. Similarly, the ejection of the Auger electron produces the doubly ionized atom whose electron properties will differ even more from the neutral case. To account for this relaxation phenomenon, separate Hartree-Fock calculations were carried out for the initial and final atomic states involved in the Auger transition. From the comments of equations (32)-(34), this means that, in general, two initial and six final state MCHF computations were carried out for each of the elements considered. In actual practice, however, only five final

states were considered since the configuration resulting from the ejection of both 3s electrons (compare (33a))presented difficulties. The wave functions and energies for this configuration were obtained, for each element, by using the coulomb integrals and wave functions computed from the configuration for the 3s3p transition (compare (33b)). It should be recalled from (52) that the structure terms involved in the computation of the LMM intermediate coupling (IC) energies contain the spin-orbit coupling parameters ξ_{3p}, ξ_{3d}. The MCHF procedure also computes these parameters utilizing an approximate approach due to Fischer which attempts to extend the results of Blume and Watson.[75] Since these results are expected to be more accurate than conventional calculations, they were adopted for this work. The use of the Hartree-Fock procedure can be summarized by noting that separate calculations are performed for each atomic configuration. The coulomb, average, and spin-orbit energies computed by the procedure are then utilized to calculate the LMM Auger energies while the wave functions allow the computation of the associated transition probabilities.

To complete this discussion on the electron wave functions, it must be noted that the MCHF procedure is not capable of producing the continuum electron function. Instead the approach taken is to assume that the Auger electron moves in a central atomic potential as it exits the atom so that it must satisfy the equation

$$\left[-\frac{\hbar^2}{2m}\nabla^2 + V(r) \right]\psi = E\psi \ . \qquad (156)$$

where $E > 0$ since the particle is not bound. The energy E is obtained

by equation (2) for the relevant transition once the coulomb energies are obtained via the MCHF computation. Hence it is necessary only to obtain V(r) and then solve for the continuum function ψ. In this work the form of V(r) was assumed to be that obtained by the Hartree-Fock-Slater (HFS) approximation to the atomic problem. Then by using the computer results developed by Hermann and Skillman[76] for the HFS approach, a potential V(r) was computed for <u>each</u> permitted final state of each element. The results of this computation were inserted into a computer program[77] which numerically solves (156) for the continuum function ψ and computes the relevant integrals $R^k(ab,cd)$ encountered in the computation of the transition probabilities (compare with (91) and (92)). The normalization chosen for the continuum function was that found in (142)--i.e., per unit energy. Note that each of the programs referenced here was modified in order to carry out the calculations of this work.

The decision to treat the Auger process in the limit of intermediate coupling (IC) was dictated by the complete lack of such computations for LMM transitions. It was also suggested by the success obtained by Asaad and Burhop[10] when they applied IC to the case of KLL transitions. This treatment, therefore, serves as a check on the need for the IC limit in the elements considered and provides as well the most general formulation--from the coupling viewpoint--of the problem. As regards this latter remark, it is to be noted that intermediate coupling is applied only to the interaction of those electrons which transit to fill the initial vacancy and form the continuum electron. The interaction of the continuum and initial (2s,2p) electrons (compare

(77)) is treated in the LS-coupling limit. It follows from this that the LMM transition probabilities are computed from (106) rather than the more general result of (97). Explicit expressions obtained from this relation are presented in Appendix C for these transition rates.

The restriction of the treatment to isolated atoms obviously ignores all molecular and solid state effects discussed in the final section of Chapter II. This omission is justified, we believe, since there exist no theoretical data for the elements in question, isolated or otherwise (although some results have appeared recently[23,24]). In addition, the contribution of the molecular and solid state effects is primarily to broaden the observed peak widths with the basic position (in energy) of the peaks being the same as for the case of isolated atoms. It follows from this that a knowledge of LMM energies and intensities, based on atomic calculations, is expected to be of interest also in molecules and solids. This is especially true in elements such as Zr, Nb, and Mo since LMM transitions in these atoms correspond to "core" transitions. Hence the band effects caused by overlapping of the valence orbitals should be quite small for these materials so that atomic calculations represent a reliable treatment for LMM transitions in such materials.

The use of the non-relativistic limit in treating the Auger process was due principally to the lack of a valid, relativistic formulation of the problem. Indeed, the only available treatment, which is valid in the relativistic limit, is due to an approximation by Möller.[78] This views the Auger process as arising from an indirect transition wherein a photon is produced and then reabsorbed by the Auger electron

(which is, of course, subsequently ejected from the atom). This is the same view originally proposed by Auger[1,2] and then discarded in the Wentzel formulation of the theory. Since the view and formulation is incorrect, it was felt that a relativistic treatment of the problem was not justified.

Finally, the Wentzel formulation of the Auger problem was assumed since experiment indicates that the Auger spectra observed does agree fairly well with that predicted on the basis of this theory. This does not, of course, mean that the two-electron formalism is correct since it may be, for example, that other peaks are simply not being resolved. Nevertheless, the basic validity seems to be indicated so our calculations assume a spectrum of the two electron type (compare Chapter II).

Results for Ti, V, Cr

The procedure outlined above describes the general assumptions made in carrying out this work. It does not, however, give the specific program which incorporates these assumptions into a viable computational scheme. Such a program was developed, of course, and it is presented in Figure 7 as a block diagram. The essential features of the scheme are readily apparent with the computation of the Hartree-Fock orbitals being the fundamental step in the procedure. Once this has been accomplished, the calculation of the Auger energies and intensities follows in a straightforward fashion by utilizing the formalism developed in Chapter II. As an aid in interpreting the steps and their relation to the formalism, pertinent equations are referenced at each step in the scheme. Note that the only deviation in the program occurs

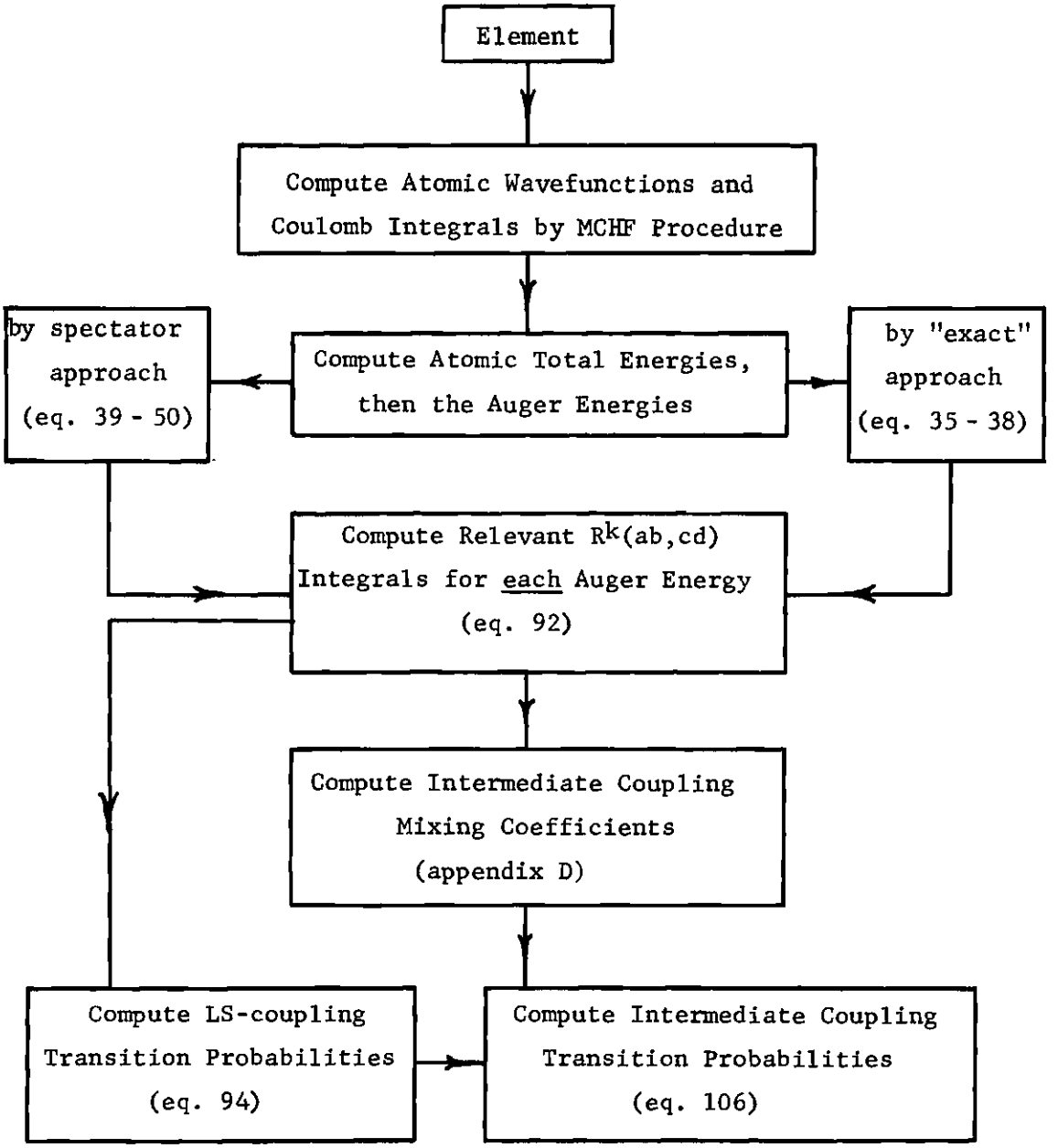

Figure 7. Block Diagram for the Computation of LMM Auger Energies and Transition Probabilities

in the calculation of the Auger energies, a fact in agreement with earlier observations. Thus it is necessary that one decide at the outset on the use of the spectator or "exact" approaches to the energy evaluation. From Chapter II, this decision depends solely on whether or not the M shell (for LMM transitions) is completely filled. If it is, then one uses the "exact" approach; otherwise, the spectator approach is required. Once the appropriate method is adopted, the computation of the transition probabilities follows the well-defined procedure of Figure 7.

In order to apply this program to the elements titanium (Ti), vanadium (V), and chromium (Cr), these comments indicate that the spectator approach must be utilized. It then follows at once from (55) that the appropriate multiplet structure arising from angular momentum coupling is obtained from the configurations

$$3s^2,\ 3s3p,\ 3s3d,\ 3p^2,\ 3p3d,\ 3d^2\ . \tag{157}$$

The structure for these configurations is presented in schematic form in Figure 8 for the (a) hydrogenic, (b) LS- , (c) intermediate and (d) jj-coupling limits. The similarity to Figure 1 for KLL transitions is readily apparent with most of the notation remaining the same. As the only exception, note that the presence of mixed states (compare (23)) in the intermediate coupling region is here denoted by an asterisk rather than quotation marks. Due to this mixing we again have that some levels, forbidden in the LS-limit, are allowed in the intermediate case as evidenced, for example, by the $3p^2(^3P_{0,2})$ levels. Now in order

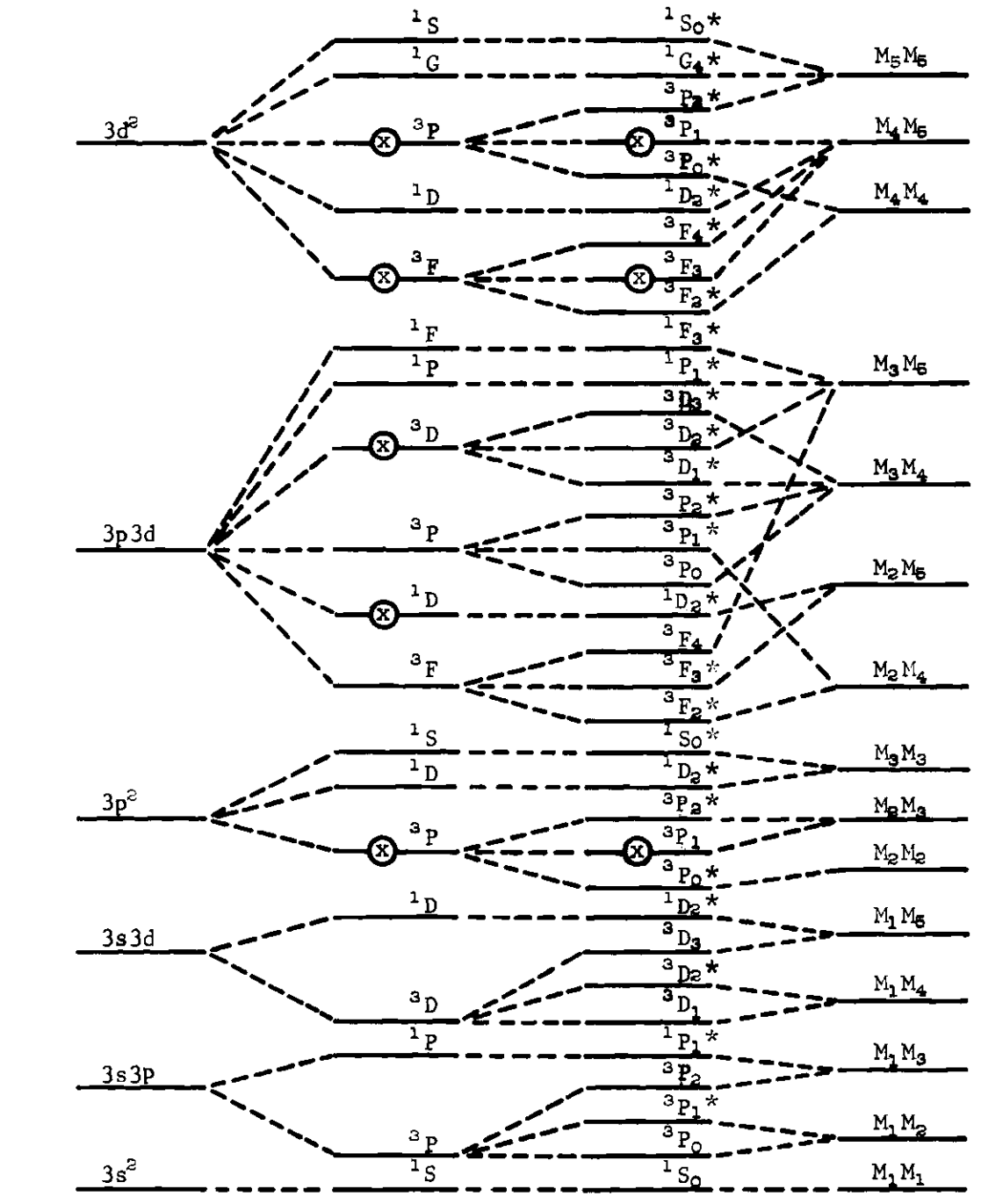

Figure 8. Schematic Energy Level Diagram for Computation of LMM Auger Energies by Spectator Approach (not to scale).

to compute the Auger energies in the desired coupling limit, it is necessary that the average energies of the configurations (157) be computed together with the energies of the structure terms appearing in Figure 8. Thus in the case of the 3s3d configuration in the LS-limit, the average energy (E_{avg}(initial) in Figure 3) locates the 3s3d level in the hydrogenic limit (a) while the structure term energies determine the splitting of the ^1D and ^3D levels. The present work treats the system in the intermediate coupling region (c) so that the structure term computation is somewhat more complex than the case of the LS-limit. It is still readily accomplished, however, using the results of Table 1.

Before proceeding to the results, a word about notation is required due to the ambiguity inherent in specifying the levels in the IC region. Following the convention set forth in the discussion following (12), these levels are specified by giving both the LS- and jj- levels to which the given IC level tends in the appropriate limit. Thus one has, for the 3s3p and $3p^2$ configurations, the levels specified as

$$3s3p\text{: } M_1M_2(^3P_0,\ ^3P_1);\ M_1M_3(^3P_2,\ ^1P_1)$$

$$3p^2\text{: } M_2M_2(^3P_0);\ M_2M_3(^3P_2,\ ^3P_1);\ M_3M_3(^1S_0,\ ^1D_2)$$

with similar designations for the other configurations. It remains to indicate whether the initial vacancy of the Auger process occurs in

the 2s or 2p subshells. This is accomplished (compare (10)) by using the notation for these levels in the jj-limit, i.e.,

$$2s \sim L_1 \qquad \text{and} \qquad 2p \sim L_2,\ L_3$$

from which it follows that a 2s transition is identified simply by using the L_1 label. Similarly, the 2p subshell should be specified by listing either the L_2 or L_3 label. The MCHF procedure utilized in this work, however, computes the orbitals and associated binding energies in the LS-limit so that only a single 2p level is obtained--i.e., the L_2 and L_3 levels are the same. It follows that our results should best be specified by including both L_2 and L_3 in the transition label. As a result the notation

$$\begin{aligned} &2s\text{: } L_1M_1M_1(^1S_0);\ L_1M_1M_2(^3P_2)\ldots \\ &2p\text{: } L_{2,3}M_1M_1(^1S_0);\ L_{2,3}M_1M_2(^3P_2)\ldots \end{aligned} \tag{158}$$

is used, in this work, to denote transitions to initial 2s or 2p vacancy states.

The results for the LMM transition energies can now be presented, and this is done in Table 2. Perhaps the most obvious feature reflected by these results is the smallness of the splittings induced by the spin-orbit interaction. Thus the maximum energy difference found for intermediate levels such as

$$3s3p\text{: } LM_1M_2(^3P_{0,1});\ LM_1M_3(^3P_2)$$

Table 2. LMM Auger Transition Energies in the Intermediate Coupling Limit (electron volts)

	Ti		V		Cr	
	L_1	$L_{2,3}$	L_1	$L_{2,3}$	L_1	$L_{2,3}$
$M_1M_1\ (^1S_0)$	402.1	302.0	452.8	344.6	516.2	404.2
$M_1M_2\ (^3P_0)$	437.7	337.7	491.0	382.8	548.2	436.1
$M_1M_2\ (^3P_1)$	437.0	337.0	490.2	382.0	547.2	435.1
$M_1M_3\ (^3P_2)$	437.0	337.0	490.1	382.0	547.2	435.1
$M_1M_3\ (^1P_1)$	426.4	326.4	479.0	370.8	535.6	423.5
$M_1M_4\ (^3D_1)$	471.7	371.7	529.7	421.5	591.6	479.5
$M_1M_4\ (^3D_2)$	471.6	371.7	529.7	421.5	591.6	479.5
$M_1M_5\ (^3D_3)$	471.6	371.6	529.6	421.4	591.5	479.4
$M_1M_5\ (^1D_2)$	467.6	367.6	525.2	417.0	587.1	475.0
$M_2M_2\ (^3P_0)$	464.4	364.4	520.0	411.8	578.4	466.3
$M_2M_3\ (^3P_1)$	464.2	364.2	519.6	411.4	578.0	465.9
$M_2M_3\ (^3P_2)$	463.7	363.8	519.2	411.0	577.4	465.3
$M_3M_3\ (^1S_0)$	456.7	356.7	511.7	403.5	569.6	457.6
$M_3M_3\ (^1D_2)$	461.0	361.0	516.3	408.1	574.4	462.3
$M_2M_4\ (^3F_2)$	504.6	404.6	565.0	456.8	628.6	516.5
$M_2M_4\ (^3P_1)$	500.1	400.1	560.2	452.0	623.7	511.6
$M_2M_5\ (^3F_3)$	504.3	404.3	564.7	456.5	628.1	516.0
$M_2M_5\ (^1D_2)$	503.4	403.4	563.7	455.6	627.2	515.1
$M_3M_4\ (^3P_0)$	499.1	399.1	560.0	451.8	623.3	511.3
$M_3M_4\ (^3P_2)$	500.2	400.3	560.4	452.2	623.9	511.8
$M_3M_4\ (^3D_1)$	499.5	399.5	559.6	451.4	623.0	510.9
$M_3M_4\ (^3D_3)$	499.3	399.3	559.4	451.2	622.8	510.7
$M_3M_5\ (^3F_4)$	503.9	403.9	564.2	456.1	627.6	515.5
$M_3M_5\ (^3D_2)$	499.4	399.4	559.5	451.3	622.8	510.7
$M_3M_5\ (^1P_1)$	493.9	393.9	553.7	445.5	617.1	505.0
$M_3M_5\ (^1F_3)$	493.0	393.0	552.7	444.5	616.1	504.0
$M_4M_4\ (^3F_2)$	538.5	438.5	603.6	495.5	672.6	560.5
$M_4M_4\ (^3P_0)$	536.8	436.8	601.4	493.2	670.4	558.3
$M_4M_5\ (^3F_3)$	538.4	438.4	603.6	495.4	672.5	560.4
$M_4M_5\ (^3F_4)$	538.4	438.4	603.5	495.4	672.4	560.3
$M_4M_5\ (^1D_2)$	536.9	436.9	601.7	493.6	670.7	558.6
$M_4M_5\ (^3P_1)$	536.8	436.8	601.4	493.2	670.3	558.3
$M_5M_5\ (^3P_2)$	536.8	436.8	601.4	493.2	670.3	558.2
$M_5M_5\ (^1G_4)$	536.1	436.1	600.7	492.5	669.7	557.6
$M_5M_5\ (^1S_0)$	532.4	432.4	596.5	488.3	665.5	553.4

is one electron volt(ev) with the minimum difference being zero. From the way the calculations are made, this small deviation reflects the fact that the LS level of the configuration ($3s3p(^3P)$ in the above example) is very little affected by the extension to intermediate coupling or, equivalently, by the introduction of the spin-orbit interaction. An immediate conclusion of these small splittings is, therefore, that LMM Auger transitions in (Ti, V, Cr) need not be treated in the intermediate coupling limit. This conclusion is valid, of course, only until experiments are capable of resolving structure with separations less than one electron volt. For clarity, note that it is assumed in the following discussion that one volt is the experimental resolution.

In order to better assess the predictions of Table 2, they are compared with available experimental data in Table 3. The experiments cited were all taken by the technique of Auger Electron Spectroscopy (AES) with the work performed by Simmons,[84] Haas et al.,[85] and Palmberg.[86] Some brief remarks are in order since the notation is changed somewhat from that of Table 2. Thus transitions such as

$$L_{2,3}M_1M_2(^3P_0,\ ^3P_1) \quad \text{and} \quad L_{2,3}M_1M_3(^3P_2)$$

are combined into the single symbol

$$L_{2,3}M_1M_{2,3}(^3P_{0,1,2}) \ .$$

This is done since the separation of the Auger energies for these

transitions is less than the experimental resolution. As a result the different peaks or lines for these transitions will appear experimentally as a single peak denoted by the above. Similar comments apply to the other combined transition labels. It should also be noted that only $L_{2,3}MM$ transitions are recorded in Table 3. This is due to the complete lack of experimental data on L_1MM transitions. This deficiency of data is probably due to inefficient ionization of the 2s subshell, at least compared to the 2p subshell, but other factors may also contribute. In any event, current experiments have not resolved these peaks and future study is necessary.

The experimental peaks listed in Table 3 are interpreted on the basis of the current theoretical predictions shown in the column labeled "calc". It should be noted that such an assignment of peak identity does not generally agree with the original interpretation given by the experimentalists. These workers had to interpret their results on the basis of the Bergstrom-Hill (B-H) predictions so discrepancies in interpretation are not surprising. As an example of the type of discrepancy encountered, we have that the peak at 335 ev observed by Simmons[84] in Ti was interpreted by him as arising from an $L_2M_1M_1$ transition--i.e., arising from a $3s^2$ type transition. Our interpretation, however, associates this peak with an $L_{2,3}M_1M_{2,3}(^3P_{0,1,2})$ line--i.e., one which arises from a 3s3p type transition. The distinction between the two interpretations is then clearly fundamental.

Some of the new interpretations given to the experimental data may seem questionable--especially for the Simmons and Haas[85] results. For example, the assignment of the 384 ev peak in Ti to the 3s3d

Table 3. Comparison of LMM Energies with Experiment: Ti, V, Cr
(all data in electron volts)

$L_{2,3}$	Ti			V			Cr		
	Calc.	B-H*	Exp.**	Calc.	B-H*	Exp.**	Calc.	B-H*	Exp.**
$M_1M_1(^1S_0)$	302	330		345	373		404	417	
$M_1M_3(^1P_1)$	326	358	327^h	371	404	386^h	424	452	423^s
$M_1M_{2,3}(^3P_{0,1,2})$	337		335^s	382			435		
$M_3M_3(^1S_0)$	357	383	355^s, 350^h	403	432	402^h, 412^h	458	483	446^s, 444^p
$M_3M_3(^1D_2)$	361		361^h, 350^p	408		395^p, 410^p	462		457^p, 469^p
$M_2M_{2,3}(^3P_{0,1,2})$	364		362^p	411			466		
$M_1M_5(^1D_2)$	368	394	384^s, 373^h	417	445	431^h, 420^p	475	497	476^p
$M_1M_{4,5}(^3D_{1,2,3})$	372		380^h, 370^p	421		428^p	480		489^p
$M_3M_5(^1P_1;^1F_3)$	393	419	403^s, 420^s	445	473	438^h	505	528	511^p, 528^p
$M_{2,3}M_{4,5}(^3P_{0,1,2})$	400		418^h, 393^p	452		438^p	512		490^h, 512^s
$M_{2,3}M_{4,5}(^3D_{1,2,3})$	400		398^p, 405^p	452		470^p	512		530^h, 530^s
$M_{2,3}M_{4,5}(^1D_2)$	404			456		445^p	516		492^s, 497^p
$M_{2,3}M_{4,5}(^3F_{2,3,4})$	404			456			516		
$M_5M_5(^1S_0)$	432	450	450^s, 452^h	488	509	475^h, 510^h	553	569	575^h
$M_{4,5}M_{4,5}(^3P_{0,1,2})$	437			493			559		573^s
$M_{4,5}M_{4,5}(^3F_{2,3,4})$	437		434^p, 445^p	493		505^p, 490^p	559		570^p
$M_{4,5}M_{4,5}(^1D_2;^1G_4)$	437			493			559		

*These values were obtained from equation (74) using $\Delta Z = 1$ for L_3MM transitions; required binding energies were taken from the report by Siegbahn.[16]

**Experimental values are those by (s) Simmons,[84] (h) Haas et al.,[85] and (p) Palmberg.[86]

transition levels might be considered as an interpretation of doubtful validity. In cases such as this, however, it must be recalled that the technique of Auger spectroscopy, as now utilized (compare Chapter I, Auger Electron Spectroscopy), is such that precise identification of the peak energies is quite difficult. This arises from complications encountered in calibration and, to a greater extent, from the fact that the data is obtained by taking the derivative of the principal experimental energy curve. This latter approach, though necessary, acts to obscure the location of the central peak with the result being an ambiguous assignment for the peak energy. This situation is, of course, well illustrated by the broad scatter of the experimental data cited in the table and, as a result, the identification of peaks is more reasonable than one might at first suspect. Note that the data by Palmberg[86], which is the most recent, seems to provide better agreement with our results than that of Haas[85] or Simmons[84] and, in this sense, may be argued to be the most accurate. Even with this data, however, there are discrepancies and the reasons for this need to be considered. The most obvious criticism would be to suspect the calculations and the associated computational scheme. This is best left for the discussion of Chapter IV, however, and it is sufficient to note at this stage that the neglect of relativistic effects is a possible error. In addition to this source of error, the experiments were performed on solid state samples rather than for isolated atoms as assumed in the calculations. Although the basic results are not expected to change drastically because of this (compare with previous remarks), one should still anticipate a work function correction being necessary. This could

then introduce a discrepancy into the observed data. In conclusion, we have found that the agreement with the available experimental energy data is adequate and, in many instances, quite good. Possible reasons for the discrepancies have been or will be discussed; the important point, however, is the re-assignment of peaks corresponding to different transitions than those obtained via Bergström-Hill predictions.

The remaining feature of the computation is that of the transition probabilities for the cases of (Ti, V, Cr). These results are presented in Table 4 and will now be discussed. Note that the data is given in atomic time units (2.42×10^{-17} sec.) or, more correctly, in inverse atomic time units. In these units the fundamental form of the relationship for transition probabilities changes from (75) to

$$\omega_{i \to f} = \pi \left| \langle f | A | i \rangle \right|^2 \rho \quad . \tag{159}$$

with the energy units being Rydbergs (13.6 ev). If one carries the analysis of Chapter II through with this form, it is found to be necessary that $\left(\frac{2\pi}{\hbar}\right)$ be everywhere replaced by (π) while the electrostatic operator, $\frac{e^2}{r_{12}}$, is replaced by $\frac{2}{r_{12}}$. With these slight changes, all other results remain formally the same except that different units are in effect. Also we recall that the energy normalization (142) is used in the calculations for the continuum function. As a result, the density of states factor is unity (compare (143)) and may be dropped from consideration. This, of course, represents an

Table 4. LMM Auger Transition Probabilities in the Intermediate Coupling Limit (in atomic time units) [multiply all entries by 10^{-3}]

	Ti		V		Cr	
	L_1	$L_{2,3}$	L_1	$L_{2,3}$	L_1	$L_{2,3}$
$M_1M_1\ (^1S_0)$	.8419	.0898	.8113	.0833	.8532	.0872
$M_1M_2\ (^3P_0)$	.2367	.2746	.2330	.2627	.2407	.2694
$M_1M_2\ (^3P_1)$	.7126	.8237	.7014	.7880	.7259	.8077
$M_1M_3\ (^3P_2)$	1.1582	1.3737	1.1664	1.3151	1.2063	1.3476
$M_1M_3\ (^1P_1)$	2.0559	.2406	2.0222	.2331	2.0655	.2395
$M_1M_4\ (^3D_1)$	.1736	.0184	.1738	.0222	.1691	.0214
$M_1M_4\ (^3D_2)$	.2898	.0306	.2904	.0370	.2820	.0357
$M_1M_5\ (^3D_3)$	.4051	.0428	.4063	.0517	.3945	.0500
$M_1M_5\ (^1D_2)$	2.5040	.1067	2.6186	.0886	2.5337	.0722
$M_2M_2\ (^3P_0)$	.00104	.3246	.00109	.2898	.00062	.2729
$M_2M_3\ (^3P_1)$	0.	.9656	0.	.8600	0.	.8071
$M_2M_3\ (^3P_2)$	.00026	1.6230	.00067	1.4497	.00022	1.3655
$M_3M_3\ (^1S_0)$	.1538	.7680	.1229	.6697	.0545	.6298
$M_3M_3\ (^1D_2)$	.0197	2.5335	.0363	2.2462	.0090	2.1132
$M_2M_4\ (^3F_2)$	.0168	.0259	.0142	.0329	.0127	.0350
$M_2M_4\ (^3P_1)$	.00658	.1425	.0089	.1668	.00756	.1458
$M_2M_5\ (^3F_3)$	.0248	.0122	.0212	.0115	.0194	.0108
$M_2M_5\ (^1D_2)$	.00076	.4368	.00083	.5171	.00094	.4723
$M_3M_4\ (^3P_0)$	.00250	.0520	.00362	.0635	.00331	.0585
$M_3M_4\ (^3P_2)$	.0114	.2444	.0159	.2931	.0142	.2651
$M_3M_4\ (^3D_1)$	.00093	.0550	.00186	.0690	.00236	.0723
$M_3M_4\ (^3D_3)$	.00038	.0947	.00085	.1019	.00113	.0940
$M_3M_5\ (^3F_4)$	.0317	.0143	.0268	.0125	.0244	.0108
$M_3M_5\ (^3D_2)$	.00110	.0826	.00190	.0964	.00217	.0940
$M_3M_5\ (^1P_1)$	.00275	.6111	.00444	.7624	.00493	.7056
$M_3M_5\ (^1F_3)$	.4274	2.2845	.7548	2.8928	.7150	2.6640
$M_4M_4\ (^3F_2)$	.0000	.1682	.00001	.3340	.00002	.2872
$M_4M_4\ (^3P_0)$	.0000	.0060	.00001	.0104	.00002	.0090
$M_4M_5\ (^3F_3)$	0.	.2353	0.	.4674	0.	.4018
$M_4M_5\ (^3F_4)$	.00004	.3028	.00012	.6015	.00015	.5172
$M_4M_5\ (^1D_2)$	.0127	.2723	.0169	.6372	.0159	.5317
$M_4M_5\ (^3P_1)$	0.	.0180	0.	.0311	0.	.0269
$M_5M_5\ (^3P_2)$	.00224	.0727	.00026	.0605	.00032	.0548
$M_5M_5\ (^1G_4)$	.4293	1.9228	.9276	3.8571	.8044	3.3088
$M_5M_5\ (^1S_0)$	.0259	.0439	.0510	.0816	.0450	.0700

enormous simplification from the situation encountered for the solid state system.

Now the data in Table 4 should be compared to experimental results in order to determine the validity of the predictions. This is, unfortunately, not possible for the elements in question since there are essentially no experimental LMM Auger intensities. Even the area of theoretical activity is relatively free of data but recently some results have been forthcoming and, in the absence of experimental data, these results are compared in Table 5 with the present computations. The theoretical results are those of Walters and Bhalla[24] and McGuire.[23] The computations of the former authors are analogous to those performed in this work with the basic difference being the use of the Hartree-Fock-Slater scheme (with an exchange term due to Herman, Van Dyke, and Ortenburger[87]) rather than the more precise Hartree-Fock computation used here. In addition, Walters and Bhalla computed total Auger transition rates (but only for initial 2p vacancies) so that they compute no multiplet structure; instead, their results are given for the possible configurations $3s^2$, 3s3p,... . In order to compare with the present results, it is therefore necessary that one form the <u>total</u> predicted transition rates from Table 4 for the different configurations. This is readily accomplished by adding the relevant results in the table. For example, the total 3s3p transition rate is obtained by adding together the predictions for the lines

$$L_{2,3}\left[M_1M_2(^3P_{0,1});\ M_1M_3(^3P_2,\ ^1P_1)\right]$$

with the result being 2.7126×10^{-3} $(au)^{-1}$. By proceeding in this fashion for all the configurations, one achieves the results listed in the row labeled "Present" in Table 5. As regards the work of McGuire[23], he performed the computations in the jj-coupling limit so that the total rates are computed from his data as in the above. It should be noted that the procedure used by McGuire in the computations involves, in our view, several major approximations which mar the value of his results. In particular, the pertinent electron wave functions were computed by utilizing an approximation to the appropriate Hermann-Skilman potential. The details of this procedure are best left to the referenced work; it is sufficient to note here that the Hermann-Skilman potential can be significantly in error so that any approximation to it must be made quite carefully.

Now consider the L_1 data in Table 5. We note that the agreement is fairly good for the configurations $3s^2$ and $3p^2$ but beyond this the disagreement is apparent. It reaches a maximum in the case of the 3s3d data with our results being larger than McGuire's by a factor of four. The reasons for this large discrepancy presumably result from the sources cited above, but it is not clear why the agreement and disagreement vary so widely. As regards the $L_{2,3}$ transition data, the additional work of Walters and Bhalla[24] is available for Ti, V, Cr with McGuire data for Ti. Comparing these results, the general pattern is one of disagreement. Only for the $3s^2$ and $3p^2$ configurations may agreement be reasonably claimed and even for $3p^2$ there are discrepancies. It is clear from the Ti data that McGuire's results sometimes agree with the present data ($3s^2$, $3p^2$), sometimes with that of Walters and

Table 5. Comparison of LMM Auger Transition Rates with Theory (in atomic units)

	3s3s	3s3p	3s3d	3p3p	3p3d	3d3d
L_1 transitions						
Ti: McGuire	.91	5.28	.86	.16	.192	.071
Present	.84	4.16	3.37	.175	.59	.47
$L_{2,3}$ transitions						
Ti: W & B	.0820	1.61	.0505	5.69	1.22	1.38
McGuire	.0900	1.64	.0600	6.14	1.34	.177
Present	.0898	2.71	.198	6.21	4.06	3.04
V: W & B	.0830	1.62	.0744	5.74	1.93	4.52
Present	.0833	2.60	.20	5.52	5.02	6.08
Cr: W & B	.0808	1.55	.107	5.48	2.87	1.24
Present	.0872	2.66	.18	5.19	4.63	5.21

The data referenced is that of McGuire[23] and Walters and Bhalla[24]; all numbers multiplied by 10^3.

Bhalla (3s3p, 3s3d, 3p3d) and with neither in the $3d^2$ case. These observations, when coupled with the analogous behavior in the L_1 data, suggest that the McGuire procedure for computations produces results which are internally inconsistent--i.e., they fluctuate. This conclusion, of course, is valid only for comparison with theoretical results so that there may be no real significance to this apparent behavior. The situation does, however, amplify the need for experimental data to check the validity of the different treatments. The general tone of disagreement, though more consistant, continues when the Walters and Bhalla data for (Ti, V, Cr) is compared with the current results. Once again, the disagreement is greatest in the 3p3d and $3d^2$ configurations although it still exists for the 3s3p and 3s3d cases. One apparent anomaly is the sudden jump and subsequent drop in the prediction by Walters and Bhalla for the $3d^2$ configuration. Thus in proceeding from Ti to Cr, these authors predict the intensity sequence

Ti	V	Cr
1.38	4.52	1.24

whereas our results, though showing the jump and drop, are not nearly so drastic--especially in going from V to Cr. A similar situation occurs in the 3p3d data. Thus our results indicate that the total 3p3d transition rate increases rather sharply ($4.06 \rightarrow 5.02$) in going from Ti to V and then decreases slightly in Cr ($5.02 \rightarrow 4.63$); in opposition to this, the Walters and Bhalla data predicts a progressive rise in the total rates with all values being less than those predicted by our

results. The source of this general disagreement in the two predictions presumably lies in the different methods (Hartree-Fock in our work, Hartree-Fock-Slater in the other) utilized to get the electron wave functions. Once again, however, the final appeal must be made to experiment if the discrepancies are to be actually resolved.

As cited previously, experimental intensity data for LMM transitions in (Ti, V, Cr) is practically non-existent. The only such data available at this time appears to be that obtained by Haas[88] for vanadium. This data was obtained by Auger spectroscopy and is just the N(E) curve described in Chapter I; it is shown in Figure 9. From the nature of this curve, it then follows that intensity measurements can be made of the various peaks. Due to the presence of an overall background signal in the data, however, these measurements are expressed in Table 6 as relative intensities rather than absolute. The designations A, B, C... in this table refer to the peaks resolved in the data; they were identified, with the aid of Table 3, and the identifications are as follows:

A	385 ev	$M_1M_{2,3}(^3P_{0,1,2})$	
B	400 ev	$M_3M_3(^1S_0, ^1D_2)$	
C	412 ev	$M_2M_{2,3}(^3P_{0,1,2})$	
D	432 ev	$M_3M_5(^1F_3)$	(160)
E	438 ev	(all other 3p3d lines)	
F	472 ev	$M_{4,5}M_{4,5}(^1G_4)$	
G	510 ev	(all other $3d^2$ line except $^1S_0$) .	

Table 6. Relative Intensities in Vanadium: Comparison with Experiment

	A	B	C	D	E	F	G
Computed	1.00	1.23	1.10	1.22	.90	1.63	.90
Experiment	1.00	1.17	1.61	2.22	2.24	2.27	1.22

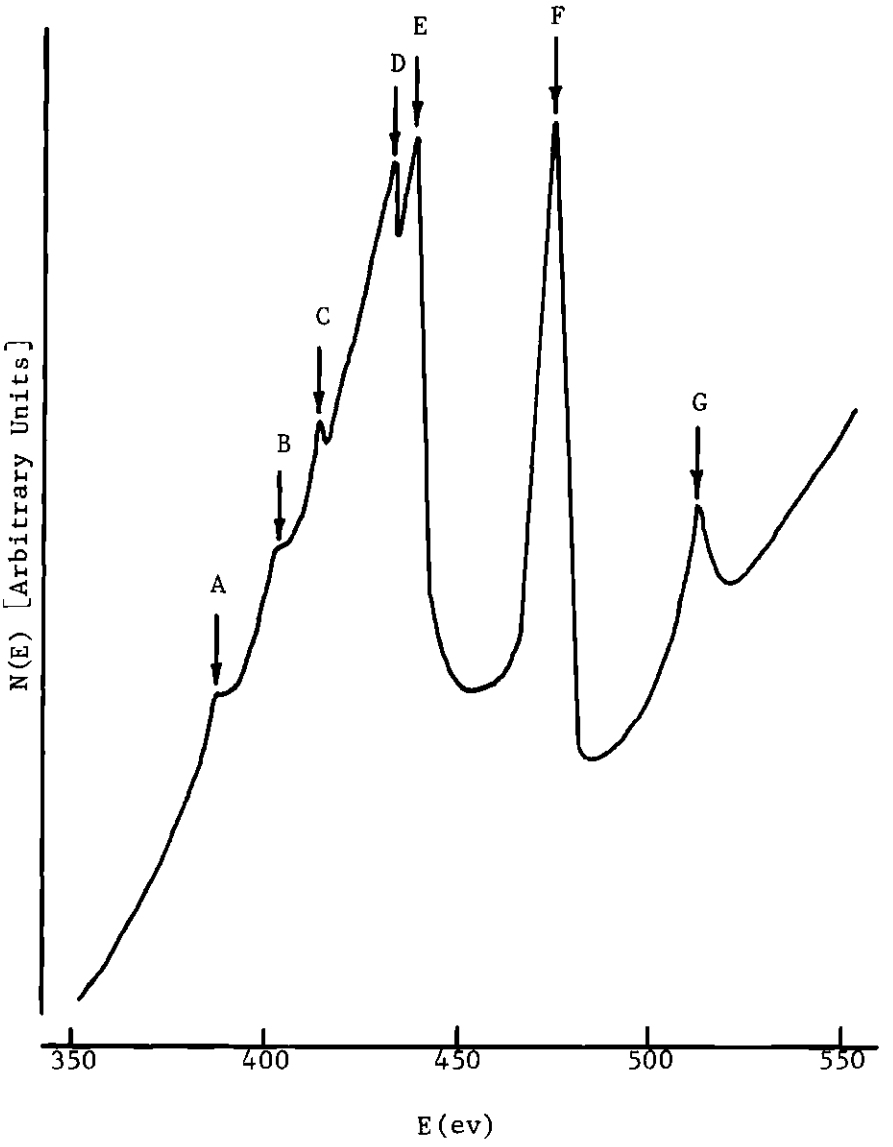

Figure 9. N(E) vs. E Curve for Vanadium

It is clear from Table 6 that the agreement is quite poor, especially for the D, E, F lines. There are, of course, many possible reasons for this disagreement other than the computations being inherently wrong. Thus the background signal in the data is not flat and, in fact, not even linear. As a result, the contribution to the different peaks due to this signal will change with their energy. It is then clear that the ratio taken in obtaining the relative intensities will not entirely eliminate the background contribution. In addition to this avenue of error, it must be recognized that the data was obtained from a solid so that the Auger electron, as it exits the sample, can undergo energy loss processes via plasmon creation or excitation of an interband transition. Although the peaks observed do not seem to have energies consistent with these energy loss mechanisms, the fact that they exist must be recognized. Finally, it is possible that our Auger energy predictions are sufficiently in error that the wrong assignment (160) has been given to the peaks observed. This would obviously give rise to incorrect intensities, perhaps leading to discrepancies such as those shown in the table. Other possibilities which may explain some of the disagreements (e.g., the experimental data could be in error) also exist but a discussion of these is not necessary at this time. We reserve the bulk of this type of comment to Chapter IV.

In conclusion, we have determined the LMM Auger energies and transition probabilities for (Ti, V, Cr). A comparison of these results with the available experimental data leads to a different interpretation of the observed lines than that based on Bergström-Hill predictions. As for the transition probabilities, the agreement with the

single experiment performed on V is quite poor. This only serves to emphasize, however, the need for more experimental data.

Results for Zr, Nb, Mo

The computation of LMM Auger energies and transition probabilities in zirconium (Zr), niobium (Nb), and molybdenum (Mo) will now be discussed. The general procedure is again that shown in Figure 7 but for these elements the "exact" method is used in computing the energies. This gives rise to only slight changes in the formalism with the primary one arising from the labels assigned to the intermediate coupling levels. Thus the discussion following (51) in Chapter II demonstrated that the structure terms which enter the energy expressions contain a spin-orbit and an electrostatic contribution. It was further shown that the difference of the spectator and exact approaches was, except for average energies, solely in the spin-orbit structure terms. Since these terms determine the degree to which pure jj-coupling is attained (Chapter II), it then follows that the energy levels of the spectator and exact views will have different labels in this limit. The difference is illustrated in Figure 10 where the schematic level diagram for the exact view is presented. The basic configurations of this view are just

$$3s^0,\ 3s3p^5,\ 3s3d^9,\ 3p^53d^9,\ 3p^4,\ 3d^8$$

as follows from (55), and these are the levels of the central field limit in the figure. Note the difference in the label assignments (as compared to Figure 8) to the levels in the jj-limit as well as the correspondence of these states with those of the intermediate region.

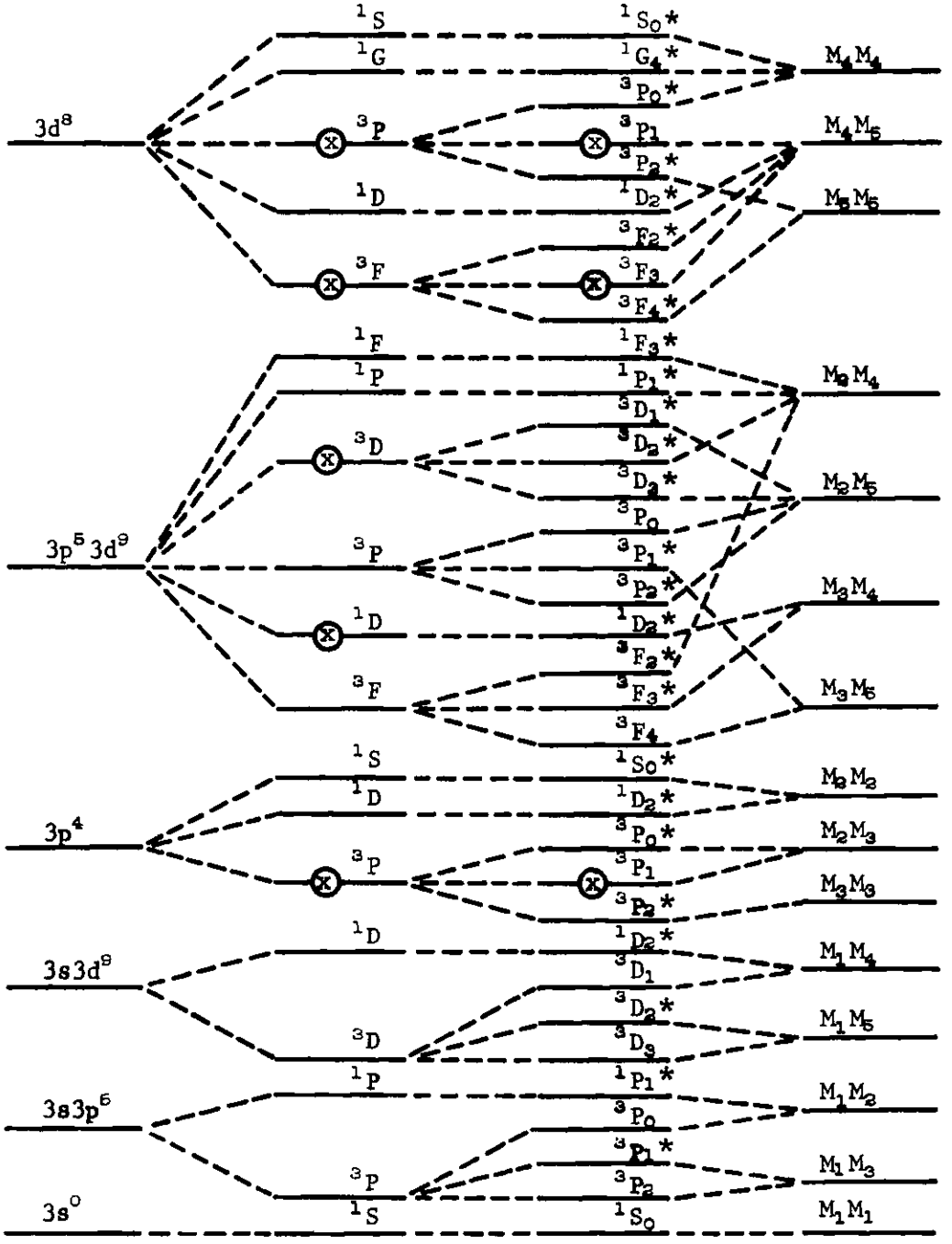

Figure 10. Schematic Energy Level Diagram for Computation of LMM Auger Energies by Direct Approach (not to scale).

Thus one has the levels arising from the $3s3p^5$ configuration labeled in the IC region as

$$M_1M_2(^1P_1, {}^3P_0) \quad \text{and} \quad M_1M_3(^3P_1, {}^3P_2)$$

while the analogous levels for the 3s3p configuration in the spectator view are denoted by

$$M_1M_2(^3P_0, {}^3P_1) \quad \text{and} \quad M_1M_3(^1P_1, {}^3P_2) \ .$$

There is, therefore, a different notation used when discussing Auger transitions computed in the intermediate coupling limit. It should be emphasized that only a difference in notation is involved, with the particular notation being dependent only on the scheme, spectator or exact, used in computing the Auger energies.

With this difference in notation now explained, the LMM Auger energies for (Zr, Nb, Mo) are presented in Table 7. This form of the data is again not particularly illuminating, but it is clear that the effect of the spin-orbit interaction has markedly increased. Thus the splitting arising from this interaction is as high as 17 ev in the $M_1M_{2,3}(^3P)$ level of molybdenum. This is to be compared with a 1 ev splitting for the same levels in Cr. A similar effect is evident for the other transition levels as well though less pronounced in those which correspond to the 3s3d, 3p3d and $3d^2$ transitions. These observations then clearly indicate the necessity of utilizing the formalism of intermediate coupling for LMM transitions in those elements whose atomic numbers (Z) are comparable with those of (Zr, Nb, Mo)--i.e., $Z \cong 40$.

Table 7. LMM Auger Transition Energies in the Intermediate Coupling Limit (electron volts)

	Zr		Nb		Mo	
	L_1	$L_{2,3}$	L_1	$L_{2,3}$	L_1	$L_{2,3}$
$M_1M_1\ (^1S_0)$	1547.8	1330.1	1649.6	1425.6	1735.7	1504.6
$M_1M_2\ (^3P_0)$	1639.0	1421.4	1743.8	1519.8	1832.8	1601.7
$M_1M_2\ (^1P_1)$	1622.7	1405.1	1727.4	1503.4	1816.4	1585.3
$M_1M_3\ (^3P_2)$	1652.2	1434.6	1758.7	1534.7	1849.7	1618.5
$M_1M_3\ (^3P_1)$	1645.3	1427.7	1751.1	1527.1	1841.3	1610.2
$M_1M_4\ (^3D_1)$	1786.1	1568.5	1898.1	1674.1	1994.5	1763.4
$M_1M_4\ (^1D_2)$	1778.2	1560.5	1890.1	1666.1	1986.4	1755.3
$M_1M_5\ (^3D_3)$	1788.6	1571.0	1901.0	1677.0	1997.8	1766.7
$M_1M_5\ (^3D_2)$	1787.3	1569.6	1899.5	1675.5	1996.1	1765.0
$M_2M_2\ (^1S_0)$	1696.1	1478.5	1802.9	1578.9	1893.9	1662.8
$M_2M_3\ (^3P_1)$	1717.2	1499.5	1825.8	1601.8	1918.7	1687.6
$M_2M_3\ (^1D_2)$	1712.3	1494.7	1820.8	1596.7	1913.6	1682.5
$M_3M_3\ (^3P_0)$	1722.1	1504.5	1831.9	1607.9	1926.2	1695.1
$M_3M_3\ (^3P_2)$	1728.8	1511.2	1839.0	1615.0	1933.8	1702.7
$M_2M_4\ (^3D_2)$	1862.0	1644.4	1976.9	1752.8	2076.1	1845.0
$M_2M_4\ (^1P_1)$	1851.0	1633.4	1965.3	1741.3	2064.0	1832.9
$M_2M_5\ (^1F_3)$	1851.8	1634.2	1966.6	1742.6	2065.9	1834.8
$M_2M_5\ (^3P_2)$	1866.9	1649.2	1981.6	1757.6	2080.7	1849.6
$M_3M_4\ (^3P_0)$	1872.4	1654.7	1988.4	1764.4	2089.1	1858.0
$M_3M_4\ (^1D_2)$	1874.0	1656.3	1990.1	1766.1	2090.8	1859.7
$M_3M_4\ (^3D_1)$	1867.6	1649.9	1983.5	1759.5	2084.0	1852.9
$M_3M_4\ (^3D_3)$	1870.6	1653.0	1986.7	1762.7	2087.3	1856.2
$M_3M_5\ (^3F_4)$	1884.1	1666.5	2000.9	1776.9	2102.2	1871.1
$M_3M_5\ (^3F_2)$	1881.4	1663.7	1997.9	1773.9	2099.1	1868.0
$M_3M_5\ (^3P_1)$	1872.6	1654.9	1988.8	1764.7	2089.5	1858.4
$M_3M_5\ (^3F_3)$	1878.8	1661.1	1995.0	1771.0	2095.8	1864.7
$M_4M_4\ (^3P_2)$	2014.6	1796.9	2136.6	1912.6	2243.2	2012.1
$M_4M_4\ (^1S_0)$	2002.4	1784.7	2123.9	1899.9	2230.1	1999.0
$M_4M_5\ (^3F_3)$	2020.7	1803.1	2143.1	1919.1	2250.2	2019.1
$M_4M_5\ (^1G_4)$	2013.7	1796.1	2135.9	1911.8	2242.6	2011.5
$M_4M_5\ (^1D_2)$	2017.2	1799.5	2139.5	1915.5	2246.5	2015.4
$M_4M_5\ (^3P_1)$	2015.1	1797.4	2137.3	1913.2	2244.1	2013.0
$M_5M_5\ (^3F_2)$	2020.0	1802.4	2142.5	1918.5	2249.6	2018.5
$M_5M_5\ (^3F_4)$	2022.8	1805.2	2145.6	1921.6	2253.0	2021.9
$M_5M_5\ (^3P_0)$	2015.1	1797.4	2137.3	1913.3	2244.2	2013.1

In order to further examine our results, a comparison with available experimental data is shown in Table 8. This data was read directly from the "Varian Chart of Auger Energies" compiled by Strausser and Uebbing[89] and, as a result, the uncertainty of the energies is rather large. The experimental peaks in the table are thus given with lower and upper bounds between which the true peak energy resides. The problem is similar to that cited in the Auger data of (Ti, V, Cr) although it is a little more severe in the present case. Allowing for this difficulty, however, the table illustrates that the agreement between experiment and theory is quite good with the maximum deviation being about 25 ev in the case of the $M_4M_4(^1S_0)$ transition in Nb. The table also demonstrates the fact that the identification of a peak with a given intermediate coupling label is ambiguous at best. Thus it is not clear whether the experimental peak observed with the range 1510-1540 ev is due to the $M_2M_3(^1D_2)$ transition or to one of the $M_{2,3}M_3(^3P_{0,1,2})$ lines. All that can be asserted with confidence is that it corresponds to one of these lines--i.e., the peak arises from a $3p^2$ type transition--with the result being that all possible assignments are given in the table. Similar considerations for the other experimental points also give rise to multiple peak assignments, and from these one concludes that the observed peaks correspond to 3s3d, 3p3d, and $3d^2$ transitions as well as those of the $3p^2$ type. One surprising feature of these conclusions is the lack of a peak corresponding to a 3s3p transition. Such a peak would be expected on the basis of our considerations with the data for (Ti, V, Cr), and the fact that it was apparently not resolved should be checked. Indeed, only if more experiments are

Table 8. Comparison of LMM Energies with Experiment for Zr, Nb, Mo (electron volts)

$L_{2,3}$	Zr			Nb			Mo		
	Calc.	B-H*	Exp.**	Calc.	B-H*	Exp.**	Calc.	B-H*	Exp.**
$M_2M_3(^1D_2)$	1495	1515	1510	1597	1599	1595	1683	1685	1675
$M_2M_3(^3P_1)$	1500		to	1602		to	1688		to
$M_3M_3(^3P_0)$	1505	1529	1540	1608	1615	1630	1695	1702	1710
$M_3M_3(^3P_2)$	1511			1615			1703		
$M_1M_4(^1D_2)$	1561	1584	1535 to	1666	1672	1625 to	1755	1758	1700 to
$M_1M_{4,5}(^3D_{0,1,2})$	1570	1607	1565	1675	1675	1660	1765	1762	1740
$M_2M_{4,5}(^1P_1, ^1F_3)$	1633	1670 to	1650	1742	1762 to	1750	1834	1853 to	1850
$M_3M_{4,5}(^1D_2, ^3P_{0,1})$	1655		to	1765		to	1858		to
$M_{2,3}M_{4,5}(^3P_2, ^3D_1)$	1650		1680	1759		1780	1851		1880
$M_3M_5(^3F_2)$	1664	1687	1675	1774	1781	1775	1868	1874	1875
$M_3M_5(^3F_3)$	1661		to	1771		to	1865		to
$M_3M_5(^3F_4)$	1667		1720	1777		1825	1871		1925
$M_4M_4(^1S_0)$	1785	1832	1755-1775	1900	1933	1860-1875	1999	2033	1960-1980

* Values obtained from equation (74) using $\Delta Z = 1$ for L_3MM transitions and Siegbahn[16] binding energies

** Data read from "Varian Chart of Auger Energies" prepared by Strausser and Uebbing.[89]

performed can the responsibility for this discrepancy be traced to features in the theory or in the data.

It should also be noted that the peak assignments listed in Table 8, though uncertain in the respect cited above, still differ from those given in the chart of Auger energies. This is expected since the latter assignments were made on the basis of the Bergström-Hill relation, and the situation is thus similar to that encountered in the results for (Ti, V, Cr). One added feature of our results is the identification of the $M_4M_4(^1S_0)$ peak listed in the table. This peak was not labeled on the chart since no Bergström-Hill prediction gives results which are close to the observed values. We have, therefore, improved on the interpretation of the observed peaks beyond that involved in a reassignment of the peak labels. A reversal of this situation also exists since the chart lists the peaks

	Zr	Nb	Mo
A	1840-1880 ev	1930-1980 ev	2020-2075 ev
B	1920-1950 ev	2025-2060 ev	2140-2175 ev

(161)

as corresponding to $L_3M_{4,5}M_{4,5}$(A) and $L_2M_{4,5}M_{4,5}$(B) lines--i.e., they arise from $3d^2$ type transitions. Our results for such transitions, however, indicate that energies for $L_{2,3}M_{4,5}M_{4,5}$ lines are significantly less that these values (compare Table 7). As a result of this, we considered the possibility of an alternate interpretation of these peaks. If the "A" peak in zirconium is chosen for definiteness, it is evident from Table 7 that the most likely candidate for this energy is a 3p3d transition which fills an initial 2s vacancy (i.e., an $L_1M_{2,3}M_{4,5}$

transition). Indeed, these results, when used in conjunction with the transition probabilities cited in Table 9, indicate that the transition $L_1M_2M_5(^1F_3)$ is the appropriate label for the observed peak. It is true, of course, that other transitions may contribute but the $^1F_3$ line is by far the most probable. A similar view can be taken for the "A" line in Nb and Mo with the conclusions being the same. The situation is more confused with the "B" line, however, and it is not clear how the peak should be assigned. The most likely candidate is again an $L_1M_{2,3}M_{4,5}$ type transition which would give discrepancies as small as 25 ev in the case of Nb. This is rather large for one to be confident of the peak assignment so that no real decision can be made. Evidently, the situation is again such that additional experimental data is required before the problem can be resolved.

The intermediate coupling transition probabilities for (Zr, Nb, Mo) are given in Table 9. Except for the slight changes in notation already mentioned, the results are similar to those obtained in Table 4. One point which can be made at once concerns the data for the $L_1M_{2,3}M_{4,5}$ transitions. The table clearly indicates that the most probable of these transitions is that of the $L_1M_2M_5(^1F_3)$ line. This observation is in obvious accord with the previous remarks made concerning the assignment of the "A" peaks cited in (161). Further discussion of the data listed in Table 9 is once again handicapped by the lack of experimental data. The comparisons which can be made are, therefore, constrained to the case of theoretical results as with the data for (Ti, V, Cr). Such a comparison, using the total transition rates computed by McGuire[23] and Walters and Bhalla[24], is given in

Table 9. LMM Auger Transition Probabilities in the Intermediate Coupling Limit (in atomic time units) [multiply all entries by 10^{-3}]

	Zr		Nb		Mo	
	L_1	$L_{2,3}$	L_1	$L_{2,3}$	L_1	$L_{2,3}$
$M_1M_1\ (^1S_0)$	1.1958	.1079	1.2404	.1076	1.2629	.1073
$M_1M_2\ (^3P_0)$	.4061	.3837	.4055	.3859	.4187	.3972
$M_1M_2\ (^1P_1)$	3.0938	.4028	3.1101	.4219	3.1140	.4455
$M_1M_3\ (^3P_2)$	2.0064	1.9112	2.0065	1.9302	2.0964	1.9682
$M_1M_3\ (^3P_1)$	1.3723	1.0786	1.4043	1.0729	1.4921	1.0861
$M_1M_4\ (^3D_1)$	.4155	.0633	.4199	.0687	.4380	.0711
$M_1M_4\ (^1D_2)$	6.9939	.0311	7.2069	.0275	7.4094	.0263
$M_1M_5\ (^3D_3)$	.9639	.1478	.9769	.1603	1.0229	.1661
$M_1M_5\ (^3D_2)$	.8076	.1041	.8503	.1124	.9289	.1158
$M_2M_2\ (^1S_0)$	.0571	.7994	.0570	.8057	.0546	.8103
$M_2M_3\ (^3P_1)$	0.	1.3024	0.	1.3921	0.	1.3700
$M_2M_3\ (^1D_2)$	.1835	3.0938	.1934	3.4088	.2031	3.3303
$M_3M_3\ (^3P_0)$	.0345	.6342	.0362	.6825	.0389	.6975
$M_3M_3\ (^3P_2)$	.0381	2.5176	.0424	2.4419	.0467	2.4871
$M_2M_4\ (^3D_2)$	.0057	.4163	.00506	.4225	.00467	.4251
$M_2M_4\ (^1P_1)$	.0804	1.6181	.0833	1.6360	.0867	1.7301
$M_2M_5\ (^1F_3)$	2.8122	6.4353	2.9075	6.6324	2.9648	6.9942
$M_2M_5\ (^3P_2)$	.0133	.5068	.0137	.5353	.0151	.5652
$M_3M_4\ (^3P_0)$	.00553	.1585	.00577	.1656	.00601	.1720
$M_3M_4\ (^1D_2)$	.00285	1.0566	.00308	1.1236	.00328	1.1847
$M_3M_4\ (^3D_1)$	.0245	.5829	.0290	.6620	.0363	.7326
$M_3M_4\ (^3D_3)$	.2513	.7434	.3120	.8818	.3774	1.0326
$M_3M_5\ (^3F_4)$	.00655	.00531	.00560	.00415	.00476	.00380
$M_3M_5\ (^3F_2)$	.00977	.32470	.0101	.3388	.0103	.3518
$M_3M_5\ (^3P_1)$	.0158	.4518	.0168	.4789	.0181	.5064
$M_3M_5\ (^3F_3)$	.02490	.0808	.0237	.0865	.0218	.0914
$M_4M_4\ (^3P_2)$	.0839	1.3691	.0919	1.5039	.1028	1.6312
$M_4M_4\ (^1S_0)$	.2838	.3841	.3009	.3981	.3160	.4240
$M_4M_5\ (^3F_3)$	0.	1.7342	0.	1.8170	0.	1.8931
$M_4M_5\ (^1G_4)$	3.3272	13.6030	3.4875	14.409	3.6268	15.052
$M_4M_5\ (^1D_2)$	.0515	1.0789	.0433	1.0518	.0360	1.0190
$M_4M_5\ (^3P_1)$	0.	.1557	0.	.1655	0.	.1791
$M_5M_5\ (^3F_2)$	.0338	1.4448	.0432	1.5588	.0561	1.6667
$M_5M_5\ (^3F_4)$	.0404	2.3694	.0508	2.4971	.0618	2.6335
$M_5M_5\ (^3P_0)$	.0112	.0648	.0146	.0718	.0187	.0812

Table 10. Comparison of Transition Rates with Theory: Zr, Nb, Mo

	3s3s	3s3p	3s3d	3p3p	3p3d	3d3d
L_1 Transitions						
Zr: McGuire	1.17	7.08	9.06	.34	3.90	10.34
Present	1.20	6.88	9.18	.313	3.25	3.83
$L_{2,3}$ Transitions						
Zr: W & B	.0980	2.07	.383	8.05	14.7	22.5
McGuire	.100	1.96	.40	8.68	14.73	24.34
Present	.108	3.78	.346	8.35	12.38	22.20
Nb: W & B	.0994	2.11	.396	8.24	15.3	23.6
Present	.108	3.81	.369	8.73	12.97	23.47
Mo: W & B	.101	2.16	.409	8.42	15.9	24.7
Present	.107	3.90	.379	8.69	13.79	24.6

The referenced work is that of McGuire[23] and Walters and Bhalla.[24] [data in atomic units, multiplied by 10^3]

Table 10. The similarity of this with Table 5 for (Ti, V, Cr) is obvious and since the data derives from identical sources, it is unnecessary to discuss the nature of these other calculations.

We concentrate at first on the L_1MM predictions of McGuire.[23] It is clear that the agreement of the two approaches is much better for Zr than was the case in Ti. Indeed, it is only in the case of the $3d^2$ transitions that the disagreement is extreme with our result being smaller by a factor of about three. It is, of course, difficult to ascertain the correctness of either prediction without experiment but, due to the excessive approximations in McGuire's work, it is most likely that our results are the more accurate. This view is substantiated when the comparison of data for $L_{2,3}$ transitions is considered for the $3d^2$ transitions. Thus the results by Walters and Bhalla[24], obtained using a technique quite similar to the Hartree-Fock approach, compare extremely well with our results for Zr, Nb and Mo. For the Zr case, however, it is evident that the McGuire data is larger than either of the other predictions. This implies that the McGuire results are too large, at least for $3d^2$ transitions, when $L_{2,3}MM$ transitions are considered. Since the same technique is applied to L_1MM transitions as for the $L_{2,3}$ variety, it is argued that the McGuire $3d^2$ results are also too large in the case of L_1 transitions. This, of course, means that the $3d^2$ total transition rate for L_1 transitions is approximately 4 (i.e., our results) and not 10 as obtained by McGuire.

An examination of the Zr data for transitions other than those of the $3d^2$ type indicates that McGuire's results still have a tendency to fluctuate when compared with the other two approaches. Thus the

McGuire values agree quite well with those of Walters and Bhalla for the 3s3p, 3s3d and 3p3d transitions as well as the $3s^2$ case. Agreement with our results is found in the $3s^2$ and $3p^2$ while the McGuire data is inconsistent with either, as cited above, for the $3d^2$ transitions. If one now extends the examination of the $L_{2,3}$ data to include Nb and Mo, it becomes clear that discrepancies still exist between the present results and those of Walters and Bhalla. These are, however, approximately the same as in the data for (Ti, V, Cr) indicating that the deviations arise from the particular approach taken. Since the primary difference in the two schemes is in the use of the Hartree-Fock-Slater (HFS) procedure by Walters and Bhalla as compared with the use of Hartree-Fock in our case, we conclude that the discrepancies in the data arise basically from the different wave functions obtained with these different procedures. A second difference in the two schemes which could explain some of the deviation is the computation of the Auger energies. Thus Walters and Bhalla[24] utilize essentially a Bergström-Hill approach with the binding energies used being obtained from their HFS results. This is evidently to be compared with our computations via the total energy approach. Since this latter procedure is the most accurate, we would conclude that our results are indeed the most accurate of those considered here. Once again, however, a final decision must reside in experiment and there are, unfortunately, very few experiments which have considered LMM transitions.

CHAPTER IV

CONCLUSIONS AND RECOMMENDATIONS

This work has presented the results of computations for LMM Auger energies and transition probabilities in the elements Ti, V, Cr, Zr, Nb, and Mo. The calculation of the energies was made by a total energy approach wherein the total energies of the initial (singly ionized) and final (doubly ionized) atomic states were computed. By taking the difference of these, the Auger energy was computed at once. The situation was complicated somewhat by the existence of multiplet spectra which produce several energies for the same Auger transition. Thus in order to obtain spectra in agreement with the predictions of the traditional two-electron Auger theory of Wentzel,[3] it was necessary to introduce two separate methods--the spectator and "exact"--for computing the relevant total energies. The spectator approach is utilized for all elements with incomplete M subshells (3s, 3p, 3d) and was therefore used in the calculations for Ti, V, and Cr. If the elements have complete M subshells, then the "exact" method is used. This was then the method used in Zr, Nb, and Mo. Explicit formulae for LMM energies which are valid in either of these schemes were obtained and presented in tabular form. These results are for the case of intermediate coupling between the two M shell electrons.

The computation of the LMM transition probabilities was straightforward, once the Auger energies were obtained, with the Wentzel

formulae being used. The primary improvement instituted in these calculations was in the use of the Hartree-Fock formalism to compute the relevant bound state electron wave functions of the problem. The results were further improved by carrying out a separate Hartree-Fock computation for each initial and final atomic state. This served to, at least partially, take into account the "relaxation" of the electron orbitals due to the transition. The results obtained by this procedure were then discussed in some detail. It should be noted that, in addition to these primary data, the formulae for LMM transition probabilities as well as the pertinent intermediate coupling mixing coefficients were also obtained (Appendices C and D).

In the discussion of the results obtained by the above procedure, the most significant feature was the lack of experimental data for all of the elements treated. Due to this deficiency, it was not possible to properly analyze the theoretical results and, therefore, the appraisal of the theory was necessarily incomplete. It was found that the energy calculations gave results which differed significantly from the traditional Bergström-Hill predictions for the LMM transitions. As a result, the interpretation of the experimental data was different from that presented in the original reports of the data. Peaks originally identified, for example, as arising from a $3s^2$ type transition in (Ti, V, Cr) were reinterpreted by our results as arising from a 3s3p type transition. In addition to this reassessment of data, a resolved but previously unlabeled peak in Zr, Nb and Mo was interpreted by our data as arising from a $3d^2$ type transition. All of this was possible by a comparison of observed and theoretical energies. The

almost complete lack of experimental intensity data for the elements in question prevented any similar comparison of our transition rate data. One conclusion which is possible without this data depends only on the basic theoretical results. Thus the small splitting of LS-coupling levels in going to the intermediate coupling (IC) formalism demonstrated that it is not necessary to treat LMM transitions in (Ti, V, Cr) in the IC limit. This then allows a significant simplification in treating such transitions in these elements. For the case of Zr, Nb, and Mo, however, the situation is changed as the splitting of the levels in the IC region becomes significant. This serves to demonstrate the necessity of using intermediate coupling when treating LMM transitions in these elements.

One additional point regarding this work should be mentioned. It is not clear that the Wentzel two-electron formulation for the Auger theory is correct. Indeed an alternate and more reasonable view would have the Auger dynamics arising from the electrostatic interaction of all electrons in the atom rather than just two as in the Wentzel treatment. Since Fano[61] recently presented a formalism capable of computing the matrix elements encountered in this view, a calculation was performed which treated LMM transitions in potassium in the Wentzel and this exact view. This served to introduce different spectra in the two schemes since the exact view includes the 4s electron in potassium when computing the Auger multiplet structure. Unfortunately, the results of this computation were ambiguous in the sense that it was not clear just how the predictions of the two views should be compared. The problem was compounded by the extremely weak coupling of the 4s electron

with the other electrons in potassium. As a result of these problems, we have not presented the details of our calculations in this work. It is sufficient to note the general result that the matrix elements encountered differ in the final results only in the angular factors; the radial integrals $R^k(ab, cd)$ are the same. The differences introduced by these angular factors are significant, however, and a calculation should be performed for an element for which ample experimental data is available. In this way, a meaningful assessment of these two views for the Auger dynamics can be accomplished.

In the process of carrying out the calculations summarized above, some potential deficiencies in the procedure have been noted. Since it is impossible to state without more experimental data that these are real defects in the treatment, we shall confine the present comments to those features which seem the most likely to introduce errors. We have stated several times that relativistic effects were neglected in performing this calculation. It was argued that the lack of a correct relativistic formulation of the Auger process made the inclusion of such effects of doubtful usefulness. But it has been reported[90] that relativistic calculations of the energy levels in Ti give rise to a shift in the 2s binding energy of as much as 40 ev. If this is true, then clearly the relativistic treatment could produce significant changes in the predicted energies. It should be noted that the reports of this shift have not been confirmed thus far. If the results presented here should be in error when reliable experimental data becomes available, however, then the inclusion of relativistic effects into the calculation should be considered. This is especially true, of course,

for the heavier elements (Zr, Nb, Mo) since the importance of relativistic effects will increase with increasing atomic number.

In addition to this neglect of relativistic phenomena, it must be recognized that the effects of the molecular and solid state have been totally ignored. Although a justification for this has been given, it may be that the effects are more significant than anticipated. This is especially true for the case of the plasmon interaction and the interband transition. An Auger electron can lose energy by these processes and thereby be displaced from the correct energy by a corresponding amount. This would then evidently lead to difficulties in interpreting observed spectra solely with the aid of Auger energies. In a similar fashion, the work function of a solid can effect the observed peak energies. It may therefore be necessary to make this adjustment in the observed energies.

As discussed in Chapter I, this calculation ignores the effect of configuration interaction (CI) in treating the LMM transitions. This was done despite the apparent success in the use of CI by Asaad in treating KLL transitions. It was pointed out by Siegbahn,[16] however, that this success was probably fortuitous being due to the use of inaccurate binding energies in Asaad's computations. On the basis of this result, we felt that inclusion of CI was not justified at this time. Subsequent results may, of course, alter this situation so that one should be aware of the possible import of configuration interaction when treating Auger transitions. A final possible improvement in the present computations is in the treatment of the continuum electron wave function. Thus we have noted in Chapter III that this function was

determined by assuming the electron to move in a Hermann-Skillman[76] central potential and then numerically solving Schrödinger's equation with this potential. A better treatment would utilize the Hartree-Fock potential for the problem. Such a treatment will inevitably introduce complications since this potential changes for each electron in the atom. But the new treatment may also introduce significant deviations in the continuum function characteristics. If this should be the case, then the predicted Auger transition probabilities will be altered as well since these quantities are extremely sensitive to the wave function character.

Now throughout this work, it has repeatedly been emphasized that there is a great need for more experimental data on LMM Auger transitions. Indeed, it is hoped that the present effort will stimulate the production of such data. If this is to be the case, there are two basic experimental techniques which will be utilized--the ESCA technique developed by Siegbahn[16] and the technique of Auger Electron Spectroscopy (AES). The latter method was discussed in some detail in Chapter I and is the one of primary interest here since results of AES were responsible for inspiring the present calculations. In this regard, we recall that the technique is, thus far, limited to an investigation of materials through the Auger energies with intensity information being lost. This arises due to the small inherent intensity of the Auger peaks relative to the other signals which appear in Auger spectroscopy and to the presence of an overall background signal. In order to identify the presence of the Auger peaks, it is then necessary that one obtain the derivative of the intensity curve (the N(E) curve

of Chapter I) and thereby destroy the meaningful intensity data. One possibility for regaining this data exists, however, and perhaps the technique can be perfected in the near future. Thus we note that the derivative curve is such that it effectively removes the background signal since this signal is almost linear over a broad range of energy. If one were to integrate this curve, it then follows that the background contribution will be largely removed and, as a result, the Auger peaks will appear more clearly. This would then enable a direct measurement of the peak intensities thereby providing a second tool in the analysis of Auger spectra. It would obviously also provide an experimental method with which the theoretical predictions, such as those produced here, could be compared. An improvement such as this would thus improve considerably the utility of the method of Auger Electron Spectroscopy.

In summary, it is hoped that the results of this work will stimulate further theoretical calculations as well as more experimental effort in the measurement of Auger energies and intensities. If the results should also play a part in inspiring the development of improvements in the AES techniques, then the present effort will have been extremely rewarding.

APPENDICES

APPENDIX A

ANGULAR MOMENTUM PROPERTIES OF SOLUTIONS TO THE SCHRÖDINGER EQUATION

The purpose of this appendix is to indicate the nature of the angular momentum dependences in the solutions of Schrödinger's equation for an atomic system. Since this problem has been exhaustively discussed,[63-65] we shall be content with a presentation of the basic results. To proceed, we introduce the atomic Hamiltonian to be used here; it is (in MKS units)

$$H = \sum_{j=1}^{N} \left(-\frac{\hbar^2}{2m} \nabla_j^2 - \frac{kZe^2}{r_j} \right) + \sum_{i<j}^{N} \frac{ke^2}{r_{ij}} + \sum_{j=1}^{N} (SO)_j \qquad \text{(A-1)}$$

where

$$k = \frac{1}{4\pi\epsilon_o} .$$

The various terms in this expression are identified by

$$\begin{aligned}
\frac{-\hbar^2}{2m} \nabla_j^2 &\sim \text{kinetic energy of } j^{th} \text{ electron,} \\
\frac{-kZe^2}{r_j} &\sim \text{mutual electrostatic interaction energy of } j^{th} \text{ electron with nucleus of charge + Ze,} \\
\frac{ke^2}{r_{ij}} &\sim \text{mutual electrostatic interaction energy of electrons i and j,}
\end{aligned} \qquad \text{(A-2)}$$

and

$$(SO)_j \sim \text{spin-orbit energy of } j^{th} \text{ electron.}$$

To facilitate computations, it is somewhat simpler to use atomic units; we therefore introduce

$$\text{energy units} \sim 1 \text{ Rydberg} = \frac{k^2 m e^4}{2\hbar^2} \simeq 13.6 \text{ ev}$$

$$\text{and length units} \sim 1 \text{ Bohr radius} = \frac{\hbar^2}{kme^2} \quad . \tag{A-3}$$

In terms of these units, one obtains

$$H = \sum_j \left(-\nabla_j^2 - \frac{2Z}{X_j} + \alpha^2 \xi(X_j) \underline{\ell}_j \cdot \underline{s}_j \right) + \sum_{i<j} \frac{2}{X_{ij}} \tag{A-4}$$

where X_j gives the displacement of the j^{th} electron in Bohr radii so that

$$r_j = X_j a_o \quad .$$

The traditional form of the spin-orbit interaction energy has been inserted into this expression with the operator

$$\underline{\ell}_j \cdot \underline{s}_j$$

being the significant feature of the interaction. It is, of course, clear that the quantities $(\underline{\ell}_j, \underline{s}_j)$ are the orbital and spin angular momenta of the j^{th} electron. As regards the quantities α and $\xi(X_j)$,

these are the fine structure constant and the spin-orbit parameter respectively.

Now Schrödinger's equation is given by

$$H\Psi = E\Psi \tag{A-5}$$

where E is in Rydbergs if (A-4) is used for the Hamiltonian. The angular momentum properties of Ψ can be examined most easily by considering the commutative properties of H with respect to the angular momentum operators of the system. Thus if one finds that H commutes with the operator $\underline{L}$ so that

$$[H, \underline{L}] = H\underline{L} - \underline{L}H = 0 ,$$

then it follows that the solutions to (A-5) can be written as simultaneous eigenstates of the operators H and $\underline{L}$. In the form of an equation, this means that

$$H\Psi = E\Psi$$

$$(\underline{L})_z\Psi = m\Psi$$

$$\underline{L}^2\Psi = L(L+1)\Psi$$

are satisfied simultaneously. Naturally if H does not commute with $\underline{L}$, then one cannot obtain such states for H and $\underline{L}$. Now in order to carry out this type of commutative operator study, it is convenient in the present case to write H as

$$H = H_1 + H_2 + H_3$$

where

$$H_1 = \sum_j \left(-\nabla_j^2 - \frac{2Z}{X_j} \right)$$

$$H_2 = \sum_j \alpha^2 \xi(X_j) \underline{\ell}_j \cdot \underline{s}_j \qquad \text{(A-6)}$$

$$H_3 = \sum_{i<j} \frac{2}{X_{ij}}$$

which evidently is just a separation of the spin-orbit and mutual electron electrostatic contributions to the total energy.

Viewed from the standpoint of perturbation theory, there are four distinct cases which can be obtained from the total H given in (A-6). Each of these gives rise to different angular momenta characterizing the solutions of (A-5) and are, therefore, discussed below.

CASE I: $H = H_1$; $H_1 >> H_2, H_3$

The commutation properties for this Hamiltonian are

$$[H, \underline{\ell}_j^2] = [H, (\underline{\ell}_j)_z] = [H, \underline{s}_j^2] = [H, (\underline{s}_j)_z] = 0 \qquad \text{(A-7)}$$

where $\underline{\ell}_j^2 = \underline{\ell}_j \cdot \underline{\ell}_j$ and $\underline{s}_j^2 = \underline{s}_j \cdot \underline{s}_j$. This then means that the eigenstates ψ_1 in

$$H_1 \psi_1 = E_1 \psi_1$$

are characterized by the quantum numbers (eigenvalues) of the operators $(\underline{\ell}_j^2)$, $(\underline{\ell}_j)_z$, $(\underline{s}_j^2)$ and $(\underline{s}_j)_z$. Further, we note that H_1 is just a sum of hydrogenic Hamiltonians h_j so that

$$H_1 = \sum_j h_j \ .$$

One then has immediately that (neglecting antisymmetry of ψ_1)

$$\begin{aligned} \psi_1 &= \varphi_1\varphi_2\cdots\varphi_N \\ E_1 &= \epsilon_1 + \epsilon_2 + \ldots + \epsilon_N \end{aligned} \qquad \text{(A-8)}$$

where

$$h_j\varphi_j = \epsilon_j\varphi_j$$

is used. But the properties of the φ_j are well-known to be such that

$$\begin{aligned} \underline{\ell}_j^2\varphi_j &= \ell_j(\ell_j+1)\varphi_j \\ (\underline{\ell}_j)_z\varphi_j &= m_\ell\varphi_j \\ \underline{s}_j^2\varphi_j &= s_j(s_j+1)\varphi_j \\ (\underline{s}_j)_z\varphi_j &= \mu_s\varphi_j \end{aligned} \qquad \text{(A-9)}$$

so that ψ_1 is indeed an eigenstate of the operators used in (A-9) as stated above. For future use, we will indicate these φ_j by the ket

$$\varphi_j \equiv |n\ell\, m_\ell\, \mu_s\rangle \tag{A-10}$$

where $(\ell,\ m_\ell,\ \mu_s)$ is the marker that the relations (A-9) are satisfied. Evidently the "j" subscript includes all of the quantum numbers indicated in (A-10). We note for completeness that the "n" label in (A-10) is the principal quantum number of hydrogenic (or central-field) theory.

CASE II: $H = H_1 + H_3$; $H_1,\ H_3 \gg H_2$

The commutation properties are here given in terms of the <u>total</u> orbital ($\underline{L}$) and spin ($\underline{S}$) angular momenta of the system. These are defined by

$$\begin{aligned} \underline{L} &= \underline{\ell}_1 + \underline{\ell}_2 + \ldots + \underline{\ell}_N = \sum_j \underline{\ell}_j \\ \underline{S} &= \underline{s}_1 + \underline{s}_2 + \ldots + \underline{s}_N = \sum_j \underline{s}_j \end{aligned} \tag{A-11}$$

and the commutative properties are

$$[H,\underline{L}^2] = [H,(\underline{L})_z] = [H,\underline{S}^2] = [H,(\underline{S})_z] = 0\ . \tag{A-12}$$

It should be noted that the basic change from the commutators listed under Case I is the fact that one now has

$$[H,(\underline{\ell}_j)_z] \neq 0 \quad \text{and} \quad [H,(\underline{s}_j)_z] \neq 0\ . \tag{A-13}$$

Hence the numbers $(m_\ell,\ \mu_s)$ are no longer meaningful in specifying the

state of the system. Instead only their sum is conserved as evidenced by the results (A-12) and the definitions in (A-11).

Now the Schrödinger equation for the system is

$$H\Psi_2 = E_2\psi_2$$

and the relations (A-12) demonstrate that ψ_2 can be written such that

$$\begin{aligned} \underline{L}^2\psi_2 &= L(L+1)\psi_2 \\ \underline{S}^2\psi_2 &= S(S+1)\psi_2 \\ (\underline{L})_z\psi_2 &= M_L\psi_2 \\ (\underline{S})_z\psi_2 &= M_S\psi_2 \quad ; \end{aligned} \tag{A-14}$$

we incorporate these symbolically by writing

$$\psi_2 = |\gamma\, LS\, M_L M_S\rangle\,. \tag{A-15}$$

Here the quantity γ includes all additional necessary quantum numbers, such as the principal values $(n_1, n_2, \ldots)$ and the individual orbital and spin momenta $(\underline{\ell}_j, \underline{s}_j)$ which couple to give $\underline{L}$ and $\underline{S}$. These functions can be expressed in terms of the hydrogenic functions of Case I but, for more than two electrons, the dependence becomes rather involved. For two electrons, it is relatively simple with the result being

$$|\gamma LSM_L M_S\rangle_{12} = \sum_{\substack{m_1 m_2 \\ \mu_1,\mu_2}} \langle \ell_1 m_1 \ell_2 m_2 | LM_L\rangle \langle s_1 \mu_1 s_2 \mu_2 | SM_S\rangle \; |n_1 \ell_1 m_1 \mu_1\rangle_1 |n_2 \ell_2 m_2 \mu_2\rangle_2\,. \tag{A-16}$$

The quantities $\langle \ell_1 m_1 \ell_2 m_2 | LM_L \rangle$ are Clebsch-Gordan coefficients while the (1,2) subscripts in $|\gamma LSM_L M_S\rangle_{12}$ denote the electron co-ordinate label. We note that this expansion is such that

$$\underline{\ell}_1^{\,2} |\gamma LSM_L M_S\rangle_{12} = \ell_1(\ell_1+1) |\gamma LSM_L M_S\rangle_{12}$$

with similar results for $\underline{\ell}_2^{\,2}$, $\underline{s}_1^{\,2}$ and $\underline{s}_2^{\,2}$. This follows from the fact that these operators still commute with H and are, therefore, good quantum numbers. A better notation for the LS-coupled (or Russell-Saunders[66]) functions would then include these quantum numbers explicitly as

$$|\gamma(\ell_1\ell_2)L(s_1s_2)\,S\,M_L M_S\rangle_{12} \qquad \text{(A-17)}$$

rather than the form of (A-16). This notation has the advantage of indicating the order of the coupling of ℓ_1 and ℓ_2 to give the resultant L and similarly for s_1, s_2 coupling to S. In addition, the form (A-17) is such that one can immediately identify the quantum numbers corresponding to electron "1" and electron "2." Thus the first listed numbers (ℓ_1, s_1) are assumed to correspond to electron "1" with (ℓ_2, s_2) being associated with electron "2."

Case III: $H = H_1 + H_2 + H_3$;

The commutative properties are now such that H commutes only with the <u>total</u> angular momentum ($\underline{J}$) of the system where

$$\underline{J} = \underline{L} + \underline{S} \qquad \text{(A-18)}$$

with the relevant commutators being

$$[H,\underline{J}^2] = [H,(\underline{J})_z] = 0 \ . \tag{A-19}$$

These relations also hold for the Hamiltonians of Cases I, II, and IV but the states are all degenerate in the J values for these cases. Hence there is no need in utilizing it to specify a particular state for such systems. It is necessary in the present case, however, and one has that the solutions ψ_3 of

$$H\psi_3 = E_3\psi_3$$

can be written as (γ not the same as in (A-15))

$$\psi_3 = |\gamma JM\rangle$$

where

$$\begin{aligned} \underline{J}^2|\gamma JM\rangle &= J(J+1)|\gamma JM\rangle \\ (\underline{J})_z|\gamma JM\rangle &= M|\gamma JM\rangle \ . \end{aligned} \tag{A-20}$$

Now it is possible to write these states as linear combinations of LS-coupled functions in analogy with the expansion of (A-16); the results are the <u>intermediate coupling</u> functions. In order to obtain these, we recall that the states of (A-16) and (A-17) are eigenstates of the operators of (A-14). But for the present case, it would be more convenient to use functions which are eigenstates of $\underline{L}^2$, $\underline{S}^2$, and $(\underline{J})_z$. Such functions are easily obtained from those of (A-16) since from (A-18),

$$M = M_L + M_S$$

so that

$$|\gamma LSJM\rangle = \sum_{M_L, M_S} \langle LM_L SM_S | JM\rangle |\gamma LSM_L M_S\rangle \ . \qquad \text{(A-21)}$$

This relation follows when the properties of Clebsch-Gordan coefficients (sometimes termed vector addition coefficients) are combined with the definition (A-18).

To proceed further, we note that the operators H_1, H_3 of the Hamiltonian are both diagonal in the L,S quantum numbers, i.e.,

$$\langle \gamma' L' S' J' M' | H_j | \gamma LSJM\rangle = \delta_{\gamma'\gamma}\delta_{L'L}\delta_{S'S}\delta_{J'J}\delta_{M'M} \qquad \text{(A-22)}$$

where $j = 1, 3$. The spin-orbit term (H_2) does not satisfy this relation, however, and instead one finds a matrix element which links different L,S states (a precise expression is given in (A-31) for two electrons). It is this term, therefore, which causes the breakdown of LS-coupling and necessitates the use of the intermediate coupling formalism. Due to this term, all (L,S) states which couple to give the same J are mixed to form the "true" states characterized by this J. This mixture enters as a sum over all the L,S pairs which can couple to give the particular J value and one has the result

$$|\gamma JM\rangle = \sum_{L,S} C^{N'}(LSJ) |\gamma LSJM\rangle \ . \qquad \text{(A-23)}$$

To illustrate this relation, consider the case of a $3p^2$ configuration. Then the possible multiplet states are

$$^1S_0;\ ^1D_2;\ ^3P_{0,1,2}$$

so that the intermediate coupling J = 2 states are obtained by a mixing of the ($^1D_2$ and $^3P_2$) pure LS-states. The result

$$|\gamma(3p^2)2M\rangle = C^{N'}(^1D_2)|\gamma(^1D_2)M\rangle + C^{N'}(^3P_2)|\gamma(^3P_2)M\rangle \qquad \text{(A-24)}$$

is thereby obtained from (A-23). We note that the coefficients $C^{N'}(LSJ)$ are termed the mixing coefficients. They are computed by solving a secular equation (consult Chapter II and Appendix D) with the N' variable indicating the coefficients which correspond to a particular solution of this equation (Appendix D presents detailed results for the mixing coefficients encountered in LMM transitions).

CASE IV: $H = H_1 + H_2$; $H_1, H_2 \gg H_3$

This case corresponds to the total spin-orbit energy being larger than the contribution of the mutual electron interaction energy. This Hamiltonian is, therefore, only approximately correct even for the very heavy elements, but it is still a useful case to consider. One could proceed by again noting that H commutes with the total angular momentum $\underline{J}$ and the z-component of this operator, but this is uninteresting here since all states are degenerate in these quantum numbers. Instead the operators of interest correspond to the <u>individual</u> total

angular momenta of each electron ($\underline{j}_k$) which are formed from the coupling

$$\underline{j}_k = \underline{\ell}_k + \underline{s}_k \ , \tag{A-25}$$

and from this one has

$$\underline{J} = \underline{j}_1 + \underline{j}_2 + \ldots + \underline{j}_N \ .$$

The commutation relations are then

$$[H, \underline{j}_k^{\,2}] = [H, (\underline{j}_k)_z] = 0 \tag{A-26}$$

so that the solutions ψ_4 of

$$H\psi_4 = E_4\psi_4$$

are such that

$$\begin{aligned} \underline{j}_k^{\,2}\psi_4 &= j_k(j_k+1)\psi_4 \\ (\underline{j}_k)_z\psi_4 &= m_k\psi_4 \ . \end{aligned} \tag{A-27}$$

These jj-coupled functions are usually denoted by (for two electrons)

$$|\gamma j_i j_2 JM\rangle \ .$$

As might be expected, it is possible to write these states in terms of the hydrogenic functions of Case I. To accomplish this, note that in

analogy with (A-21) one has

$$|n\ell jm\rangle = \sum_{m_\ell \mu} \langle \ell m_\ell s\mu | jm\rangle |n\ell m_\ell \mu\rangle$$

from which it follows that

$$|\gamma j_1 j_2 JM\rangle = \sum_{m_1 m_2} \langle j_1 m_1 j_2 m_2 | JM\rangle |n_1 \ell_1 j_1 m_1\rangle |n_2 \ell_2 j_2 m_2\rangle \qquad \text{(A-28)}$$

is the expanded jj-coupling function.

It is sometimes necessary to work in both the LS- and jj-limits so that a knowledge of the <u>recoupling coefficient</u> connecting the states of these two limits is desirable. Thus we have--for two electrons--the result

$$|n_1 \ell_1 n_2 \ell_2 LSJM\rangle = |(\ell_1 \ell_2)L(s_1 s_2)S, JM\rangle =$$

$$\sum_{j_1 j_2} \langle ((\ell_1 s_1) j_1 (\ell_2 s_2) j_2,\ JM | (\ell_1 \ell_2)L(s_1 s_2)S, JM\rangle^* \qquad \text{(A-29)}$$

$$|(\ell_1 s_1) j_1 (\ell_2 s_2) j_2,\ JM\rangle$$

with the recoupling coefficient being

$$\langle ((\ell_1 s_1) j_1 (\ell_2 s_2) j_2,\ JM | (\ell_1 \ell_2)L(s_1 s_2)S, JM\rangle \ .$$

The reason for calling this a <u>recoupling</u> coefficient is obvious since the change in the two states is in the different coupling order of the

individual angular momenta. It may be shown[64,70] that this coefficient is given by

$$\sqrt{(2j_1+1)(2j_2+1)(2L+1)(2S+1)} \begin{Bmatrix} \ell_1 \ell_2 L \\ s_1 s_2 S \\ j_1 j_2 J \end{Bmatrix} \tag{A-30}$$

where $\begin{Bmatrix} \end{Bmatrix}$ is the Wigner 9-j symbol.[64]

By using this result, it is then straightforward to evaluate the matrix element of the spin-orbit energy (H_2) in the LS-coupling scheme. This is true since H_2 is diagonal in the jj-coupling limit. The result of such a computation is just

$$\langle L'S'JM| \sum_{k=1}^{2} \xi_{n_k \ell_k} \underset{\sim}{\ell}_k \cdot \underset{\sim}{s}_k |LSJM\rangle =$$

$$\sum_{j_1 j_2} \left[\frac{(2j_1+1)(2j_2+1)}{2}\right] [L', S', L, S]^{\frac{1}{2}} \begin{Bmatrix} \ell_1 s_1 j_1 \\ \ell_2 s_2 j_2 \\ L' S' J \end{Bmatrix} \begin{Bmatrix} \ell_1 \ell_2 L \\ s_1 s_2 S \\ j_1 j_2 J \end{Bmatrix} *$$

$$\sum_{k} \xi_{n_k \ell_k} \left[j_k(j_k+1) - \ell_k(\ell_k+1) - \frac{3}{4}\right] \tag{A-31}$$

where the notation $[\,L\,]^{\frac{1}{2}} = \sqrt{2L+1}$ is used. The mixing of the different LS-states is well-illustrated here in accordance with previous remarks.

APPENDIX B

EVALUATION OF AVERAGE AND STRUCTURE TERM ENERGIES

In this appendix the general formula for computing the average energy of any electron configuration is given. The definition of the average energy is that given by Slater[63] and therefore does not include the contribution from a spin-orbit interaction. Instead only the contribution of the kinetic energy and electron-electron interaction energies are considered. Using the notation introduced in Appendix A, this means that only those terms which arise from matrix elements of the H_1 and H_3 operators are considered.

The wave functions used in these matrix elements are of the hydrogenic or central field type defined in (A-10). As a result, the H_1 contribution to the average energy is in terms of the quantities

$$I(n\ell) = \int_0^\infty P_{n\ell}(r)\left[-\frac{\partial^2}{\partial r^2} + \frac{\ell(\ell+1)}{r^2} - \frac{2Z}{r} \right] P_{n\ell}(r)\, dr \qquad \text{(B-1)}$$

where $\frac{P_{n\ell}(r)}{r}$ is the radial portion of the wave function. Similarly, the H_3 contribution is in terms of the radial integrals

$$R^k(ab,cd) = \int_0^\infty \int_0^\infty \frac{2r_<^k}{r_>^{k+1}} P_a(r_1)P_b(r_2)P_c(r_1)P_d(r_2)dr_1dr_2 \qquad \text{(B-2)}$$

where $P_a(r)$ corresponds to $P_{n_a\ell_a}(r)$ in analogy with the functions of

(B-1). Note that $(r_<, r_>)$ are defined by the relations

$$r_1 > r_2 \begin{cases} r_< = r_2 \\ r_> = r_1 \end{cases} \quad \text{and} \quad r_1 < r_2 \begin{cases} r_< = r_1 \\ r_> = r_2 \end{cases} \tag{B-3}$$

so that (B-2) can, if desired, be written as the sum of two integrals. This definition for $R^k(ab,cd)$ is valid for Rydberg units as is assumed here for H_1 and H_3. Finally, it is frequently true that one has the cases

$$(a = c \quad \text{and} \quad b = d) \quad \text{or} \quad (a = d \quad \text{and} \quad b = c)$$

in the definition (B-2). In these cases it is conventional to introduce the notation

$$F^k(ab) \equiv R^k(ab,\ ab)$$

and (B-4)

$$G^k(ab) \equiv R^k(ab,\ ba) \ .$$

In terms of these quantities, we now write down the average energy for the configuration

$$1s^2 2s^2 2p^6 3s^k 3p^m 3d^n 4s^2 \tag{B-5}$$

which enables the calculation of the average energy of any 3d transition metal. To extend to elements of atomic number such that the 4s shell is not filled, it is only necessary to treat all 4s contributions as zero; a similar statement holds for the other orbitals. With

these preliminary remarks, the average energy of (B-5) is

$$
\begin{aligned}
E_{avg} = & \sum_j f_j I(n_j \ell_j) + \bar{E}(1s^2) + \bar{E}(2s^2) + 15\bar{E}(2p^2) \\
& + \frac{k(k-1)}{2}\bar{E}(3s^2) + \frac{m(m-1)}{2}\bar{E}(3p^2) + \frac{n(n-1)}{2}\bar{E}(3d^2) \\
& + \bar{E}(4s^2) + 4\bar{E}(1s2s) + 12\bar{E}(1s2p) + 2k\bar{E}(1s3s) \\
& + 2m\bar{E}(1s3p) + 2n\bar{E}(1s3d) + 4\bar{E}(1s4s) + 12\bar{E}(2s2p) \qquad \text{(B-6)} \\
& + 2k\bar{E}(2s3s) + 2m\bar{E}(2s3s) + 2n\bar{E}(2s3d) + 4\bar{E}(2s4s) \\
& + 6k\bar{E}(2p3s) + 6m\bar{E}(2p3p) + 6n\bar{E}(2p3d) + 12\bar{E}(2p4s) \\
& + km\bar{E}(3s3p) + kn\bar{E}(3s3d) + 2k\bar{E}(3s4s) + mn\bar{E}(3p3d) \\
& + 2m\bar{E}(3p4s) + 2n\bar{E}(3d4s) \ .
\end{aligned}
$$

The notation in this relation is such that $\bar{E}(n_1\ell_1 n_2\ell_2)$ is the average energy of the <u>two</u> electron configuration $n_1\ell_1 n_2\ell_2$. We list below the results for several average energies of this type. As for the parameter f_j, this is just the number of electrons in the orbital $n_j\ell_j$.

It is clear that the average energy of the total configuration (B-5) has been expressed in terms of the average interaction energies of all possible two electron configurations which can occur in (B-5). The results necessary to accomplish such an expansion are obtained from

the fact that the average energy for a configuration $(n_1\ell_1)^p(n_2\ell_2)^q$ is given by

$$E_{avg}(\ell_1{}^p\ell_2{}^q) = E_{avg}(\ell_1{}^p) + E_{avg}(\ell_2{}^q) + pq\, E_{avg}(\ell_1\ell_2)$$

and (B-7)

$$E_{avg}(\ell_1{}^p) = \frac{p(p-1)}{2} E_{avg}(\ell_1{}^2) \quad .$$

By using these expressions on (B-5) (or for any other configuration), an expression such as (B-6) is obtained. It then remains to compute the average energies of the two electron configurations. This is straightforward since one has the results

$$E_{avg}(n_1\ell_1n_2\ell_2) = \frac{1}{2}\left[2F^\circ(n_1\ell_1n_2\ell_2) - \sum_\ell g_{\ell\ell_1\ell_2} G^\ell(n_1\ell_1n_2\ell_2)\right]$$

and (B-8)

$$E_{avg}((n_1\ell_1)^2) = \frac{2\ell_1+1}{4\ell_1+1}\left[2F^\circ(n_1\ell_1n_1\ell_1) - \sum_\ell g_{\ell\ell_1\ell_1} F^\ell(n_1\ell_1n_1\ell_1)\right]$$

where

$$g_{\ell\ell_1\ell_2} = \frac{(\langle \ell_1 0 \ell 0 | \ell_2 0\rangle)^2}{2\ell_2+1} \quad .$$

The limits on ℓ in the above are in integer steps as 0,1,2, ... with the upper limit being set by the properties of the Clebsch-Gordan

coefficient. If the relations (B-8) are utilized, one can obtain the following results for the configurations which occur for s, p, and d electrons:

$$
\begin{aligned}
\bar{E}(s^2) &= F^0(ss) \\
\bar{E}(p^2) &= F^0(pp) - \frac{2}{25} F^2(pp) \\
\bar{E}(d^2) &= F^0(dd) - \frac{2}{63} F^2(dd) - \frac{2}{63} F^4(dd) \\
\bar{E}(ss') &= F^0(ss') - \frac{1}{2} G^0(ss') \\
\bar{E}(sp) &= F^0(sp) - \frac{1}{6} G^1(sp) \\
\bar{E}(sd) &= F^0(sd) - \frac{1}{10} G^2(sd) \\
\bar{E}(pp') &= F^0(pp') - \frac{1}{6} G^0(pp') - \frac{1}{15} G^2(pp') \\
\bar{E}(pd) &= F^0(pd) - \frac{1}{15} G^1(pd) - \frac{3}{70} G^3(pd) \\
\bar{E}(dd') &= F^0(dd') - \frac{1}{10} G^0(dd') - \frac{1}{35} G^2(dd') - \frac{1}{35} G^4(dd') .
\end{aligned}
\tag{B-9}
$$

In these relations, the "n" label has been dropped and, where necessary, a prime is used to indicate that different n values are to be used.

As the final point, we write down the structure term energies which are utilized in evaluating the LMM transition energies. The following results are for LS-states and are obtained from the compilation by Slater;[63] for further details this reference should be consulted.

It is to be noted that the average energies have been removed from the following terms--i.e., the structure terms are with respect to the average configuration energy and are not absolute. The results are

Configuration	Structure Term
$sp(^1P)$	$\frac{1}{2} G^1(sp)$
$sp(^3P)$	$-\frac{1}{6} G^1(sp)$
$sd(^1D)$	$\frac{3}{10} G^2(sd)$
$sd(^3D)$	$-\frac{1}{10} G^2(sd)$
$p^2(^1S)$	$\frac{12}{25} F^2(pp)$
$p^2(^1D)$	$\frac{3}{25} F^2(pp)$
$p^2(^3P)$	$-\frac{3}{25} F^2(pp)$
$pd(^3F)$	$\frac{2}{35} F^2(pd) - \frac{1}{3} G^1(pd) + \frac{15}{490} G^3(pd)$
$pd(^3D)$	$-\frac{1}{5} F^2(pd) + \frac{4}{15} G^1(pd) - \frac{3}{70} G^3(pd)$
$pd(^3P)$	$\frac{1}{5} F^2(pd) - \frac{105}{490} G^3(pd)$
$pd(^1F)$	$\frac{2}{35} F^2(pd) + \frac{7}{15} G^1(pd) + \frac{27}{490} G^3(pd)$
$pd(^1D)$	$-\frac{1}{5} F^2(pd) - \frac{2}{15} G^1(pd) + \frac{63}{490} G^3(pd)$
$pd(^1P)$	$-\frac{1}{5} F^2(pd) + \frac{2}{15} G^1(pd) + \frac{147}{490} G^3(pd)$

(B-10)

(cont'd) Configuration	Structure Term
$d^2(^3F)$	$-\frac{58}{441} F^2(dd) + \frac{5}{441} F^4(dd)$
$d^2(^3P)$	$\frac{77}{441} F^2(dd) - \frac{70}{441} F^4(dd)$
$d^2(^1G)$	$\frac{50}{441} F^2(dd) + \frac{15}{441} F^4(dd)$
$d^2(^1D)$	$-\frac{13}{441} F^2(dd) + \frac{50}{441} F^4(dd)$
$d^2(^1S)$	$\frac{140}{441} F^2(dd) + \frac{140}{441} F^4(dd)$.

We note that the above terms also are valid for the complementary configurations of those shown. Thus (sp^5) has the same structure splitting as (sp), (sd^9), the same as (sd), and similarly for the other configurations.

APPENDIX C

INTERMEDIATE COUPLING TRANSITION PROBABILITIES

The expression obtained for the LMM transition probabilities are presented in this appendix. The results were obtained by using equation (106) in Chapter II so that only the interaction of the M shell electrons are treated in intermediate coupling. In addition, note that the density of states factor, $\frac{2\pi\rho}{\hbar}$ or π, depending on the units being used, is omitted from the following results. Any application of these relations must thus include these factors.

The results are first given for an initial 2s vacancy with the notation being that used for the (Ti,V,Cr) lines. If (Zr, Nb, Mo) or a similar element is treated, the only changes are those illustrated in Figure 10 of Chapter III. The 2s transition probabilities are then

$$L_1M_1M_1(^1S_0) = \left|R^0(2sE0,3s^2)\right|^2$$

$$A = R^0(2sE1,3s3p) - \frac{1}{3}R^1(2sE1,3p3s)$$

$$B = A + \frac{2}{3}R^1(2sE1,3p3s)$$

$$L_1M_1M_2(^3P_0) = \frac{1}{2}|A|^2$$

$$\left.\begin{matrix} L_1M_1M_2(^3P_1) \\ \\ L_1M_1M_3(^1P_1) \end{matrix}\right] = \frac{3}{2}\left[|C^N(^3P_1)|^2|A|^2 + |C^N(^1P_1)|^2|B|^2\right]$$

$$L_1M_1M_3(^3P_2) = \frac{5}{2}|A|^2$$

$$C = R^0(2sE2,3s3d) - \frac{1}{5}R^2(2sE2,3d3s)$$

$$D = C + \frac{2}{5}R^2(2sE2,3d3s)$$

$$L_1M_1M_4(^3D_1) = \frac{3}{2}|C|^2$$

$$\left.\begin{matrix} L_1M_1M_4(^3D_2) \\ L_1M_1M_5(^1D_2) \end{matrix}\right] = \frac{5}{2}\left[|C^N(^3D_2)|^2|C|^2 + |C^N(^1D_2)|^2|D|^2\right]$$

$$L_1M_1M_5(^3D_3) = \frac{7}{2}|C|^2$$

$$\left.\begin{matrix} L_1M_2M_2(^3P_0) \\ L_1M_3M_3(^1S_0) \end{matrix}\right] = \frac{1}{3}|C^N(^1S_0)|^2|R^1(2sE0,3p^2)|^2$$

$$L_1M_2M_3(^3P_1) = 0$$

$$\left.\begin{matrix} L_1M_2M_3(^3P_2) \\ L_1M_3M_3(^1D_2) \end{matrix}\right] = \frac{2}{3}|C^N(^1D_2)|^2|R^1(2sE2,ep^2)|^2$$

$$A = -\frac{\sqrt{2}}{3}R^1(2sE1,3p3d) - \frac{\sqrt{2}}{5}R^2(2sE1,3d3p)$$

$$B = -\frac{\sqrt{2}}{3}R^1(2sE1,3p3d) + \frac{\sqrt{2}}{5}R^2(2sE1,3d3p)$$

$$C = \frac{1}{\sqrt{7}}\left[R^1(2sE3,3p3d) + \frac{3}{5}R^2(2sE3,3d3p)\right]$$

$$D = \frac{1}{\sqrt{7}}\left[R^1(2sE3,3p3d) - \frac{3}{5}R^2(2sE3,3d3p)\right]$$

$$\left.\begin{matrix} L_1M_2M_4(^3F_2) \\ L_1M_2M_5(^1D_2) \\ L_1M_3M_4(^3P_2) \\ L_1M_3M_5(^3D_2) \end{matrix}\right] = \frac{5}{2}\left[|C^N(^3F_2)|^2|D|^2 + |C^N(^3P_2)|^2|B|^2\right]$$

$$\left.\begin{matrix} L_1M_2M_4(^3P_1) \\ L_1M_3M_4(^3D_1) \\ L_1M_3M_5(^1P_1) \end{matrix}\right] = \frac{3}{2}\left[|C^N(^3P_1)|^2|B|^2 + |C^N(^1P_1)|^2|A|^2\right]$$

$$\left.\begin{matrix} L_1M_2M_5(^3F_3) \\ L_1M_3M_4(^3D_3) \\ L_1M_3M_5(^1F_3) \end{matrix}\right] = \frac{7}{2}\left[|C^N(^3F_3)|^2|D|^2 + |C^N(^1F_3)|^2|C|^2\right]$$

$$L_1M_3M_4(^3P_0) = \frac{1}{2}|B|^2$$

$$L_1M_3M_5(^3F_4) = \frac{9}{2}|D|^2$$

$$\left.\begin{matrix} L_1M_4M_4(^3P_0) \\ L_1M_5M_5(^1S_0) \end{matrix}\right] = \frac{1}{5}\left|C^N(^1S_0)\right|^2\left|R^2(2sE0,3d^2)\right|^2$$

$$L_1M_4M_5(^3P_1) = 0$$

$$\left.\begin{matrix} L_1M_4M_4(^3F_2) \\ L_1M_4M_5(^1D_2) \\ L_1M_5M_5(^3P_2) \end{matrix}\right] = \frac{2}{7}\left|C^N(^1D_2)\right|^2\left|R^2(2sE2,3d^2)\right|^2$$

$$L_1M_4M_5(^3F_3) = 0$$

$$\left.\begin{matrix} L_1M_4M_5(^3F_4) \\ L_1M_5M_5(^1G_4) \end{matrix}\right\} = \frac{6}{35}|C^N(^1G_4)|^2|R^2(2sE4,3d^2)|^2 .$$

In the case of the transition probabilities for an initial 2p vacancy, the $L_{2,3}$ shell label is not included. It is understood, however, that it is necessary when specifying the transition. With this preliminary remark, the expressions for $L_{2,3}$ MM transitions are

$$M_1M_1(^1S_0) = \frac{1}{9}|R^1(2pE1,3s^2)|^2$$

$$A_\pm = \frac{1}{3}R^1(2pE0,3s3p) \mp R^0(2pE0,3p3s)$$

$$B_\pm = -\frac{\sqrt{2}}{3}R^1(2pE2,3s3p) \pm \frac{\sqrt{2}}{5}R^2(2pE2,3p3s)$$

$$M_1M_2(^3P_0) = \frac{1}{6}[|A_-|^2 + |B_-|^2]$$

$$\left.\begin{matrix} M_1M_2(^3P_1) \\ M_1M_3(^1P_1) \end{matrix}\right\} = \frac{1}{2}[|C^N(^3P_1)|^2(|A_-|^2+|B_-|^2)+|C^N(^1P_1)|^2(|A_+|^2+|B_+|^2)]$$

$$M_1M_3(^3P_2) = \frac{5}{6}[|A_-|^2 + |B_-|^2]$$

$$C_\pm = \sqrt{\frac{2}{15}}[R^1(2pE1,3s3d) \pm R^1(2pE1,3d3s)]$$

$$D_\pm = \frac{-1}{\sqrt{5}}[R^1(2pE3,3s3d) \pm \frac{3}{7}R^3(2pE3,3d3s)]$$

$$M_1M_4(^3D_1) = \frac{1}{2}[|C_-|^2 + |D_-|^2]$$

$$\left.\begin{matrix} M_1M_4(^3D_2) \\ M_1M_5(^1D_2) \end{matrix}\right\} = \frac{5}{6}\left[|C^N(^3D_2)|^2(|C_-|^2+|D_-|^2)+|C^N(^1D_2)|^2(|C_+|^2+|D_+)^2)\right]$$

$$M_1M_5(^3D_3) = \frac{7}{6}\left[|C_-|^2 + |D_-|^2\right]$$

$$T = R^0(2pE1,3p^2) + \frac{2}{5}R^2(2pE1,3p^2)$$

$$U = T - \frac{3}{5}R^2(2pE1,3p^2)$$

$$|S|^2 = |T - \frac{9}{25}R^2(2pE1,3p^2)|^2 + \frac{54}{625}|R^2(2pE3,3p^2)|^2$$

$$\left.\begin{matrix} M_2M_2(^3P_0) \\ M_3M_3(^1S_0) \end{matrix}\right\} = \frac{1}{3}\left[|C^N(^1S_0)|^2|T|^2+|C^N(^3P_0)|^2|U|^2\right]$$

$$M_2M_3(^3P_1) = |U|^2$$

$$\left.\begin{matrix} M_2M_3(^3P_2) \\ M_3M_3(^1D_2) \end{matrix}\right\} = \frac{5}{3}\left[|C^N(^1D_2)|^2|S|^2 + |C^N(^3P_2)|^2|U|^2\right]$$

$$\alpha_\pm = R^0(2pE2,3p3d)+\frac{1}{5}R^2(2pE2,3p3d) \pm \frac{9}{35}R^3(2pE2,3d3p)$$

$$\pm \frac{1}{15}R^1(2pE2,3d3p)$$

$$\beta_\pm = -\sqrt{2}\left[\frac{1}{5}R^2(2pE0,3p3d) \pm \frac{1}{3}R^1(2pE0,3d3p)\right]$$

$$\gamma_\pm = R^0(2pE2,3p3d) - \frac{1}{5}R^2(2pE2,3p3d) \pm \frac{1}{5}R^1(2pE2,3d3p)$$

$$\mp \frac{3}{35}R^3(2pE2,3d3p)$$

$$\sigma_{\pm} = R^0(2pE2,3p3d) + \frac{2}{35} R^2(2pE2,3p3d) \pm \frac{2}{5} R^1(2pE2,3d3p)$$

$$\pm \frac{1}{245} R^3(2pE2,3d3p)$$

$$\epsilon_{\pm} = -6\sqrt{3} \left[\frac{1}{35} R^2(2pE4,3p3d) \pm \frac{1}{49} R^3(2pE4,3d3p)\right]$$

$$\left.\begin{matrix} M_2M_4(^3F_2) \\ M_3M_4(^3P_2) \\ M_2M_5(^1D_2) \\ M_3M_5(^3D_2) \end{matrix}\right] = \frac{5}{6} \left[|C^N(^3F_2)|^2(|\sigma_-|^2 + |\epsilon_-|^2) + |C^N(^1D_2)|^2|\gamma_+|^2 + |C^N(^3D_2)|^2|\gamma_-|^2 + |C^N(^3P_2)|^2(|\alpha_-|^2 + |\beta_-|^2)\right]$$

$$\left.\begin{matrix} M_2M_4(^3P_1) \\ M_3M_4(^3D_1) \\ M_3M_5(^1P_1) \end{matrix}\right] = \frac{1}{2} \left[|C^N(^3P_1)|^2(|\alpha_-|^2 + |\beta_-|^2) + |C^N(^3D_1)|^2|\gamma_-|^2 + |C^N(^1P_1)|^2(|\alpha_+|^2 + |\beta_+|^2)\right]$$

$$\left.\begin{matrix} M_2M_5(^3F_3) \\ M_3M_4(^3D_3) \\ M_3M_5(^1F_3) \end{matrix}\right] = \frac{7}{6} \left[|C^N(^3F_3)|^2(|\sigma_-|^2 + |\epsilon_-|^2) + |C^N(^3D_3)|^2|\gamma_-|^2 + |C^N(^1F_3)|^2(|\sigma_+|^2 + |\epsilon_+|^2)\right]$$

$$M_3M_4(^3P_0) = \frac{1}{6} \left[|\alpha_-|^2 + |\beta_-|^2\right]$$

$$M_3M_5(^3F_4) = \frac{3}{2} \left[|\sigma_-|^2 + |\epsilon_-|^2\right]$$

$$\Gamma = \frac{-1}{\sqrt{15}} \left[2R^1(2pE1,3d^2) + \frac{9}{7} R^3(2pE1,3d^2)\right]$$

$$\Sigma_1 = \frac{-1}{5\sqrt{21}} \left[7R^1(2pE1,3d^2) + \frac{9}{7} R^3(2pE1,3d^2)\right]$$

$$\Sigma_2 = \frac{1}{5}\sqrt{\frac{2}{7}} \left[R^1(2pE3,3d^2) + \frac{12}{7} R^3(2pE3,3d^2)\right]$$

$$B_1 = \sqrt{\frac{6}{35}} \left[R^1(2pE3,3d^2) + \frac{1}{21} R^3(2pE3,3d^2)\right]$$

$$B_2 = -\frac{5}{21}\sqrt{\frac{6}{7}} R^3(2pE5,3d^2)$$

$$\Pi = \frac{1}{\sqrt{5}} \left[R^1(2pE1,3d^2) - \frac{3}{7} R^3(2pE1,3d^2)\right]$$

$$K = \frac{2}{\sqrt{70}} \left[-R^1(2pE3,3d^2) + \frac{3}{7} R^3(2pE3,3d^2)\right]$$

$$\left.\begin{matrix} M_4M_4(^3P_0) \\ M_5M_5(^1S_0) \end{matrix}\right] = \frac{1}{3} \left[|C^N(^3P_0)|^2|\Pi|^2 + |C^N(^1S_0)|^2|\Gamma|^2\right]$$

$$M_4M_5(^3P_1) = |\Pi|^2$$

$$\left.\begin{matrix} M_4M_4(^3F_2) \\ M_4M_5(^1D_2) \\ M_5M_5(^3P_2) \end{matrix}\right] = \frac{5}{3} \left[|C^N(^3F_2)|^2|K|^2 + |C^N(^1D_2)|^2(|\Sigma_1|^2 + |\Sigma_2|^2) + |C^N(^3P_2)|^2|\Pi|^2\right]$$

$$M_4M_5(^3F_3) = \frac{7}{3} |K|^2$$

$$\left.\begin{matrix} M_4M_5(^3F_4) \\ M_5M_5(^1G_4) \end{matrix}\right] = 3 \left[|C^N(^3F_4)|^2|K|^2 + |C^N(^1G_4)|^2(|B_1|^2 + |B_2|^2)\right] .$$

One closing remark regarding the use of the above expressions is necessary. Thus the values of the mixing coefficients to be inserted in the given relations must be matched with the line being treated. For example, if one desires to compute the $L_{2,3}M_4M_4$ ($^1P_0$) transition probability, then the mixing coefficients should have the values obtained when the energy of the Auger electron corresponds to the $M_4M_4(^3P_0)$ transition.

APPENDIX D

INTERMEDIATE COUPLING MIXING COEFFICIENTS

This appendix presents the formalism required to compute the intermediate coupling mixing coefficients which are encountered in treating LMM Auger transitions. In addition, tables are given which list the coefficients obtained for the elements Ti, V, Cr, Zr, Nb and Mo. To begin, recall from equation (28) of Chapter II that the secular equation arises from ($C_K \equiv C^N$ of Appendix C).

$$\sum_{L,S}^{N} C_K(LSJ)\left[\langle L'S'JM|H|LSJM\rangle - E(J)\delta_{L'L}\delta_{S'S}\right] = 0 \qquad \text{(D-1)}$$

where H is the system Hamiltonian. For the case of (N = 2), the secular equation resulting from this relation is just (30) of Chapter II, i.e.,

$$\det\begin{bmatrix} \alpha_1 & \alpha_2 \\ \alpha_3 & \alpha_4 \end{bmatrix} = 0 \qquad \text{(D-2)}$$

where

$$\begin{aligned} \alpha_1 &= \langle L_1S_1JM|H|L_1S_1JM\rangle - E(J) \\ \alpha_2 &= \alpha_3 = \langle L_1S_1JM|H|L_2S_2JM\rangle \\ \alpha_4 &= \langle L_2S_2JM|H|L_2S_2JM\rangle - E(J) \quad . \end{aligned} \qquad \text{(D-3)}$$

The values L_1S_1 and L_2S_2 are the two (L,S) pairs which couple to give the total angular momentum J while E(J) is the desired energy eigenvalue. Now the relation (D-2) must hold since the system of equations which results from (D-1) is

$$\begin{aligned} C_1\alpha_1 + C_2\alpha_2 &= 0 \\ C_1\alpha_3 + C_2\alpha_4 &= 0 \end{aligned} \qquad \text{(D-4)}$$

where $[C_1 = C(L_1S_1J)$ and $C_2 = C(L_2S_2J)]$ and non-trivial solutions for C_1, C_2 are desired. We shall now examine the system (D-4) for these non-trivial solutions.

We have at once from (D-2) that

$$\alpha_1\alpha_4 = \alpha_2\alpha_3$$

which evidently requires

$$C_2 = -\frac{\alpha_1}{\alpha_2} C_1 = -\frac{\alpha_3}{\alpha_4} C_1 \quad , \qquad \text{(D-5)}$$

provided that $\alpha_2, \alpha_4 \neq 0$.

But the wave function $\Psi(J)$ is

$$\Psi(J) = C_1\phi_1 + C_2\phi_2 \qquad \text{(D-6)}$$

so that (D-5) gives

$$\Psi(J) = C_1\left(\phi_1 - \frac{\alpha_1}{\alpha_2}\phi_2\right) \quad .$$

By now demanding that $\Psi(J)$ be normalized, we obtain

$$\langle \Psi | \Psi \rangle = 1 = C_1^2 \left(1 + \frac{\alpha_1^2}{\alpha_2^2} \right)$$

where it is assumed that the LS-coupled states (ϕ_1, ϕ_2) are orthonormal. But this then gives

$$C_1 = \frac{\pm 1}{\sqrt{1 + \left(\frac{\alpha_1}{\alpha_2} \right)^2}} \qquad \text{(D-7)}$$

or

$$\Psi(J) = \frac{\phi_1 - \frac{\alpha_1}{\alpha_2} \phi_2}{\sqrt{1 + \left(\frac{\alpha_1}{\alpha_2} \right)^2}} \quad , \qquad \text{(D-8)}$$

where the positive sign of (D-7) has been chosen for definiteness. These results then provide the mixing coefficients and the resulting normalized wave functions for a given solution E(J) to the secular equation (D-2). It is straightforward to verify that there are two solutions included in (D-8) and that they are, in fact, orthogonal. Thus one has from (D-3) that

$$\begin{aligned} \alpha_1 &= \alpha_1(E) = a - E \\ \alpha_2 &= \alpha_3 = b \\ \alpha_4 &= d - E \quad . \end{aligned} \qquad \text{(D-9)}$$

Using this notation, the secular equation of (D-2) gives

$$(a - E)(d - E) - b^2 = 0$$

or

$$E^2 - (a+d)E + (ad - b^2) = 0;$$

this then gives immediately the result that

$$E_{1,2} = \frac{(a+d) \pm \sqrt{(a+d)^2 - 4(ad-b^2)}}{2} \qquad \text{(D-10)}$$

It is then clear that E_1 and E_2 are related by

$$E_1 E_2 = ad - b^2 \quad \text{and} \quad E_1 + E_2 = a + d \ . \qquad \text{(D-11)}$$

If we now adopt the notation

$$\alpha_1(E_1) = \alpha_{11} \ , \ \alpha_1(E_2) = \alpha_{12} \ ,$$

we find two solutions Ψ_1, Ψ_2 as

$$\Psi_1 = \frac{\phi_1 - \frac{\alpha_{11}}{\alpha_2}\phi_2}{\sqrt{1 + \left(\frac{\alpha_{11}}{\alpha_2}\right)^2}} \quad \text{and} \quad \Psi_2 = \frac{\phi_1 - \frac{\alpha_{12}}{\alpha_2}\phi_2}{\sqrt{1 + \left(\frac{\alpha_{12}}{\alpha_2}\right)^2}} \ . \qquad \text{(D-12)}$$

That these are normalized is easy to check as is their orthogonality.

Thus the latter property follows since

$$\langle \Psi_1 | \Psi_2 \rangle = \frac{1 + \dfrac{\alpha_{11}\,\alpha_{12}}{(\alpha_2)^2}}{\sqrt{1 + \left(\dfrac{\alpha_{11}}{\alpha_2}\right)^2}\,\sqrt{1 + \left(\dfrac{\alpha_{12}}{\alpha_2}\right)^2}} \tag{D-13}$$

where the orthonormality of ϕ_1, ϕ_2 is used. But one has

$$1 + \frac{\alpha_{11}\,\alpha_{12}}{(\alpha_2)^2} = \frac{(\alpha_2)^2 + (a-E_1)(a-E_2)}{(\alpha_2)^2} = \frac{b^2 + E_1E_2 + a^2 - a(E_1+E_2)}{b^2}$$

which from (D-11) gives

$$\frac{b^2 + ad - b^2 + a^2 - (a+d)a}{b^2} \equiv 0 \ .$$

Thus we have the result from (D-13) that

$$\langle \Psi_1 | \Psi_2 \rangle = 0 \ . \tag{D-14}$$

In a similar fashion, the normalization of Ψ_1, Ψ_2 can be checked.

The mixing coefficients for a (3 x 3) secular equation can be obtained in the same manner. We shall not write down the detailed matrix elements which enter this equation but treat it symbolically as in (D-2). Then the system of equations encountered in the (3 x 3) case has the form

$$\begin{aligned} C_1\alpha_1 + C_2\alpha_2 + C_3\alpha_3 &= 0 \\ C_1\alpha_4 + C_2\alpha_5 + C_3\alpha_6 &= 0 \\ C_1\alpha_7 + C_2\alpha_8 + C_3\alpha_9 &= 0 \end{aligned} \tag{D-15}$$

so that the relevant secular equation is

$$\det \begin{bmatrix} \alpha_1 & \alpha_2 & \alpha_3 \\ \alpha_4 & \alpha_5 & \alpha_6 \\ \alpha_7 & \alpha_8 & \alpha_9 \end{bmatrix} = 0 \ . \tag{D-16}$$

These results clearly indicate that the equations of (D-15) are linearly dependent so that at least one of the equations is redundant and can be ignored. If, for example, one has

$$\det \begin{bmatrix} \alpha_2 & \alpha_3 \\ \alpha_5 & \alpha_6 \end{bmatrix} \neq 0 \ ,$$

then the result may be written as

$$\begin{aligned} C_2\alpha_2 + C_3\alpha_3 &= -C_1\alpha_1 \\ C_2\alpha_5 + C_3\alpha_6 &= -C_1\alpha_4 \end{aligned} \tag{D-17}$$

from which the results

$$C_2 = \frac{\begin{vmatrix} -C_1\alpha_1 & \alpha_3 \\ -C_1\alpha_4 & \alpha_6 \end{vmatrix}}{\begin{vmatrix} \alpha_2 & \alpha_3 \\ \alpha_5 & \alpha_6 \end{vmatrix}} \qquad \text{and} \qquad C_3 = \frac{\begin{vmatrix} \alpha_2 & -C_1\alpha_1 \\ \alpha_5 & -C_1\alpha_4 \end{vmatrix}}{\begin{vmatrix} \alpha_2 & \alpha_3 \\ \alpha_5 & \alpha_6 \end{vmatrix}}$$

are obtained immediately. These can be rewritten as

$$C_2 = \frac{\alpha_4\alpha_3 - \alpha_1\alpha_6}{\alpha_2\alpha_6 - \alpha_3\alpha_5} C_1 = k_1 C_1 \qquad \text{and } C_3 \frac{\alpha_1\alpha_5 - \alpha_2\alpha_4}{\alpha_2\alpha_6 - \alpha_3\alpha_5} C_1 = k_2 C_1 \tag{D-18}$$

respectively. The value of C_1 is then obtained by requiring that

$$\Psi = C_1\phi_1 + C_2\phi_2 + C_3\phi_3 = C_1(\phi_1 + k_1\phi_2 + k_2\phi_3)$$

be normalized; the result is then that the mixing coefficients for the 3 x 3 secular equation are

$$C_1 = \frac{1}{\sqrt{1 + k_1^{\,2} + k_2^{\,2}}}$$

$$C_2 = k_1 C_1 \; ; \; C_3 = k_2 C_1 \; . \tag{D-19}$$

It is to be noted that similar results will be obtained regardless of which equation in (D-15) is ignored, so long as the relevent (2 x 2) determinant in the (3 x 3) coefficient matrix is different from zero.

Finally, we have the case of the (4 x 4) secular equation which is required when treating the (J = 2) states of the 3p3d transitions. The system of equations is

$$\begin{aligned} C_1\alpha_1 + C_2\alpha_2 + C_3\alpha_3 + C_4\alpha_4 &= 0 \\ C_1\alpha_5 + C_2\alpha_6 + C_3\alpha_7 + C_4\alpha_8 &= 0 \\ C_1\alpha_9 + C_2\alpha_{10} + C_3\alpha_{11} + C_4\alpha_{12} &= 0 \\ C_1\alpha_{13} + C_2\alpha_{14} + C_3\alpha_{15} + C_4\alpha_{16} &= 0 \end{aligned} \tag{D-20}$$

from which the secular equation is

$$\det \begin{bmatrix} \alpha_1 & \alpha_2 & \alpha_3 & \alpha_4 \\ \alpha_5 & \alpha_6 & \alpha_7 & \alpha_8 \\ \alpha_9 & \alpha_{10} & \alpha_{11} & \alpha_{12} \\ \alpha_{13} & \alpha_{14} & \alpha_{15} & \alpha_{16} \end{bmatrix} = 0 \ . \qquad \text{(D-21)}$$

If one again ignores the last equation as in the (3 x 3) case and assume that

$$D = \det \begin{bmatrix} \alpha_2 & \alpha_3 & \alpha_4 \\ \alpha_6 & \alpha_7 & \alpha_8 \\ \alpha_{10} & \alpha_{11} & \alpha_{12} \end{bmatrix} \neq 0 \ ,$$

then the following results are obtained for the mixing coefficients:

$$C_2 = k_1 C_1 = -\frac{\det \begin{bmatrix} \alpha_1 & \alpha_3 & \alpha_4 \\ \alpha_5 & \alpha_7 & \alpha_8 \\ \alpha_9 & \alpha_{11} & \alpha_{12} \end{bmatrix}}{D} C_1 ; \quad C_3 = k_2 C_1 = -\frac{\det \begin{bmatrix} \alpha_2 & \alpha_1 & \alpha_4 \\ \alpha_6 & \alpha_5 & \alpha_8 \\ \alpha_{10} & \alpha_9 & \alpha_{12} \end{bmatrix}}{D} C_1 ;$$

$$C_4 = k_3 C_1 = -\frac{\det \begin{bmatrix} \alpha_2 & \alpha_3 & \alpha_1 \\ \alpha_6 & \alpha_7 & \alpha_5 \\ \alpha_{10} & \alpha_{11} & \alpha_9 \end{bmatrix}}{D} C_1 ; \qquad C_1 = \frac{1}{\sqrt{1 + k_1^2 + k_2^2 + k_3^2}} \ . \qquad \text{(D-22)}$$

The value of C_1, is, of course, determined by requiring that

$$\Psi = C_1\phi_1 + C_2\phi_2 + C_3\phi_3 + C_4\phi_4$$

be normalized.

These results then give the relevant expressions for computing the intermediate coupling (IC) mixing coefficients which occur in treating LMM Auger transitions. The specific values of the coefficients obtained in this work by using these results are listed in Tables 11-16. A few remarks regarding the use of these tables is in order. Thus we have used the symbol

$$C^N(LSJ)$$

to indicate an IC mixing coefficient with the understanding that "N" denotes the solution of the secular equation--i.e., the energy eigenvalue--used when computing the coefficients.

In order to present these coefficients in tabular form, the (LSJ) values of the IC coefficients are listed in the leftmost column of each box in the table. For example, the mixed levels for a 3s3p transition are those of the $^1P_1$ and $^3P_1$ states; these symbols are accordingly listed in the leftmost column of the "3s3p" box. The "N" value for each coefficient is denoted by the headings of each column with ^1P and ^3P being appropriate for the 3s3p transition. It is perhaps clear that these headings correspond to the possible LS-multiplets obtainable from the configuration listed in the table. This is, of course, not an accident as may be seen by examining one case in detail.

For reasons of simplicity, the case chosen is that of the 3s3p transition. One has that the IC wave functions and energies for this system are given by (compare Table I and Equation (D-6))

$$\Psi^N(J=1) = C^N(^1P_1)\psi(^1P_1) + C^N(^3P_1)\psi(^3P_1)$$

and

$$E_{1,2} = \frac{G^1(3s3p)}{6} - \frac{\xi_{3p}}{4} \pm \sqrt{\left(\frac{G^1}{3} + \frac{\xi_{3p}}{4}\right)^2 + \frac{\xi_{3p}^2}{2}}$$

where it is assumed that

$$E_1 \sim E_+ \qquad \text{and} \qquad E_2 \sim E_- \ .$$

The functions $\psi(^1P_1)$, $\psi(^3P_1)$ are <u>pure</u> LS-coupled states as defined in Appendix A. In addition, the N variable has two values corresponding to whether E_1 or E_2 is used to compute the IC coefficients. One could label this variable with the values (1,2), but then it would not be particularly clear which solution is involved. A better procedure is possible since we have

$$\lim_{\xi_{3p} \to 0} \begin{aligned} E_1 &= + \frac{G^1(3s3p)}{2} = E(^1P) \\ E_2 &= - \frac{G^1(3s3p)}{6} = E(^3P) \end{aligned} \qquad \text{(D-24)}$$

where the final step follows from (B-10) of Appendix B. Thus it follows that, in the limit of a zero spin-orbit interaction, the energy E_1 reduces to the energy for the pure ^1P state; similarly E_2 corresponds to the energy of the pure ^3P state. One can, therefore, label the energies $E_{1,2}$ by the LS-state to which they correspond when the spin-orbit parameter vanishes. The "N" label of $C^N(LSJ)$ can then be denoted by these same LS-state labels, and this is done in the tables. To illustrate the use of this notation, we can list the results for the 3s3d and 3s3p transitions in Ti obtained from Table 11. Thus one has

$$\begin{aligned}
&3s3p: \quad E(^1P) \sim 1; \quad C^1(^1P_1) = .999550 \quad C^1(^3P_1) = .030002 \\
&\qquad\quad E(^3P) \sim 2; \quad C^2(^1P_1) = .030005 \quad C^2(^3P_1) = -.999550 \\
&\\
&3s3d: \quad E(^1D) \sim 1; \quad C^1(^1D_2) = .999974 \quad C^1(^3D_2) = .007227 \\
&\qquad\quad E(^3D) \sim 2; \quad C^2(^1D_2) = .007142 \quad C^2(^3D_2) = -.999974
\end{aligned}$$

with similar results for the remaining configurations.

A final remark concerning the accuracy of the coefficients listed in the tables is in order. In all cases, the normalization of the IC function is accurate to 7 decimal places, assuming that the LS-states are also normalized (to 1). The IC states are also orthogonal with the maximum deviation being a value of (.0005) for the overlap integral between the ^3P and ^3F IC functions of the $3d^2$ transition in Cr.

Table 11. Titanium Intermediate Coupling Mixing Coefficents for LMM Transitions

3s3p		^1P	^3P									
	$^1P_1$	.999550	.030005									
	$^3P_1$	.030002	-.999550									
3s3d		^1D	^3D									
	$^1D_2$	.999974	.007142									
	$^3D_2$	.007227	-.999974									
$3p^2$		^1S	^3P		^1D	^3P						
	$^1S_0$	.996641	.081886	$^1D_2$	.993174	.116628						
	$^3P_0$	-.081890	.996642	$^3P_2$	.116639	-.993176						
$3d^2$		^1D	^3P	^3F		^1S	^3P		^1G	^3F		
	$^1D_2$	.921841	.386912	.022587								
	$^3P_2$	-.387001	.922079	-.000458	$^1S_0$	.999912	.013187	$^1G_4$	.999945	.010283		
	$^3F_2$	-.020971	-.008306	.999745	$^3P_0$	-.013232	.999913	$^3F_4$	.010459	-.999947		
3p3d		^3P	^1D	^3D	^3F		^1P	^3P	^3D		^3D	^1F	^3F
	$^3P_2$	.954685	.069842	.289178	.008621								
	$^1D_2$	.073787	-.976905	-.001682	-.200532	$^1P_1$	.998329	.044356	.037011	$^3D_3$	.998711	.029793	.041086
	$^3D_2$	.287925	.029353	-.956764	-.029027	$^3P_1$	-.028562	.935879	-.351156	$^1F_3$	-.028941	.999356	-.021197
	$^3F_2$	-.015227	.199791	.031256	-.979219	$^3D_1$	-.050232	.349519	.935585	$^3F_3$	-.041683	.019994	.998931

Table 12. Vanadium Intermediate Coupling Mixing Coefficients for LMM Transitions

3s3p		^1P	^3P									
	$^1P_1$	.999395	.034784									
	$^3P_1$	.034787	-.999395									
3s3d		^1D	^3D									
	$^1D_2$	.999961	.008766									
	$^3D_2$	.008788	-.999962									
$3p^2$		^1S	^3P		^1D	^3P						
	$^1S_0$	.995621	+.093477		$^1D_2$	.990771	.135544					
	$^3P_0$	-.093477	.995621		$^3P_2$	.135543	-.990772					
$3d^2$		^1D	^3P	^3F		^1S	^3P		^1G	^3F		
	$^1D_2$	.992212	.121784	.026027	$^1S_0$	.999873	.015883	$^1G_4$	.999936	.011358		
	$^3P_2$	-.121831	.992554	-.000530	$^3P_0$	-.015913	.999874	$^3F_4$	.011356	-.999936		
	$^3F_2$	-.025920	-.002491	.999661								
3p3d		^3P	^1D	^3D	^3F		^1P	^3P	^3D		^3D	^1F	^3F
	$^3P_2$	.942755	.081687	.323143	.010859	$^1P_1$	.997762	.054399	.038881	$^3D_3$	.998284	.034684	.047198
	$^1D_2$	.086383	-.971607	.000992	-.220245	$^3P_1$	-.033410	.909288	-.414811	$^1F_3$	-.033564	.999140	-.024349
	$^3D_2$	.321499	.035012	-.945702	-.032610	$^3D_1$	-.057929	.412597	.909077	$^3F_3$	-.047990	.022738	.998589
	$^3F_2$	-.019742	.219274	.034996	-.974839								

Table 13. Chromium Intermediate Coupling Mixing Coefficients for LMM Transitions

$3s3p$		^1P	^3P									
	$^1P_1$	.999202	-.039940									
	$^3P_1$	.039942	-.999202									
$3s3d$		^1D	^3D									
	$^1D_2$	.999946	.010365									
	$^3D_2$	.010381	-.999946									
$3p^2$		^1S	^3P		^1D	^3P						
	$^1S_0$	.994338	.106262	$^1D_2$	.987583	.157090						
	$^3P_0$	-.106262	.994338	$^3P_2$	.157098	-.987584						
$3d^2$		^1D	^3P	^3F		^1S	^3P		^1G	^3F		
	$^1D_2$	.989572	.140648	.031393	$^1S_0$	.999813	.019308	$^1G_4$	.999904	.013820		
	$^3P_2$	-.140618	.990051	-.000766	$^3P_0$	-.019331	.999814	$^3F_4$	.013856	-.999904		
	$^3F_2$	-.031199	-.004180	.999507								
$3p3d$		^3P	^1D	^3D	^3F		^1P	^3P	^1D		^3D	^1F	^3F
	$^3P_2$	.927704	.097944	.359980	.013760	$^1P_1$	.996872	.067803	.040592	$^3D_3$	.992594	.041235	.055722
	$^1D_2$	.103982	-.964839	.003773	-.241370	$^3P_1$	-.039505	.872447	-.487104	$^1F_3$	-.039659	.998789	-.029111
	$^3D_2$	.357564	.044224	-.932094	-.037310	$^3D_1$	-.068454	.483982	.872400	$^3F_3$	-.056855	.026833	.998022
	$^3F_2$	-.026488	.239867	.040025	-.969618								

Table 14. Zirconium Intermediate Coupling Mixing Coefficients for LMM Transitions

3s3p		^1P	^3P									
	$^1P_1$	.957692	.287796									
	$^3P_1$	-.287796	.957692									
3s3d		^1D	^3D									
	$^1D_2$	.990817	.135208									
	$^3D_2$	-.135211	.990817									
$3p^2$		^1S	^3P		^1D	^3P						
	$^1S_0$	.8009162	.598787	$^1D_2$	.910327	.413890						
	$^3P_0$	.598776	-.800908	$^3P_2$	-.413890	.910323						
$3d^2$		^1D	^3P	^3F		^1S	^3P		^1G	^3F		
	$^1D_2$	.551728	.703472	.448060	$^1S_0$	.980614	.195946	$^1G_4$	.993924	.110048		
	$^3P_2$	.722576	-.671384	.164449	$^3P_0$	.195950	-.980615	$^3F_4$	-.110072	.993926		
	$^3F_2$	.416510	.233175	-.878748								
3p3d		^3P	^1D	^3D	^3F		^1P	^3P	^3D		^3D	^1F	^3F
	$^3P_2$	.369932	.561589	.684686	.281111	$^1P_1$	.865277	.110456	.488985	$^3D_3$	.893291	.237050	.381912
	$^1D_2$	-.456293	.120192	-.204264	.857701	$^3P_1$	.254722	-.936998	-.239124	$^1F_3$	.288610	-.953843	-.083016
	$^3D_2$	-.375790	-.617745	.688901	.050691	$^3D_1$	.431755	.331412	-.838876	$^3F_3$	.344580	.184365	-.920463
	$^3F_2$	-.716749	.537180	.122047	-.427500								

Table 15. Niobium Intermediate Coupling Mixing Coefficients for LMM Transitions

$3s3p$		^1P	^3P									
	$^1P_1$	.949699	.313166									
	$^3P_1$	-.313165	.949698									
$3s3d$		^1D	^3D									
	$^1D_2$	.988445	.151579									
	$^3D_2$	-.151581	.988445									
$3p^2$		^1S	^3P		^1D	^3P						
	$^1S_0$	.785269	.619155	$^1D_2$	.904960	.425496						
	$^3P_0$	.619155	-.785269	$^3P_2$	-.425496	.904960						
$3d^2$		^1D	^3P	^3F	^1S	^3P		^1G	^3F			
	$^1D_2$	.493737	.714368	.495886	$^1S_0$	.976476	.215623	$^1G_4$	.992869	.119208		
	$^3P_2$	.733380	-.648480	.204002	$^3P_0$	.215627	-.976477	$^3F_4$	-.119211	.992869		
	$^3F_2$	.467309	.262966	-.844086								
$3p3d$		^3P	^1D	^3D	^3F		^1P	^3P	^3D		^3D	^1F	^3F
	$^3P_2$	.338501	.568980	.687526	.298303	$^1P_1$	.849327	.122586	.513433	$^3D_3$	.873167	.253619	.416245
	$^1D_2$	-.461817	.081982	-.212416	.857252	$^3P_1$	.268257	-.937934	-.219816	$^1F_3$	.313312	-.946214	-.080712
	$^3D_2$	-.346599	-.641744	.682725	.043825	$^3D_1$	.454622	.324427	-.829498	$^3F_3$	.373384	.200890	-.905663
	$^3F_2$	-.742975	.507647	.126785	-.417389								

Table 16. Molybdenum Intermediate Coupling Mixing Coefficients for LMM Transitions

3s3p		^1P	^3P									
	$^1P_1$	.940757	.339082									
	$^3P_1$	-.339082	.940757									
3s3d		^1D	^3D									
	$^1D_2$	.985582	.169161									
	$^3D_2$	-.169201	.985589									
$3p^2$		^1S	^3P		^1D	^3P						
	$^1S_0$	.770528	.637405	$^1D_2$	.899843	.436212						
	$^3P_0$	.637406	-.770529	$^3P_2$	-.436214	.899844						
$3d^2$		^1D	^3P	^3F	^1S	^3P		^1G	^3F			
	$^1D_2$	.430588	.722514	.540883	$^1S_0$	.971699	.236166	$^1G_4$	.991699	.128551		
	$^3P_2$	.739970	-.625646	.246768	$^3P_0$	.236222	-.971713	$^3F_4$	-.128584	.991703		
	$^3F_2$	.516758	.294179	-.804084								
3p3d		^3P	^1D	^3D	^3F		^1P	^3P	^3D		^3D	^1F	^3F
	$^3P_2$	.313218	.571526	.689801	.315394	$^1P_1$	.833455	.136377	.535485	$^3D_3$	.850428	.270033	.451539
	$^1D_2$	-.464990	.047945	-.220144	.856175	$^3P_1$	.280820	-.939136	-.197959	$^1F_3$	.338477	-.937849	-.076625
	$^3D_2$	-.322134	-.660612	.677110	.036113	$^3D_1$	.475912	.315317	-.821016	$^3F_3$	.402749	.217993	-.888955
	$^3F_2$	-.762829	.484407	.131272	-.407660								

BIBLIOGRAPHY[†]

1. P. Auger, Comptes Rendus 180, 65 (1925); 182, 773 (1926).
2. P. Auger, J. Phys. Rad. 6, 205 (1925).
3. G. Wentzel, Z. Physik 43, 524 (1927).
4. E. H. S. Burhop, Proc. Roy. Soc. (London) A148, 272 (1935).
5. L. Pincherle, Nuovo Cimento 12, 81 (1935).
6. E. G. Ramberg and F. K. Richtmeyer, Phys. Rev. 51, 913 (1937).
7. H. S. Massey and E. H. S. Burhop, Proc. Roy. Soc. (London) A153, 661 (1936).
8. R. A. Rubenstein and J. N. Snyder, Phys. Rev. 97, 1653 (1955).
9. R. A. Rubenstein, Ph.D. Thesis, University of Illinois, 1955.
10. W. N. Asaad and E. H. S. Burhop, Proc. Phys. Soc. 71, 369 (1958).
11. P. Erman, I. Bergström, Y. Y. Chu and G. T. Emery, Nucl. Phys 62, 401 (1965).
12. R. L. Graham, I. Bergström and F. Brown, Nucl. Phys. 39, 107 (1962).
13. E. J. Callan, Phys. Rev. 124, 793 (1961).
14. W. N. Asaad, Nucl. Phys. 44, 399 (1963).
15. W. N. Asaad, Nucl. Phys. 66, 494 (1965).
16. K. Siegbahn, et al., Air Force Materials Laboratory Technical Report No. AFML-TR-68-189, 1968 (unpublished).
17. E. J. McGuire, Phys. Rev. 185, 1 (1969); A2, 273 (1970).
18. D. L. Walters and C. P. Bhalla, Phys. Rev. A3, 1919 (1971); A3, 519 (1971).

[†]Abbreviations herein follow the form recommended by the American Institute of Physics.

19. V. O. Kostrun, M. H. Chen and B. Crasemann, Phys. Rev. A3, 533 (1971).

20. W. N. Asaad, in Role of Atomic Electrons in Nuclear Transformations (Nuclear Energy Information Center, Warsaw, 1963), Vol. 3, p. 371.

21. E. J. Callan, in Reference 20, p. 398.

22. W. N. Asaad and W. Mehlhorn, Z. Physik 217, 304 (1968).

23. E. J. McGuire, Phys. Rev. A3, 587 (1971).

24. D. L. Walters and C. P. Bhalla, Phys. Rev. A4, 2164 (1971).

25. B. Crasemann, M. H. Chen and V. O. Kostrun, Phys. Rev. A4, 2161 (1971).

26. E. J. McGuire, Phys. Rev. A5, 1043, 1052 (1972).

27. M. A. Listengarten, Izv. Akad. Nauk USSR (ser. fiz.) 24, 1041 (1960). (Trans. Bulletin 24, 1050).

28. I. Bergström and C. Nordling, in Alpha-, Beta- and Gamma-Ray Spectroscopy, Chapter XXV, p. 1523, North Holland Publishing Co., Amsterdam (1965).

29. K. D. Sevier, Low Energy Electron Spectrometry, Wiley-Interscience, New York (1972).

30. E. H. S. Burhop, The Auger Effect and Other Radiationless Transitions, Cambridge University Press (1952).

31. D. Chattarji and B. Talukdar, Phys. Rev. 174, 44 (1968).

32. W. N. Asaad, Proc. Roy. Soc. (London) A249, 555 (1959).

33. M. A. Listengarten, Izv. Akad. Nauk USSR (ser. fiz.) 25, 792 (1961). (Trans. Bulletin 25, 803).

34. M. A. Listengarten, Izv. Akad. Nauk USSR (ser. fiz.) 26, 182 (1962). (Trans. Bulletin 26, 182).

35. L. H. Toburen and R. G. Albridge, Nucl. Phys. A90, 529 (1967).

36. O. Hörnfeldt, Ark. Fysik 23, 235 (1962).

37. J. L. Wolfson and A. P. Baerg, Can. J. Phys. 42, 1781 (1964).

38. H. Körber and W. Mehlhorn, Z. Physik 191, 217 (1966).

39. B. Cleff and W. Mehlhorn, Z. Physik 219, 311 (1969).

40. E. Sokolowski and C. Nordling, Ark. Fysik 14, 557 (1959).

41. O. Hornfeldt, A. Fahlman and C. Nordling, Ark. Fysik 23, 155 (1962).

42. F. A. Johnson and J. S. Foster, Can. J. Phys. 31, 469 (1953).

43. R. L. Graham, F. Brown, G. T. Ewan and J. Uhler, Can. J. Phys. 39, 1086 (1961).

44. G. T. Ewan and J. S. Merritt, Can. J. Phys. 38, 324 (1960).

45. J. S. Dionisio, in Reference 20, p. 440.

46. W. Mehlhorn and D. Stalherm, Z. Physik 217, 294 (1968).

47. M. O. Krause, Phys. Lett. 19, 14 (1965).

48. S. K. Haynes, in Inner Shell Ionization Phenomena and Future Applications, p. 559, North-Holland Publishing Co., Amsterdam (1973).

49. C. J. Allan and K. Siegbahn, Uppsala Univ. Internal. Rpt. UUIP-754, 1971).

50. K. Siegbahn, Uppsala Univ. Internal. Rpt. UUIP-752, 1971.

51. L. N. Tharp, Ph.D. Thesis, Georgia Institute of Technology, 1968.

52. C. C. Chang, Surface Science 25, 53 (1971).

53. C. S. McKee and M. W. Roberts, Chem. in Britain 6, 106 (1970).

54. P. W. Palmberg, in CRC Critical Reviews in Solid State Sciences, Vol. 3, CRC Press, 1972.

55. G. W. Simmons, W. H. Hicklin and R. K. Hart, in Proc. of 24th Annual Symposium on Frequency Control, p. 111 (1970).

56. R. E. Weber and W. T. Peria, J. Appl. Phys. 38, 4355 (1967).

57. J. C. Rivere, Physics Bulletin 20, 85 (1969).

58. A. Fahlman, K. Hamrin, R. Nordberg, C. Nordling and K. Siegbahn, Phys. Lett. 20, 159 (1966).

59. T. W. Haas, J. T. Grant and G. J. Dooley III, J. Appl. Phys. 43, 1853 (1972).

60. L. N. Tharp and E. J. Scheibner, J. Appl. Phys. 38, 3320 (1967).

61. U. Fano, Phys. Rev. 140, A67 (1965).

62. B. W. Shore, Phys. Rev. 139, A1042 (1965).

63. J. C. Slater, Quantum Theory of Atomic Structure, Vols. I and II, McGraw-Hill Book Co. (1960). General Reference.

64. E. U. Condon and G. H. Shortley, The Theory of Atomic Spectra, Chapters 3 and 6-13, Cambridge University Press (1967).

65. A. Messiah, Quantum Mechanics, Vols. I and II, North-Holland Publishing Co., Amsterdam (1962). General Reference.

66. H. N. Russell and F. A. Saunders, Astrophys. J. 61, 38 (1925).

67. C. F. Fischer, Comp. Phys. Comm. 1, 151 (1969).

68. I. Bergström and R. Hill, Ark. Fysik 8, 21 (1954).

69. B. W. Shore and D. H. Menzel, Principles of Atomic Spectra, Wiley and Sons, New York (1968). General Reference.

70. A. R. Edmonds, Angular Momentum in Quantum Mechanics, Princeton University Press, New Jersey (1960). General Reference.

71. M. Jacob and G. C. Wick, Ann. Phys. (New York) 7, 404 (1959).

72. W. R. Frazer, Elementary Particles, Prentice-Hall, Inc., New Jersey (1966).

73. G. Racah, Phys. Rev. 63, 367 (1943).

74. G. F. Amelio, Ph.D. Thesis, Georgia Institute of Technology, 1968.

75. M. Blume and R. E. Watson, Proc. Roy. Soc. (London) A270, 127 (1962).

76. F. Hermann and S. Skillman, Atomic Structure Calculations, Prentice-Hall, Inc., New Jersey (1963).

77. S. T. Manson, private communication.

78. C. Möller, Ann. Physik 14, 531 (1932).

79. G. L. Connell and Y. P. Gupta, Mat. Res. and Stand. 11, 8 (1971).

80. L. A. Harris, Anal. Chem. 40, 24A (1968); J. Appl. Phys. 39, 1419 (1968).

81. N. J. Taylor, Vacuum 19, 474 (1969).

82. N. J. Taylor, J. Vac. Sci. and Tech. 6, 241 (1969).

83. G. F. Amelio, Surface Science 22, 301 (1970).

84. G. W. Simmons, J. Coll. and Interface Sci. 34, 343 (1970).

85. T. W. Haas, J. T. Grant and G. J. Dooley III, Phys. Rev. B1, 1449 (1970).

86. P. W. Palmberg, private communication (1972).

87. F. Hermann, J. P. Van Dyke and I. B. Ortenburger, Phys. Rev. Lett. 22, 807 (1969).

88. T. W. Haas, private communication.

89. Y. E. Strausser and J. J. Uebbing, "Varian Chart of Auger Energies," Varian Vacuum Div., Palo Alto, California (1971).

90. T. Collins, private communication.

VITA

James Daniel Phillips was born October 20, 1943, in De Queen, Arkansas. On October 23, 1964 he was married to Cynthis Jane Davis of Texarkana, Texas; they have two children, Ronald Eugene and Dale Alan.

Mr. Phillips attended public schools in the Texarkana, Texas school system graduating with honors from Texas Senior High in May, 1961. He entered Texas Tech University, following one year at Texarkana College, in September, 1962, and graduated with honors in May, 1965, with a B. S. degree in Physics. After enrolling at the Georgia Tech Institute of Technology the next fall, he received an M.S. degree in Physics in June, 1967.

While at Texas Tech and Texarkana College, he was named to several honorary societies including Phi Theta Kappa, Lychonos and Sigma Pi Sigma. He was also selected to the Dean's List for each period in attendance at these institutions and received the Texaco Scholarship at Texas Tech in 1964. During his tenure at Georgia Tech, he received an NDEA graduate fellowship and held positions both as a graduate teaching (1967-1969) and graduate research assistant (1969-1972).